FUNCTIONAL ORGANIZATION AND ONTOGENY OF THE OPTOKINETIC REFLEX IN *XENOPUS LAEVIS*

Graduate School of
Systemic Neurosciences

LMU Munich

Dissertation der Graduate School of Systemic Neurosciences
der Ludwig-Maximilians-Universität München

Johanna Schuller

29. August 2017

Supervisor/1st reviewer: Prof. Hans STRAKA

2nd reviewer: Prof. Stefan GLASAUER

3rd reviewer: Prof. Uwe ILG

Defense: Munich, 8th of December 2017

ACKNOWLEDGEMENT

Years passed by, but memories will remain!

I am grateful to the people who supported me in one way or another within the last years and made this work possible.

Thank you …

… Hans Straka for being my supervisor, for providing your laboratory to conduct my thesis, for tons of scientific ideas and for your patience and support across the last years and especially within the last weeks!

… my dear colleagues for the good times in and outside the laboratory and the many laughs, cakes and coffees - and Francisco and Sara for proof-reading parts of my thesis.

… Alex for helping me with the analysis program, for answering all my questions on basic Matlab codes and for sharing your technological view on biological systems!

… Gerd for thorough proof-reading of this manuscript and plenty of helpful comments and Julia for compilation of the style sheet!

… Stefan Glasauer and John Simmers for your valuable input during my thesis committees.

… to my external reviewer Uwe Ilg for reviewing my thesis.

… to the team of the Graduate School of Systemic Neurosciences, for the interesting events and courses during my PhD program, the financial support and the good mood.

… to the Graduiertenkolleg 1091 and the IFB for financial support.

… to my friends for telling me, I can do it - and Céline and Nadine for your wise sayings, many quiffees and deep friendship.

… to my parents and to my siblings Julia and Florian - for your endless support, for believing in me and for never letting me down!

ABSTRACT

Visuo-vestibular reflexes together with spinal efference copy-driven eye movements minimize visual disturbances during vertebrate locomotion. The optokinetic closed-loop system provides feedback about the quality of compensation and elicits motor output to optimize image stabilization. Large surround visual motion stimulation evokes the optokinetic reflex characterized by slow following and fast resetting eye movements. This study investigated the horizontal optokinetic response of *Xenopus laevis* with a focus on its functional organization and developmental changes during metamorphosis. Constant velocity and sinusoidal optokinetic stimulation with a vertically striped pattern evoked eye movements in semi-intact *in vitro* preparations with a functional visual system. Pre-metamorphic tadpoles showed a large amplitude optokinetic response with low-pass filtering characteristics and the onset of the optokinetic reflex correlated with maturation of swimming behavior. Simultaneous motion recordings of one eye and extracellular multiple- and single-unit recordings of the contralateral extraocular nerves during optokinetic stimulation revealed a differential recruitment and task-specific contribution of abducens motoneurons. Type I units were active during slow and fast phases, type II units fired during fast phases and spinal efference copy-driven eye movements. Optokinetic performance incurred a drastic decline during metamorphosis. A reduced ocular motility, a low response gain and a lack of fast resetting phases became apparent with the modification of body plan and change of locomotor pattern. The functionality of the optokinetic system in tadpoles and frogs mirror the specific requirements of the respective mode of life. These findings show that *Xenopus laevis* can serve as a viable animal model to gain insight in the fundamental functionality of the optokinetic system in vertebrates and open up the approach to new questions e.g. concerning the interaction of the optokinetic system and intrinsic spinal efference copies during locomotion.

TABLE OF CONTENTS

1 INTRODUCTION

Around 540 million years ago in the Cambrian period at the beginning of the Paleozoic era, rapid diversification of life forms generated the first representatives of all modern animal phyla (Lamb et al., 2007; Valentine et al., 1999). With the increase of complex organisms, the transition from aquatic to terrestrial habitats several million years later was a crucial step in evolution. Challenged by the novel physical and biological conditions, animals changed their morphological and physiological mechanisms to adapt for a life in the specific niches (Ashley-Ross et al., 2013). Besides respiration, feeding and reproduction, capabilities - such as sight and the ability to move - were and still are essential for survival (Biewener, 2003; Lamb et al., 2007).

Early organisms evolved simple systems, which were able to signal light by light-dependent chemical reactions way before the Cambrian explosion (Lamb et al., 2007). With the behaviors becoming more complex, more sophisticated sensory organs and neural processing were required (Nilsson, 2013). Likely deriving from the same ancient photoreceptive cell type (Arendt et al., 2009), but shaped by different developmental events and natural selection (Gehring, 2011), visual systems of spectacularly high spatial acuity and optical resolving power evolved independently in arthropods, cephalopods and vertebrates (Lamb et al., 2009; Suzuki et al., 2015).

During self-generated body movements in vertebrates, the image is moving on the retina since the eye position in space is changing relative to the environment. Without compensation of this retinal image slip, locomotion would lead to blurred vision (Land, 1999). Therefore, not only body posture but also gaze must be continuously stabilized during locomotion to guarantee a stable perception of the world. The development of an ocular motor system in vertebrates (Fig. 1A) with its adjustment for species-specific requirements allows moving the eyes within the head and increase the ability to maintain a stable gaze during self-motion.

1.1 THE OCULAR MOTOR SYSTEM

Extraocular muscles and their neuronal innervations are the important components of the ocular motor system for gaze stabilization.

Besides slight modifications in arrangement and innervation, six extraocular muscles (EOMs) are highly conserved in all vertebrates. Their arrangement in three antagonistically operating pairs allows torsional, vertical and horizontal movements of the eye by rotating the eye ball. The superior (SO) and inferior oblique (IO) muscles are responsible for intorsion and extorsion. The superior rectus muscle (SR) elevates and the inferior rectus muscle (IR) depresses the eye ball in the vertical plane. Eye rotation in the horizontal plane is mediated by the adducting medial rectus muscle (MR) moving the eye ball in the nasal direction and the abducting lateral rectus muscle (LR) moving the eye in the temporal direction (Horn and Leigh, 2011) (Fig. 1B).

The extraocular muscles are the effector organs of voluntary and reflexive eye movements. For an optimal and accurate execution of the different eye movements, the EOMs have to be activated with extremely high precision (Spencer and Porter, 2006). Such high-precision control is accomplished by the innervation by three different cranial nerves (CNs) that guarantee a fine-tuning of differential muscle activation. The lateral rectus muscle is innervated by the abducens nerve (CN VI), the superior oblique muscle by the trochlear nerve (CN IV) and all other extraocular muscles are supplied by the oculomotor nerve (CN III). Three separate motor nuclei in the brain give rise to the extraocular motor nerves. While the oculomotor nucleus (nIII) is located in the mesencephalon, the trochlear (nIV) and abducens (nVI) nuclei are found in the hindbrain (Gilland and Baker, 2005) (Fig. 1C). Interconnection of the extraocular motor nuclei of both sides innervating antagonistic muscle pairs facilitates conjugated movements of both eyes in the same direction (Baker and Highstein, 1975). To enable concurrent eye movements in the horizontal plane for example, abducens neurons on one side innervate the ipsilateral lateral rectus muscle, while simultaneously active ipsilateral abducens interneurons

send excitatory projections to the contralateral oculomotor nucleus (Evinger, 1988; Straka and Dieringer, 1991), which innervates the medial rectus muscle on the contralateral side.

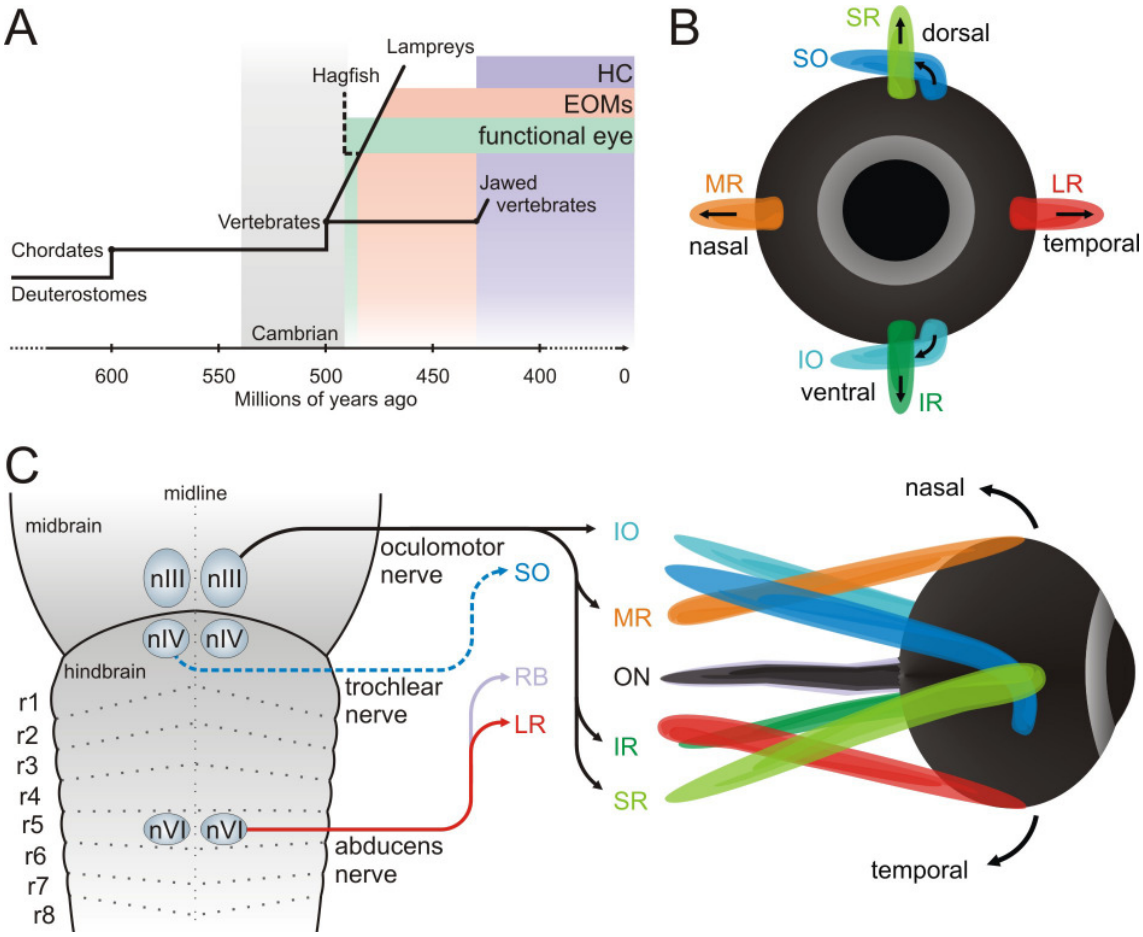

Figure 1: Ocular motor system in vertebrates. (A) Simplified evolutionary tree of the important structures for gaze stabilization in the horizontal plane (Fritzsch and Beisel, 2003; Lamb, 2013). (B) The eye of larval *Xenopus* (front view) with indication of the primary pulling directions of the extraocular muscles. (C) Schematic map of the cranial nerve efferent nuclei in the frog hindbrain and the corresponding extraocular musculature (top view). In all vertebrates the oculomotor (nIII) and trochlear (nIV) nuclei are found in the midbrain and the rostral part of the hindbrain segment r1, respectively. In anurans and mammals the abducens nuclei (nVI) are situated in rhombomere 5 (Gilland and Baker, 2005). In frogs, an additional extraocular muscle for retraction of the eye bulb, the retractor bulbi muscle, is innervated by the abducens nerve. EOM, extraocular muscle; HC, horizontal semicircular canal; IO, inferior oblique; IR, inferior rectus; LR, lateral rectus; MR, medial rectus; ON, optic nerve; r1-8, rhombomeres 1-8; RB, retractor bulbi; SO, superior oblique; SR, superior rectus.

1.2 GAZE STABILIZING REFLEXES

Body and head movements activate the vestibular system and an optic flow is generated across the retina. Both sensory systems, i.e. the vestibular and visual systems, elicit reflexive behaviors, which complement each other (Dieringer et al., 1992). Together with eye movements driven by spinal efference copy signals (Combes et al., 2008; Lambert et al., 2012), the reflexes ensure image stabilization during self- and passively induced movements (Fig. 2). Present in all vertebrates, the ocular motor control system mediating vestibulo-ocular and optokinetic reflexes is phylogenetically the oldest and builds a base for other eye movement systems, e.g. for smooth pursuit eye movements or target-directed saccades (Büttner and Büttner-Ennever, 2006; Spencer and Porter, 2006).

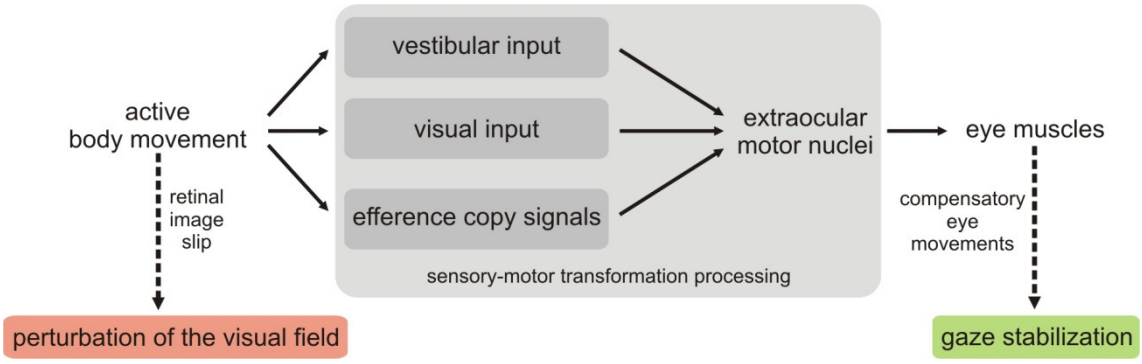

Figure 2: Gaze stabilization. Active head and body movements generate an image slip on the retina and lead to perturbation of the visual field. Transformation of the generated sensory input in the vestibular and visual systems as well as spinal efference copy signals lead to compensatory eye movements which counteract body movement related image displacements.

1.2.1 Vestibular system and vestibulo-ocular reflex (VOR)

The vestibular system consists of the vestibular labyrinth in which the sensory hair cells are located, first-order vestibular neurons innervating the hair cells, and the central vestibular nucleus (Straka and Dieringer, 2004).

The labyrinth is a set of interconnected chambers located bilaterally in the otic capsule. A membranous labyrinth is enclosed within bony walls that build the outer structure of the labyrinth. It comprises three semicircular canals

oriented perpendicular to each other and the two otolith organs utricle and saccule in mammals. In all non-mammalian vertebrates including monotremes an additional labyrinthine end organ, the lagena, exists (Straka et al., 2003). The membranous labyrinth within the osseous labyrinth is filled with endolymph. The purpose of this complex fluid-filled structure is to transmit the mechanical energy resulting from head movements to the sensory receptors of the vestibular system – the hair cells.

Vestibular hair cells possess up to several hundred stereocilia which increase in length towards a longer kinocilium. Deflection of the stereocilia towards the kinocilium leads to a depolarization, away from the kinocilium to a hyperpolarization of the hair cell via mechanically gated transduction channels. The combination of the direction selectivity of the hair cells themselves, their arrangement within the sensory epithelium and the position of the sensory epithelia within the vestibular organs enable the vestibular system to sense head translation and rotation in any direction (Goldberg et al., 2012).

The otolith organs primarily detect linear vertical and horizontal accelerations as well as static changes of head position relative to gravity. The maculae, the sensory epithelia in the otolith organs, are oriented nearly vertically in the saccule and horizontally in the utricle. Hair cells lie between supporting cells and project their hair bundles into a gelatinous layer, which is overlain by calcium carbonate crystals (otoconia). During head movement, the hair bundles are deflected due to the inertia of the otoconia which displace the gelatinous layer (Purves et al., 2012).

The semicircular canals detect angular accelerations. On the base of each canal, a bulbous expansion called ampulla contains the sensory epithelium (crista). The hair cell bundles project in a gelatinous mass (cupula) which protrudes into and spans the canal lumen of the ampulla. Functioning as a viscous barrier, the cupula and thus the stereocilia are deflected by the endolymph during angular movements and convert minimal rotations of the head into alterations of the hair cell membrane potential. The canals on both

sides of the head form three nearly coplanar canal pairs (Blanks et al., 1975; Blanks and Precht, 1976). Each canal pair acts opposite synergistically, i.e. when for example the hair cells in the left horizontal canal are depolarized, the hair cells in the right horizontal canal are hyperpolarized and vice versa.

The polarization of the hair cells is encoded in the spike discharge of the afferent bipolar first-order vestibular neurons, which synapse with the hair cells. Their ascending fibers form the vestibular branch of the VIIIth cranial nerve and project to second-order vestibular neurons of the vestibular nucleus in the brainstem. Besides descending and ascending projections to e.g. spinal and cerebellar networks (Matesz et al., 2002), the vestibular nucleus is also an early station for visual-vestibular sensory integration (Allum et al., 1976; Beraneck and Cullen, 2007). In addition, many of the second-order vestibular neurons act as premotor cells and are part of very short-latency circuits that drive compensatory eye and head movements in response to vestibular stimulation (Straka and Dieringer, 2004).

While some reflex arcs act to maintain the posture of head (vestibulo-cervical reflex) and body (vestibulo-spinal reflex), the purpose of the vestibulo-ocular reflexes (VORs) is to stabilize gaze during head movements (Purves et al., 2012). Vestibular stimulation in one direction elicits eye movements in the opposite direction via a three-neuronal reflex arc of vestibular afferents, central vestibular neurons and extraocular motoneurons (Baker et al., 1981). While linear acceleration induces the linear VOR (lVOR), rotational acceleration evokes the angular VOR (aVOR). Each of the three semicircular canal pairs is closely linked to the alignment and pulling actions of one of the three extraocular muscle pairs (Ezure and Graf, 1984; Simpson and Graf, 1981). In case of the horizontal vestibulo-ocular reflex, head rotation to the left leads to depolarization of the hair cells in the left horizontal semicircular canal and thus excitation of the left vestibular nucleus. Second-order vestibular neurons excite the contralateral abducens neurons and interneurons, which evoke contraction of the right lateral rectus muscle and via midline-crossing

projections of the abducens interneurons to the left oculomotor nucleus contraction of the medial rectus muscle of the left eye. In parallel, inhibitory second-order vestibular projections to the ipsilateral abducens neurons and interneurons decrease the motor drive of the left lateral rectus and right medial rectus muscles. Therefore, rotation of the head to the left results in conjugated eye movements to the right to counteract retinal image slip (Fig. 3A).

Fast processing of sensory signals and transformation in motor output by this reflex arc (Straka and Dieringer, 2004) makes the vestibular system perfectly suited to compensate for high accelerations of head and body (Straka and Simmers, 2011). However, the motor output, i.e. the movement of the eyes, does not influence the sensory reception and no internal feedback is available to correct for imperfect retinal slip compensation. Thus, the vestibular system operates as an open-loop control system (Miles and Lisberger, 1981; Precht, 1979). Feedback about the quality of gaze stabilization is exclusively provided by the visual system.

1.2.2 Visual system and optokinetic reflex circuitry

The majority of vertebrates achieve high-resolution vision with paired camera-type lens eyes. Through the lens, light is precisely focused on the retina, a hemispheric surface covered with photoreceptors (Martinez-Morales and Wittbrodt, 2009). An image of the environment is mapped onto the retinal surface conserving the relationship of neighboring points. Photopigments in the photoreceptor cells transform the photons of light into an electrochemical signal. The signal is passed on to the retinal ganglion cells and via their axons, which form the optic nerve, to information processing thalamic, pretectal and tectal structures in the brain (Prasad and Galetta, 2011).

Rods and cones are the two photoreceptor cell types of the vertebrate retina. Differences lie in the light absorption spectra of the photopigments, all of which are a modified form of the protein opsin. Rods contain rhodopsin and absorb a broad spectrum of light. Light sensitivity and a high intraretinal

convergence allow vision even in dim light although with decreased visual acuity. Cones contain iodopsins. With their limited absorption spectra responsible for color vision in some vertebrates, cones require much brighter illumination and have far less convergence than rods. Numbers and distribution of photoreceptors in the retina vary between species, but follow the typical pattern of more rods in the periphery and more cones in the central area (see Liem et al., 2001).

Besides the photoreceptors, four further cell layers build up the retina. Bipolar cells in the bipolar cell layer synapse with one or several photoreceptor cells and project to the ganglion cells in the ganglion cell layer. Further interconnections between photoreceptors and bipolar cells are mediated by horizontal cells in the outer plexiform layer and amacrine cells in the inner plexiform layer connect bipolar and ganglion cells horizontally. The complex inhibitory and excitatory arrangement provides the basis for signal processing of spatiotemporal information within the retina and facilitates motion detection (Borst and Egelhaaf, 1989; Clifford and Ibbotson, 2002).

Discrimination of image movement directions appears already at the level of retinal ganglion cells (Barlow and Hill, 1963) or even before (Briggman et al., 2011; Euler et al., 2002). Stimuli in the preferred direction excite the cells, while stimuli in the opposite direction lead to inhibition. Thus, the retina with its ability to detect image movement directions and motion changes of the visual surround forms the sensory key element for the optokinetic closed-loop system.

Retinorecipient projection sites important for the reflexive optokinetic system are located in the midbrain and pretectum. While in teleosts only one nucleus, the pretectal area, contains direction-selective neurons for all directions of stimulus movement (Klar and Hoffmann, 2002), the representation of horizontal and vertical stimulus directions is sorted in different nuclei in all tetrapods (Distler and Hoffmann, 2011; Masseck and Hoffmann, 2009). In amphibians, reptiles and birds a pretectal neuropil referred to as nucleus lentiformis mesencephali (nLM) relays information of horizontal visual

stimulation of the contralateral eye, predominantly in temporo-nasal direction. The nucleus of the basal optic roots (nBOR) belongs to the accessory optic system (AOS) and processes contralateral stimuli in vertical and all other remaining directions (Cochran et al., 1984; Gruberg and Grasse, 1984 (frog); Fan et al., 1995 (turtle); Wallman et al., 1981 (chicken); Winterson and Brauth, 1985 (pigeon)). However, anatomical interspecies differences concerning e.g. the relative size of the nuclei as well as differences in the functional interconnection to other brain regions exist (Giolli et al., 2006). On the basis of anatomical, functional and neuronal connections and response properties, the nucleus of the optic tract (NOT) and the dorsal, medial and lateral terminal nuclei (DTN/MTN/LTN) in mammals are considered to be homologous to nLM and nBOR (Collewijn, 1975; Katte and Hoffmann, 1980; McKenna and Wallman, 1985). Inhibitory pretectal-AOS interconnections exist as well as reciprocal connections between ipsi- and contralateral nLMs and nBORs, respectively (for review see Giolli et al., 2006). Comparative functional studies across species underline the crucial role of the pretectal nucleus (in mammals: NOT together with DTN) as optokinetic relay station for horizontal eye movements and the importance of the accessory optic nucleus for vertical eye movements. In frogs (Montgomery et al., 1981; Straka and Dieringer, 1991) and pigeons (Brecha and Karten, 1979; Wylie et al., 1997), but not in turtle (Weber et al., 2003), these nuclei have been shown to send efferent projections to the ipsilateral extraocular motor nuclei – the nLM to the abducens nucleus, the nBOR to the oculomotor and trochlear nuclei. Also in rabbit, NOT neurons project directly to the ipsilateral abducens nucleus (Holstege and Collewijn, 1982) (Fig. 3B). Besides these major connections, further parallel visual motion processing pathways and the involvement of additional brain structures functioning as velocity-to-position integrator or velocity storage elements were shown in several species (Pastor et al., 1994 (goldfish); Delgado-Garcia et al., 1989; Lopez-Barneo et al., 1982 (cat); Cannon and Robinson, 1987 (primate).

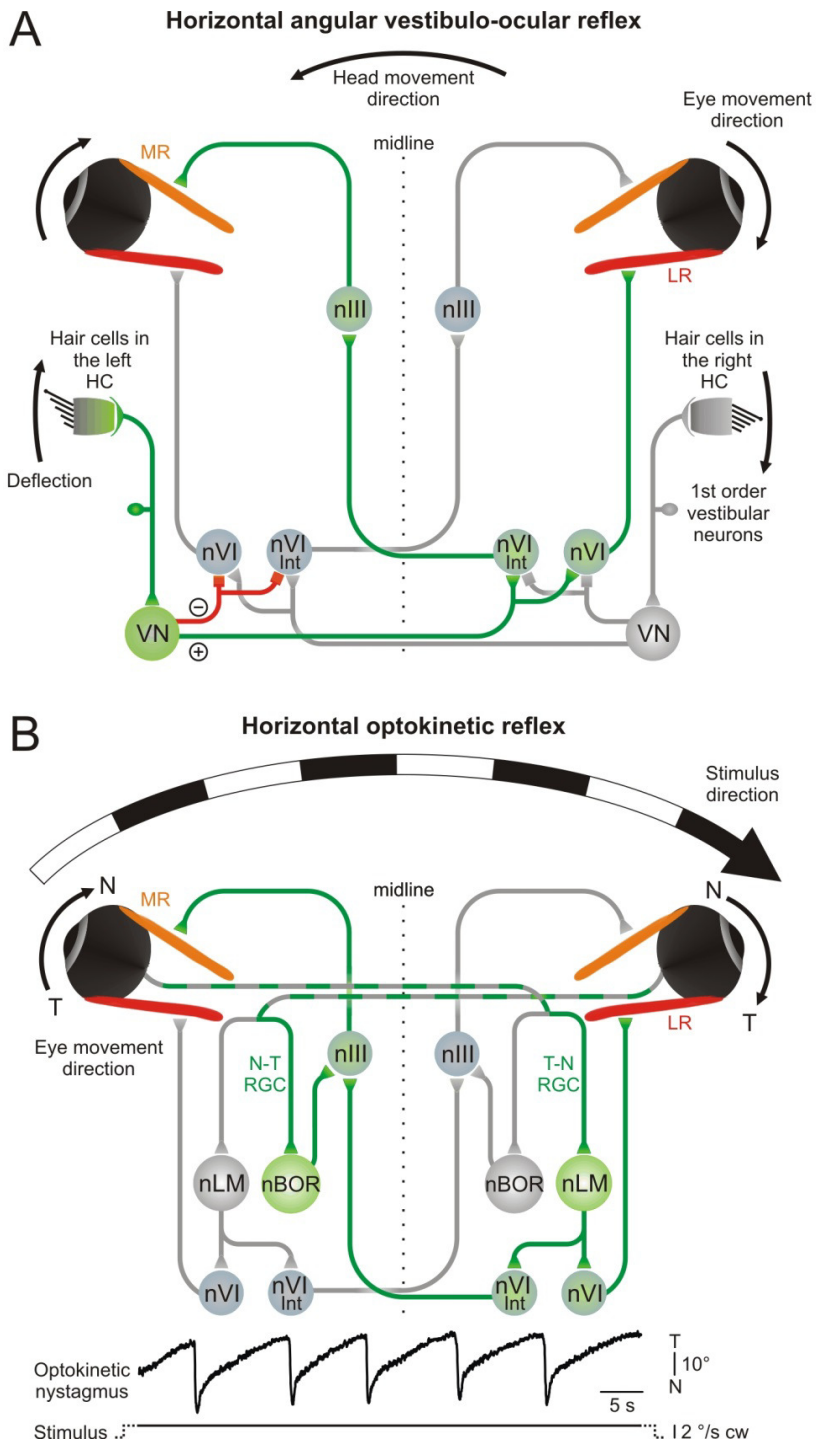

Figure 3: Gaze stabilizing reflex circuitries. (A) Horizontal angular vestibulo-ocular reflex pathway. (B) Horizontal optokinetic reflex pathway and right eye position of *Xenopus laevis* (stage 50) during constant velocity stimulation. AOS, accessory optic tract; cw, clockwise; HC, horizontal semicircular canal; Int, interneurons; LR, lateral rectus muscle; MR, medial rectus muscle; N, nasal; nIII, oculomotor nucleus; nVI, abducens nucleus; nBOR, nucleus of the basal optic roots; nLM, nucleus lentiformis mesencephali; N-T, naso-temporal; LR, lateral rectus; RGC, retinal ganglion cell; T, temporal; T-N, temporo-nasal; VN, vestibular nucleus.

1.2.2.1 The optokinetic reflex (OKR)

Large-field visual stimulation as sensory input to the described circuitry results in slow following movements of the eyes, the optokinetic response. Longer lasting unidirectional stimulation evokes the optokinetic reflex (OKR), a sequence of involuntary eye movements. Three subtypes of optokinetic reflexes exist dependent on stimulus orientation: the vertical/oblique OKR (vOKR) elicited by upward and downward directed vertical stimulation, the horizontal OKR (hOKR) in response to horizontal stimulation and the torsional OKR (tOKR) evoked by visual stimulation in the roll plane.

The optokinetic reflex behavior consists of a slow and a fast component. Slow eye movements (slow phases) by which the eye is following the visual stimulus, are interrupted by fast eye movements (fast phases) in opposite direction, resetting the eye in the orbit (Büttner and Büttner-Ennever, 2006). The eye position changes during optokinetic reflex behavior follow a typical saw-tooth-like pattern composed of slow and fast phases (Ilg, 1997). This response pattern can be evoked by constant unidirectional velocity stimulation and is also called optokinetic nystagmus. During horizontal visual stimulation in clockwise direction temporo-nasal (T-N) direction-selective retinal ganglion cells in the left eye's retina are exited, which project to the pretectal area on the contralateral side. Naso-temporal (N-T) direction-selective retinal ganglion cells of the right eye project onto neurons of the contralateral accessory optic system (AOS). The pretectal nucleus lentiformis mesencephali (nLM) and the nucleus of the basal optic roots (nBOR) in the AOS innervate extraocular motor nuclei on the ipsilateral side respectively, leading to a contraction of the left medial rectus muscle (MR) and the right lateral rectus muscle (LR). Eyes follow the stimulus pattern in a conjugated manner (Fig. 3B).

Slip velocity of retinal images is reduced during slow phases. The optokinetic gain as the ratio of eye movement velocity to image movement velocity is a measure of the quality of compensation during slow phases (Collewijn, 1969, 1980). An optokinetic gain of one indicates a perfect

compensation of the image movement by the evoked eye movements. A low gain implies a high residual retinal image slip. The fast phases are necessary to enable the eyes to continuously compensate image slip and stabilize the retinal image. Without fast phases the eyes would reach their anatomical most eccentric positions and could not further follow the visual stimulus, which is e.g. the case in frog (Dieringer et al., 1982).

To maintain visual acuity, the optokinetic system works hand in hand with the simultaneously active vestibular and proprioceptive systems. The optokinetic closed-loop system receives feedback about remaining retinal slip and elicits motor output to optimize gaze stabilization. Due to the fact that not only the eyes but also the head contributes to minimize image displacement on the retina, major differences exist in the extent and the interaction of compensatory eye and head movements. Thus, the performance and appearance of the OKR as well as the quality of retinal slip compensation are subject to large variability between different species.

1.2.2.2 Studies on compensatory eye movements and the optokinetic system

The mechanisms and structures underlying vision and eye movements have drawn researchers' interest for centuries (for review see Wade, 2010). Studies on the optokinetic reflex and retinal slip compensation exist for numerous species within the different vertebrate groups. A multitude of different techniques helped to identify the optokinetic circuitry and its function. Purely behavioral studies with visual stimulation using black and white striped bar or random dot patterns characterized the velocity profiles of various species. While mammals can compensate for relatively high pattern velocities, reptiles and amphibians are restricted to lower velocity ranges (Dieringer et al., 1982). Neuroanatomical studies illustrated the crucial structures and neuronal connectivity of the reflex system, as described above (Graf et al., 2002; Lazar et al., 1989). Pharmacological and electrophysiological approaches supplemented existing knowledge on a molecular and cellular basis by investigating

neurotransmitters and properties of the neurons involved in visuomotor processing (e.g. Bonaventure et al., 1985; Delgado-Garcia et al., 1986a, b).

In addition to the basic functionality of the optokinetic reflex circuitry, researchers also addressed the reasons and advantages of the different optokinetic response profiles for the different species and approached this problem in comparative studies concerning morphology, development and neuronal connectivity. Monocular horizontal visual stimulation experiments demonstrated an asymmetry of the optokinetic behavior manifested as larger response to a preferred stimulus direction (i.e. temporo-nasal) in some species (e.g. Klar and Hoffmann, 2002 (rainbow trout); Wallman and Velez, 1985 (chicken); Hess et al., 1985 (rat)), but not in others (Hoffmann et al., 2004 (ferret); Distler et al., 1999 (primates)). The presence or absence of a fovea (Masseck et al., 2008; Tauber and Atkin, 1968), eye position in head (i.e. frontal- versus lateral-eyed) along with the size of the binocular field (Gioanni et al., 1981), the correlation of both eyes and different lifestyles (Dieringer et al., 1992; Fritsches and Marshall, 2002) were discussed as potential factors influencing optokinetic performance (for review see Masseck and Hoffmann, 2009).

Like OKR symmetry and asymmetry, the participation of head and eye components in gaze stabilization is influenced by locomotor patterns and anatomical body constructions. While fishes and mammals predominantly use eye movements, most birds, reptiles and amphibians mainly counterbalance retinal image slip by compensatory head movements (for review see Land, 2015). To ascertain the functional boundaries of the optokinetic system only, experiments under head-fixed conditions were perfectly suited, as demonstrated e.g. in primate (Cohen et al., 1977) and rabbit (Collewijn, 1969). But the interest in the proper ratio of head and eye movement components for gaze stabilization and the question of how the multiple gaze stabilizing systems act together to maximize retinal slip compensation, shifted researchers' focus towards experimentation under head-unrestrained conditions. Dieringer and

colleagues for example performed a multitude of experiments under head-restrained and unrestrained conditions to identify the role of optokinetically elicited eye and head movements in adult frogs (Dieringer and Precht, 1982; Dieringer et al., 1982).

1.2.2.3 Gaze stabilization in frogs

The optokinetic system of adult frogs is predominantly sensitive to slow motion visual stimulation. Accurate eye tracking movements compensate for image displacements of velocities down to a few degrees per hour (Dieringer and Daunicht, 1986). However, the ocular motor range is small in amplitude. In the grass frog *Rana temporaria* the angle of ocular displacements typically averages ±4° around resting position. This narrow eye movement range limits the deflection amplitude of ocular slow following and fast resetting phases and restricts optokinetic performance for high stimulus velocities. Instead, higher retinal slip velocities are compensated by head movements with a range of up to 40° in frogs (Dieringer and Precht, 1982).

Studies on visually elicited compensatory movements in frogs were done already in the early 20th century. However, they mainly examined aspects of resulting head movements, not eye movements (Birukow, 1937, 1952; Butz-Kuenzer, 1957). The poor optokinetic performance in comparison to the clearly detectable head movements even led to the assumption of some investigators that frogs do not execute any eye movements at all – a misapprehension which was disproved later along with the investigation of gaze stabilizing reflexes (Grüsser and Grüsser-Cornehls, 1976; Walls, 1942).

Electrophysiological and neuroanatomical studies examined the optokinetic reflex pathway in frogs to be disynaptic. Direct connections via interconnecting neurons located in the retinorecipient pretectal area to abducens motoneurons close the three-neuronal retino-ocular reflex arc (Cochran et al., 1984). Complemented by various behavioral studies, the optokinetic system is well

explored in adult frogs these days, but still little is known about larval optokinetic performance and potential developmental changes during metamorphosis.

1.2.2.4 Larval Xenopus laevis as an ideal model organism to study the OKR

The amphibian genus *Xenopus* is a frequently-used animal model in developmental biology. Because of the availability of embryos in large numbers, their external development, low costs and the ability to withstand extensive surgical intervention and culture *in vitro*, *Xenopus* also serves as attractive first-line and high-throughput model in biomedical and pharmaceutical approaches (Brändli, 2004; Wheeler and Brändli, 2009). In the field of neuroscience, the aquatic frog already contributed to understanding general vertebrate principles concerning the development of central circuits for sensory signal processing, for instance of the visual, vestibular, olfactory and auditory systems (for review see Straka and Simmers, 2011).

As the optokinetic system is well preserved in all vertebrates, the African clawed frog *Xenopus laevis* provides ideal opportunities to investigate the basic functionality of this fundamental circuitry. The fact that cortical structures are sparsely developed compared to mammals (Northcutt and Kicliter, 1980) and the absence of a fovea in frogs (Gordon and Hood, 1976) are rather conducive than unfavorable for studying this reflex: Lesion studies in mammals showed that the visual cortex is not directly involved in optokinetic reflex behavior (Pasik et al., 1959 (primate)) and only modulates certain response parameters, e.g. the symmetry of the OKR (Distler and Hoffmann, 2003; Ventre, 1985; for review see Huang and Neuhauss, 2008). Moreover, goal-directed saccades and smooth pursuit eye movements of foveate animals influence and distort optokinetic reflex performance in a way that the optokinetic system cannot be accessed without activating the pursuit system simultaneously (for review see Ilg, 1997). This is consequently diminished in afoveate animals (Collewijn, 1969 (rabbit); Huang and Neuhauss, 2008 (zebrafish)).

In addition, the ontogenetic development of *Xenopus* involves a complete alteration of lifestyle. During metamorphosis the body plan is remodeled and the locomotor pattern transforms from larval tail-based undulatory swimming to limb-based forward propulsion in adult frogs (Combes et al., 2004; Nieuwkoop and Faber, 1994) (Fig. 4). The possibility to study all developmental stages from embryo to adult allowed tracing drastic changes in the organization and developmental plasticity of the spinal cord circuitry during metamorphosis of *Xenopus* (Beyeler et al., 2008). Along with the changes in locomotor patterns, larvae and adults also employ different eco-physiological niches. The adult frogs as sit-and-wait predators spend most of the time motionless, lurking for food. Their body movements are limited compared to the filter-feeding larvae, which undulate constantly in the water. Considering the special importance of the optokinetic reflex during locomotion, the fact that adult frogs show a limited optokinetic response performance (Dieringer, 1987) shifts attention towards the development and possible changes of the optokinetic reflex in larval *Xenopus.*

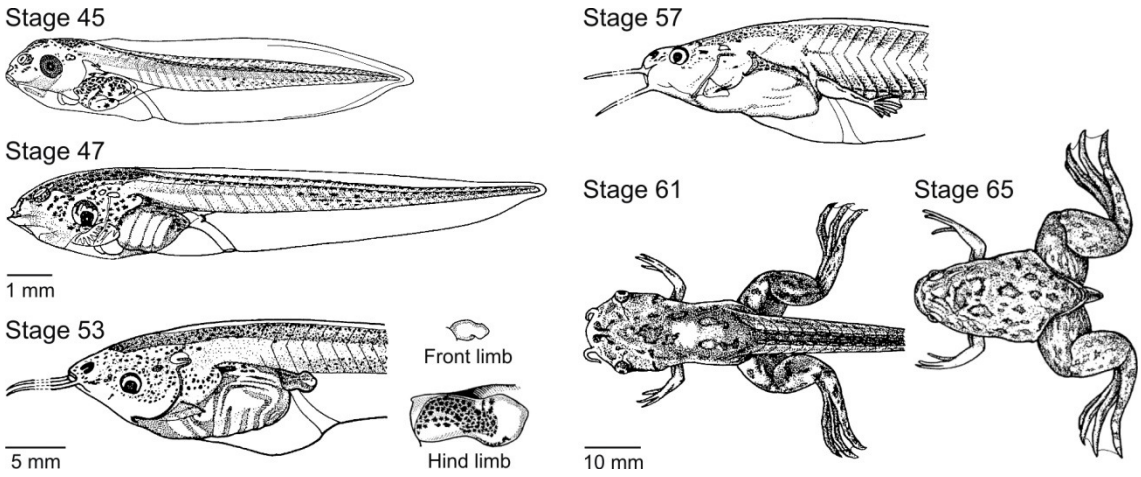

Figure 4: Developmental stages of *Xenopus laevis*. Staging of the tadpoles is conducted on the basis of morphological characteristics (e.g. tentacles, hind- and forelimb buds, form of the head/body). During metamorphosis animals differentiate from larval tadpoles to adult frogs by a complete body transformation (Modified from Nieuwkoop and Faber, 1994. Permission granted by Taylor and Francis Group, LLC).

A crucial step for the establishment of *Xenopus* as an animal model for developmental studies on sensory and sensory-motor systems was the achievement of stable *in vitro* preparations, i.e. either semi-intact or even further

reduced forms of the functional central nervous system (Straka and Simmers, 2011). A high robustness and long survival of the tissue make the preparation well suited for experiments using a multitude of neuroanatomical and physiological techniques (Luksch et al., 1996). While morpho-physiological investigations can only be performed *in vivo* in most vertebrates, these isolated preparations allow the application of a wide range of methodologies. Due to the easy accessibility of the transparent otic capsules in *Xenopus* larvae, especially investigations on cellular and network aspects of vestibulo-ocular reflex organization successfully employed the preparation (Straka and Simmers, 2011).

The transparency of the preparation of larval and juvenile individuals is also advantageous for monitoring the optokinetic response. Easy access to the extraocular nerves and the laterally positioned dark contrasting eyes facilitated the examination of visually induced motor output not only on a cellular but also on a systemic basis. Pairing electrophysiological recordings with noninvasive eye movement tracking (Beck et al., 2004a) allows direct comparison of extraocular motoneuronal output signals and actual behavioral response.

1.3 AIMS OF THE STUDY

The optokinetic system in adult frogs is well explored in contrast to the scarcity of comparable data in the tadpole. The possibility to monitor eye movements in semi-intact *in vitro* preparations of tadpoles with the full response spectrum opens up a wide range of experiments. Thus, this study is supposed to outline the fundamental functionality of the optokinetic system in *Xenopus* by pursuing the following objectives:

First of all, the existence of a stable horizontal optokinetic response in tadpoles has to be demonstrated and its basic parameters have to be characterized. These parameters will encompass eye movement amplitude and velocity as well as the gain of the optokinetic response. Systematic variation of the stimulus parameters will provide information on spatial frequency

characteristics and velocity sensitivity of the system controlling the optokinetic reflex.

It can be expected that optokinetic responses in larval *Xenopus* are not independent of their state of development, so that the developmental changes of optokinetic response properties will be tracked over the entire timeline from onset until metamorphic climax.

Optic tract tracing and injection of fluorescent dyes into extraocular motor nuclei will visualize the basic neuronal components of the reflex circuitry, thus providing the anatomical substrate of the optokinetic pathway in the tadpole.

Extraocular motor nerve recordings during large field visual motion stimulation will provide further insight into the control mechanisms and dynamics of the neuronal motor components of the optokinetic circuitry. The response profile of the motoneurons may allow classification of different types of neurons which can be compared to functionally distinct groups in other paradigms, e.g. the vestibulo-ocular reflex.

More generally, the study aims to contribute to the understanding of how the optokinetic system alters during the dramatic reorganization of body plan in metamorphosis from tadpole to frog, which is paralleled by a fundamental change in locomotor behavior from tail-based undulatory swimming to limb-based linear forward movements.

2 MATERIALS AND METHODS

2.1 ANIMALS

Tadpoles and froglets of *Xenopus laevis* were obtained from the breeding facility at the Biocenter Martinsried of the Ludwig-Maximilians-University Munich. Housed in fresh-water tanks at 16-17 °C on a 12/12 h light-dark cycle, tadpoles were fed daily with *Spirulina* (*Spirulina platensis*; Naturwaren Blum, Germany) and froglets with frog pellets (ssniff Spezialdiäten GmbH, Germany). Permission for the experiments was granted by the governmental institution at the Regierung von Oberbayern/ Government of Upper Bavaria (55.2-1-54-2532.3-59-12) and all procedures were in keeping with the *Principles of Animal Care* (publication no. 86-23; revised 1985 by the National Institutes of Health).

2.2 SEMI-INTACT *IN VITRO* PREPARATION

Experiments were performed on 91 animals at developmental stages between 45 and 66, determined by characteristic anatomical features (Nieuwkoop and Faber, 1994) (Fig. 4). Surgery was conducted under anesthesia with tricaine methanesulfonate (MS-222, 0.05 %, Pharmaq Ltd., UK) in ice cooled frog Ringer (in mM: 75 NaCl, 25 $NaHCO_3$, 11 glucose, 2 $CaCl_2$, 2 KCl and 0.5 $MgCl_2$ (0.1 for Magnesium reduced Ringer), pH 7.4) under a binocular microscope (SZX16, objective SDF plapo 0.8x, Olympus, Germany). Animals were decapitated and decerebrated (Fig. 5A). Decapitation included the removal of the lower jaw, cardiovascular system, gills, digestive tract and other viscera. Additionally, the tail was disconnected at the level of the upper spinal cord (Fig. 5A). To prevent movement of the remaining tail stump, spinal ventral roots were separated from the musculature. Depending on the specific experimental paradigm further surgical interventions were made.

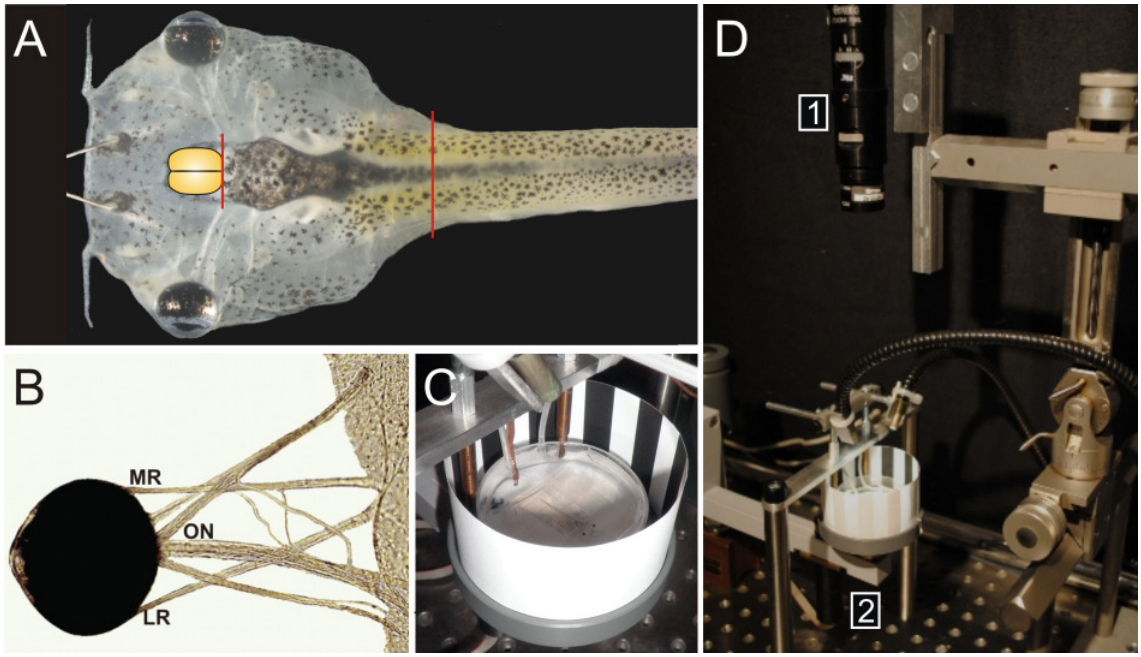

Figure 5: *In vitro* preparation and experimental setup. (A) *In vitro* preparation after decapitation (top view). Red lines indicate cutting areas for the removal of telencephalon and tail. (B) For electrophysiological recordings: Dissection of abducens and oculomotor nerve branches innervating the lateral (LR) and medial (MR) recti of the left eye with an intact optic nerve (ON) (Modified from Lambert et al., 2008. Permission granted by J Neurosci). (C) For horizontal visual stimulation the *in vitro* preparation was positioned in the center of the optokinetic drum. (D) Experimental setup for optokinetic stimulation with striped pattern driven by a DC motor from below (D – 2) and eye movement recordings from above (D – 1, camera).

- *Experiments with binocular visual stimulation*: For visualization of eye movements, eyes were kept with their sensory and motor innervation intact. The persisting functionality of the central nervous system (Straka and Simmers, 2011) with the intact visual and ocular motor circuitry enabled elicitation of eye movements by optokinetic stimulation.

- *Extraocular nerve recordings*: For multi- and single-unit recordings of the abducens or oculomotor nerves of the left eye, only the right eye was kept intact. The left eye was freed from skin and connective tissue covering the eye musculature, the nerve branch for electrophysiological recordings was segregated from its motor target, and all other ocular motor nerves were severed to immobilize the eye in its normal position (Fig. 5B).

- *Fictive swimming*: Fictive swimming is the neural correlate of actual swimming behavior. In some preparations, the tail remained connected to the head and the spinal cord, attached to the brain, was dissected. The spinal ventral roots were isolated from the tail musculature. Electrophysiological recordings of the ventral roots' activity (spinal segments 8-10) consisted of rhythmic bursting, being indicative of locomotor activity. Thus, the influence of efference copies of the motor command for the tail musculature on ocular motor network neuron activity could be monitored.

2.3 EXPERIMENTAL SETUP

2.3.1 Optokinetic stimulation and eye movement recordings

Horizontal eye movements were induced by a vertically striped paper drum (black/white pattern, stripe frequency 16.4°) (Fig. 5C) with a diameter of 6.8 cm. Driven by a servo-controlled DC motor (motor 2232-024SR, gear drive 22E, encoder IE2-512, motion controller MCDC3006S; reduction 546:1; Faulhaber, Germany) (Fig. 5D2), the pattern was rotated in the horizontal plane. The stimulus drum was raised from below around the specimen holder, fixing the Petri dish (5 cm diameter) with the pinned down *in vitro* preparation in the center of the drum. The whole chamber was illuminated from above by a cold-light source (60 % intensity, ZLED CLS6000, ZETT OPTICS GmbH, Germany) or for measuring spontaneous eye movements in the dark by an infra-red lamp (850 nm, ABUS Security-center, Germany). The dish with the preparation was continuously perfused with oxygenated Ringer's solution at 17.0 ± 0.2 °C at a rate of approximately 4 ml/min.

Optokinetic stimuli were provided step-wise or sinusoidally. In each category, stimuli were presented in randomized order of the variable parameters.

- *Constant velocity stimulation*: Constant velocity step stimuli had a duration of 140 s: 10 s with a stationary drum, 60 s with the pattern moving at

constant angular velocity in clockwise direction, 60 s moving in counterclockwise direction and 10 s with the drum stationary (Fig. 6D). Constant drum angular velocities ranged from ±0.2 to ±20 °/s.

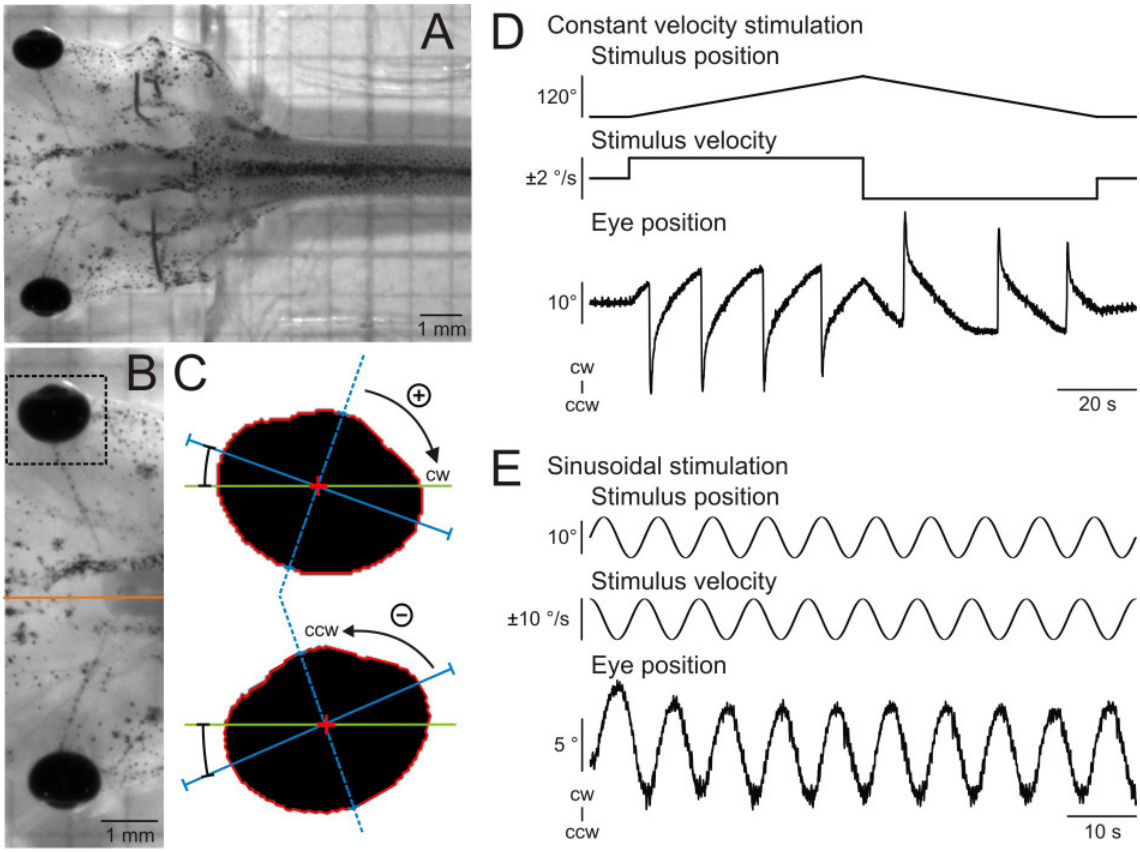

Figure 6: Eye movement analysis. (A) The preparation was monitored from above with the rostrocaudal axis of the animal aligned to the horizontal border of the image. (B) Recording of the region around the eyes during optokinetic stimulation. For eye movement analysis, a region of interest (ROI) for each eye was chosen (rectangle). (C) After conversion into a black and white image, an ellipse was drawn around the eye. The algorithm calculated the angle between the major axis (solid blue line) of the eye ellipse and the horizontal image border (green line). Angles were chosen in a way that eye movement in clockwise direction resulted in an increase of the eye position angle and vice versa. (D) Constant velocity stimulation in clockwise (cw) and counterclockwise (ccw) direction provoked an optokinetic reflex (stage 52, stimulation ±2 °/s). (E) During sinusoidal stimulation, the eyes followed the pattern in a sinusoidal manner (stage 52, stimulation 0.125 Hz, ±10 °/s).

- *Sinusoidal stimulation*: Each trial of sinusoidal stimulation consisted of 10 cycles (Fig. 6E). Two stimulation paradigms were used. For one subset of experiments, stimulus frequency was varied between 0.032 and 1.0 Hz and

stimulus peak velocity was kept constant at ±10 °/s. For this subset of stimuli, the amplitude and the phase shift of the eye movement response gave information about the frequency response of the optokinetic system. The second subset of sinusoidal stimulation consisted of nine stimuli with different peak velocities between ±0.5 and ±50 °/s at a stimulus frequency of 0.125 Hz. With these stimuli, the optokinetic system was tested for linearity of the eye movement response to the different stimulus velocities.

Eye movements were recorded from above with a video camera (GRAS-03K2M, Point Grey Research Inc., Canada), equipped with suitable zoom objectives and lenses (Mini TV Tube 1.5x, Optem Zoom 70XL, variable working distance auxiliary lens, Qioptiq Photonics GmbH & Co. KG, Germany) (Fig. 5D1). Videos were captured at a frame rate of 49.86 Hz with the imaging software FlyCap2 (version 2.4.3.10, Point Grey Research Inc., Canada), and video onset was triggered externally via the data acquisition and analysis software Spike2 (version 7.04, Cambridge Electronic Design Ltd., UK).

2.3.2 Electrophysiological recordings

Concurrent to optokinetically elicited eye movements in the intact right eye as described in 2.3.1, extraocular motor nerve activity was recorded with glass suction electrodes from the left eye. Recordings consisted of multi- and single-unit spike discharges of abducens or oculomotor nerve fibers, projecting to the left lateral and medial recti eye muscles (Fig. 5B). Glass electrodes (GB150-8P, Science Products GmbH, Germany) were pulled with a horizontal electrode puller (P-87, Sutter Instruments Co., USA) and the tip diameter was individually adjusted to the size of the nerve branch. The spike discharge of either the abducens or the oculomotor nerve branch was recorded, amplified (EXT 10-2F, npi electronic GmbH, Germany), digitized at 18.5 kHz (CED 1401, Cambridge Electronic Design Ltd., UK) and stored for later analysis. In some preparations spinal ventral root signals during spontaneous fictive swimming were recorded in addition to extraocular motor discharge and eye movements.

The recording procedure was the same as for the extraocular nerves. All electrophysiological experiments were conducted in Magnesium reduced Ringer.

2.3.3 Modifications for experiments with monocular visual stimulation

During experiments with monocular visual stimulation only, eye movements of both eyes were recorded. A reduced subset of optokinetic constant velocity and sinusoidal stimuli was provided. The experimental design consisted of three conditions:

1. *Binocular:* For control conditions, *in vitro* preparations were tested with both eyes intact (Fig. 7A).
2. *Monocular:* A blank white circular background was positioned on the left side of the Petri dish, covering the whole left hemisphere (180°) of the drum (Fig. 7B). With this arrangement, optokinetic stimulation was provided only to the right eye.
3. *Monocular, disconnected:* For this condition, the left optic nerve was cut (Fig. 7C). The right eye was optokinetically stimulated.

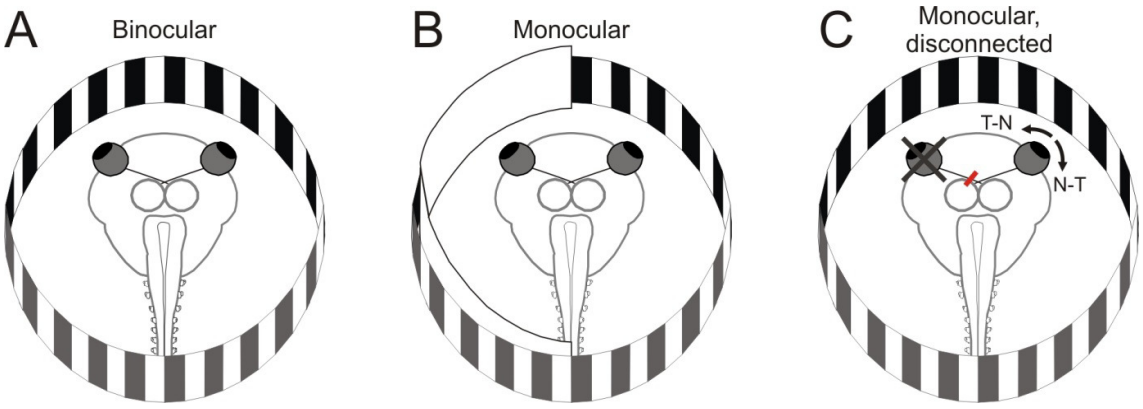

Figure 7: Monocular visual stimulation. (A) Optokinetic performance under binocular stimulus conditions. (B) Monocular stimulation of the right eye by covering the left side of the drum with a white circular background. (C) Monocular stimulation after cutting the left optic nerve (red mark indicates cutting area). For all conditions horizontal movements of both eyes were recorded. Stimulation of the intact eye was provided in naso-temporal (N-T) and temporo-nasal direction (T-N).

In the monocular condition with a severed left optic nerve any retinal input of the left eye was removed, whereas during the monocular condition with a stationary white background a constant visual input was present. Thus, the comparison of eye movement behaviors during sinusoidal stimulation between both monocular conditions allowed testing functional interactions between bilateral central relay nuclei involved in optokinetic reflex behavior. Constant velocity stimulation in clockwise and counterclockwise directions allowed comparing the eye movement behavior of the intact right eye for the binocular versus both monocular conditions and gave insight into the directional symmetry of the optokinetic reflex.

2.4 DATA ANALYSIS

2.4.1 Eye movement analysis

The video processing was done in MATLAB (R2015a, The MathWorks Inc., USA), based on a program written in LabView by Beck et al. (2004a). In order to extract eye position from the video recordings, use was made of the contrast between the transparent body of the preparation and the dark eyes. After conversion of the recorded video into black and white, a region of interest (ROI) around the eye was selected and automatically applied to each frame (Fig. 6B). The software fitted an ellipse around the eye ball. The eye position was determined as the angle of the major axis of the ellipse relative to the horizontal border of the video image (Fig. 6C). As a standard during experiments, care was taken to align the longitudinal axis of the *in vitro* preparation to the horizontal border of the recorded image (Fig. 6A). The angles determined from consecutive frames of the video sequences represented the time course of eye positions. Calculation of eye position angles was chosen such that eye movements in clockwise direction corresponded to an increase of eye position angle values and vice versa.

2.4.2 Eye movement parameters

During constant velocity stimulation, the eyes performed an optokinetic reflex (Fig. 6D). Eye movements consisted of slow following movements (slow phase, SP) in stimulus direction interrupted by oppositely directed fast resetting movements (fast phases, FP) (Fig. 8A). During sinusoidal stimulation eyes followed the pattern with respective cyclic oscillations (Fig. 6E). Response parameters, which will be explained in the following paragraphs, were computed based on the eye position over time. Values were calculated for each eye of each animal separately.

The conjugation of left and right eye movements was determined via linear regression and linear correlation analyses between right and left eye positions. The ocular motor range was calculated as the range within which the eye was moving during 97 % of the stimulus time (Fig. 8D). This yielded a reliable value for the natural working range of the eye during following movements in the horizontal plane.

2.4.2.1 Parameters extracted from constant velocity stimulation data

Gain was defined as the ratio between change in eye position over time and stimulus velocity and served as a measure for the quality of optokinetic behavior. Because eye position angles increased non-linearly during slow phases and optokinetic reflex performance changed considerably during ontogeny, slow phase performance during constant velocity stimulation was evaluated as following: Position traces analyzed in MATLAB were imported into the Spike2 program. Eye position range was restricted by two horizontal cursors. Cursor 1 was positioned at the maximal deflection reached by the first slow phase following clockwise stimulation; cursor 2 was positioned at the minimal deflection reached by the first slow phase following counterclockwise stimulation (Fig. 8B). Only the intermediate parts between the two cursors were considered for slope and gain calculations. For the final average gains, gain values were averaged over all slow phases for each stimulus velocity.

Furthermore, eye movements in naso-temporal (N-T) and temporo-nasal (T-N) direction were processed separately to detect potential stimulus direction-specific differences.

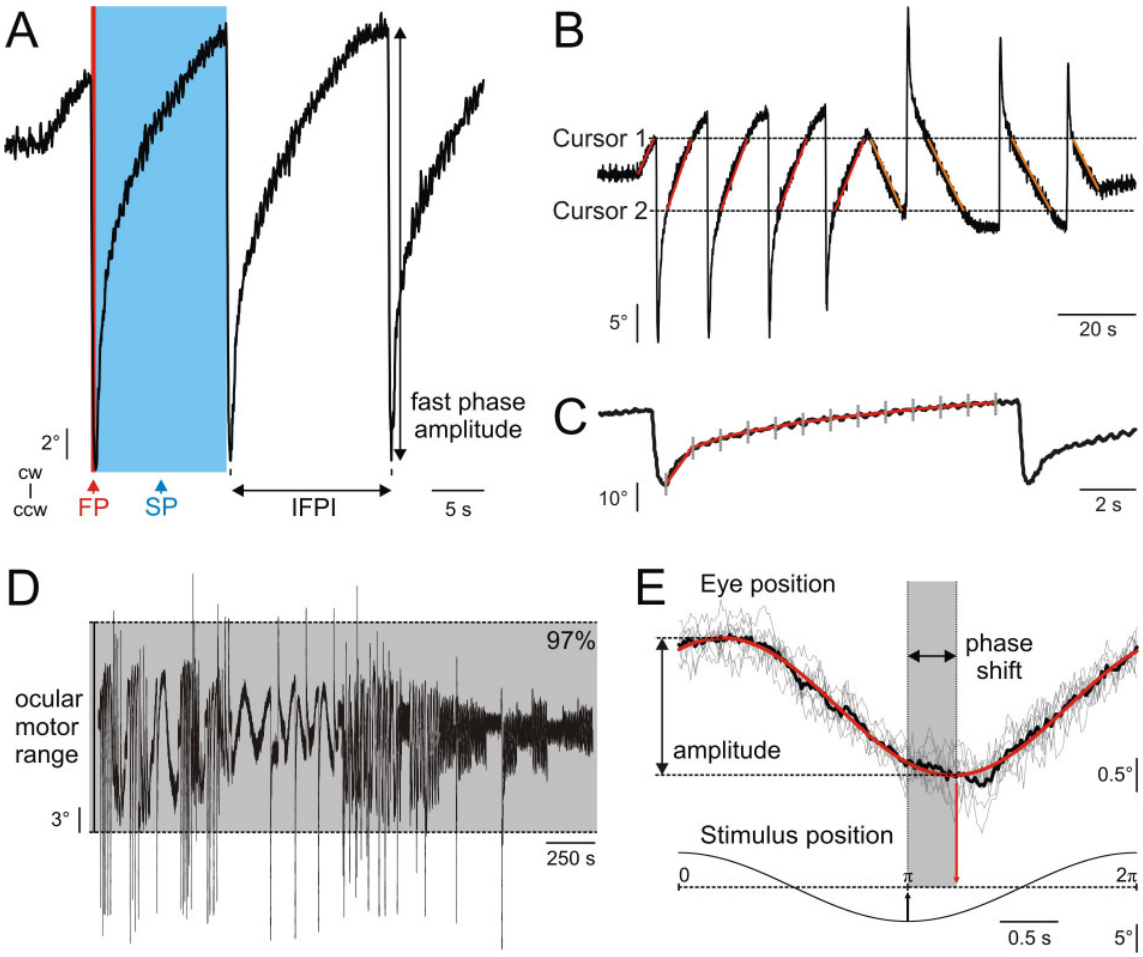

Figure 8: Parameters calculated from eye position traces. (A) The optokinetic reflex consisted of slow following movements (SPs, blue) and fast resetting phases (FPs, orange). Number of fast phases, fast phase amplitude and inter-fast-phase-interval (IFPI) were identified. Slow phase gain was calculated by two different methods shown in B and C. (B) Gain calculated from the intermediate range of the slow phases. The range was limited by two cursors set to the maximum and minimum deflection reached during the first slow phase in clockwise (cw) and counterclockwise (ccw) directions. (C) Gain calculated by dividing the slow phase in 1 s bins – one gain value per bin. Orange lines indicate the calculated slopes. (D) Ocular motor range calculations minimized distortion by the eye's overshoot during fast phases (selected example, stage 52). (E) For sinusoidal eye movements, eye movement amplitude for gain calculations and the phase shift were determined by fitting a sine (red curve) to the averaged position cycles (stage 52, 0.25 Hz, ±10 °/s, gray = single cycles, black = average).

To correlate gain and eye position, each slow phase was binned in 1 s windows and the gain was calculated for each window (Fig. 8C). The eyes' mean position during each bin was directly correlated to the gain of the respective window, giving information about the change of optokinetic performance dependent on eye position.

To quantify the fast resetting movements, the number of fast phases, fast phase amplitude and inter-fast-phase-intervals (IFPIs) were calculated for both movement directions (Fig. 8A). To exclude fast eye movements resulting from retractions of the eyes into the head, the minimal distance between two fast phases was set to 4 s and only quick eye movements with an absolute peak velocity greater than 32.5 °/s were characterized as fast phases.

2.4.2.2 Parameters extracted from sinusoidal stimulation data

The sinusoidal eye position traces consisting of 10 cycles were evaluated on the basis of single cycles (Fig. 8E). As the response to sinusoidal stimulation reached steady state only after the first half-cycle, the leading and trailing half-cycles were omitted, and therefore only 9 cycles were evaluated. Cycles were averaged and a sine wave was fitted to the averaged position trace. The amplitude of the sinusoidal fit was used for calculating the gain and also yielded information of the phase shift indicating whether the eye was leading (phase value > 0) or following the stimulus sine wave with a certain delay (phase value < 0).

2.4.3 **Spike train analysis**

Single units were extracted from the recording traces using the spike sorting tool implemented in Spike2. In MATLAB peri-stimulus time histograms (PSTHs) with 40 bins were generated for each single unit recorded during sinusoidal optokinetic stimulation. A circular normal distribution fit on the PSTHs revealed the stimulus-dependent peak discharge rates and firing patterns as well as the half-widths of the modulation depth. Linear regression analysis between the

firing activity of the left extraocular motor nerves and the position as well as velocity of the right eye classified the coding specificity of the single units. The phase relation was calculated between the maximum of modulation depth of each unit and the maximum eye deflection in the relevant direction.

2.4.4 Data representation and statistics

Eye position and velocity data were averaged over the right and the left eye for each individual. Afterwards, mean values were calculated by averaging over animals. Pooled data were expressed as mean values ± standard deviations (SD), if not indicated differently as median or standard error of the mean (SEM).

Statistical analyses were calculated using MATLAB. The critical level of statistical significance was set to $p = 0.05$. To test of normality, the Shapiro-Wilk test was used due to its power for data of small sample sizes. The adequate statistical tests (t-test, analysis of variance (ANOVA), Wilcoxon signed-rank test) were performed dependent on the probability distributions of the data and the experimental design. Linear regression and linear correlation analyses evaluated the relation between the right and the left eyes as well as between eye position and motor nerve discharge. Kendall rank correlation was used as a non-parametric measure of correlation.

2.5 TRACER EXPERIMENTS AND ANATOMY

To anatomically outline the optokinetic reflex circuitry in *Xenopus* tadpoles, tracer substances were injected into different target structures in isolated *in vitro* preparations. After exposing the target structures (eyes and brainstem) by removing the skin and the surrounding tissue, the surface of the preparation was carefully dried to prevent dilution of the dye. For tracing the optic tract, the lens of the eye was removed. Crystals of dextran Alexa Fluor 488 (Life Technologies GmbH, Germany) moisturized with dimethyl sulfoxide (DMSO, 99.9 %, Sigma-Aldrich, Germany) were inserted into one eyeball with fine insect

pins (diameter 0.1 mm) and the opening was closed by fixing the overlying tissue with small amounts of superglue.

To illustrate the connection between optic tract and abducens motor nuclei, Alexa Dextran 546 (Life Technologies GmbH, Germany) was additionally injected from ventral into the contralateral side of rhombomere 5 at the level of the abducens nucleus (Straka et al., 1998).

After an application time of 5 minutes in the dark, preparations were rinsed with oxygenated Ringer solution and stored in the fridge at 13.5 °C. The preparations were incubated for 48-72 h before the brains were removed and fixed in 4 % paraformaldehyde (PFA) in 0.1 M phosphate buffer (PB) overnight. For whole mount preparations, the tectum was longitudinally split along the rostrocaudal midline and the brain was flattened and pinned to a Sylgard floor before fixation. After washing 3x for 10 min with 0.1 M PB, whole mount brains were mounted on slides and cover slipped with Vectashield mounting medium (Vector Laboratories Inc., USA). For cryostat sectioning (CM3050 S, Leica Biosystems, Germany), fixed brains were stored overnight in 30 % sucrose in 0.1 M PB to prevent freezing artifacts. Thereafter brains were frozen, embedded in TissueTek (Sakura Finetek GmbH, Germany) and transversally cut into sections of 30 µm. The mounted sections were cover slipped with Vectashield medium.

The probes were imaged with a confocal laser scanning microscope (Leica SP5 II, Leica Microsystems GmbH, Germany) at wavelengths of 488 nm and 561 nm. This allowed visualization of the optic tract and its projection areas as well as the neurons connecting the optic tract and the abducens motor nuclei (see 3.3).

3 RESULTS

Testing different developmental stages of *Xenopus laevis* – before, during and after metamorphosis – showed an enormous variation of optokinetic response properties. To solve the question if a horizontal optokinetic reflex is present in larvae and to what extent it changes throughout development, data were separated into two parts. The first section describes the characteristics of the horizontal optokinetic reflex (hOKR) in larval stages from 50 to 55. Within this developmental period the reflex behavior was robust. Ontogenetic changes in optokinetic performance are depicted in the second section. A clear decline of eye movements was detected with proceeding development. While in the third section the anatomical circuitry of the optokinetic reflex pathway is outlined, the description of the neuronal activity of the extraocular motor nerves during optokinetic reflex performance and sinusoidal following movements forms the last part. Different units with different firing characteristics turned out to be in charge of controlling the diverse components of eye movements.

3.1 HORIZONTAL EYE MOVEMENT BEHAVIOR

In the following paragraph eye movement behaviors of *Xenopus laevis in vitro* preparations of ontogenetic stages 50-55 are described.

3.1.1 Eye resting position and spontaneous eye movements

During rest, eyes were oriented laterally in the head with a very small deflection in nasal direction. The mean angle between both eyes in the horizontal plane measured 175.0 ± 9.7°, i.e. an angle of 87.5 ± 4.9° between each eye and the nasal tip of the rostrocaudal midline of the animal (n = 15) (Fig. 9A).

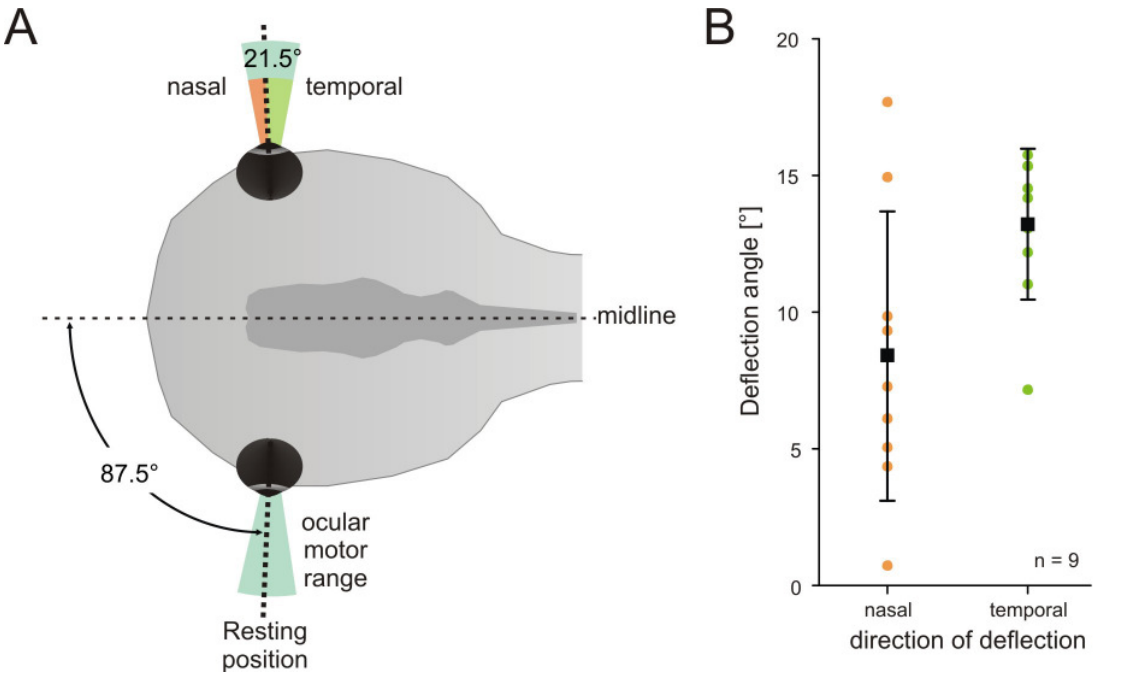

Figure 9: Eye resting position and ocular motor range. (A) During rest, eyes were directed laterally with a minimal nasal tendency (2.4°). In response to visual stimulation, the eyes moved within an ocular motor range of 21.5° (dark green area) around the resting position. (B) The angle of deflection from eye resting position in the temporal direction was larger than in nasal direction. Black squares show mean angles ± standard deviations of nine tested individuals (colored dots).

During recordings under dark and light conditions (n = 6) without visual stimulation some preparations showed sporadic retraction movements of the eye bulb into the head due to retractor bulbi muscle activity. However, spontaneous large amplitude eye movements in the temporo-nasal horizontal plane were virtually absent under both illumination conditions (Fig. 10A).

In the dark, eyes remained still with slight jitter movements within a range of 0.46 ± 0.10° around resting position with a mean velocity of 5.71 ± 0.96 °/s. Under light condition, when the striped pattern was visible but stationary, a significant decrease in spontaneous movement range (Wilcoxon signed-rank test, $p = 0.0313$) and velocity (paired t-test, $p < 0.001$) compared to eye movement behavior in the dark condition occurred (Fig. 10B). Eyes stayed within a movement range of 0.37 ± 0.13° with a mean velocity of 3.94 ± 0.53 °/s.

Spectral analysis with a high-pass filter of 0.1 Hz depicted the frequency content of the eye positions during both conditions (Fig. 10C). The white noise level in the dark was generally elevated due to the minor contrast of the video recordings. Frequencies around 2 Hz were strongly represented during the light condition, but not in the dark. Thus, this oscillation was most likely induced by visual feedback generated by the stationary pattern.

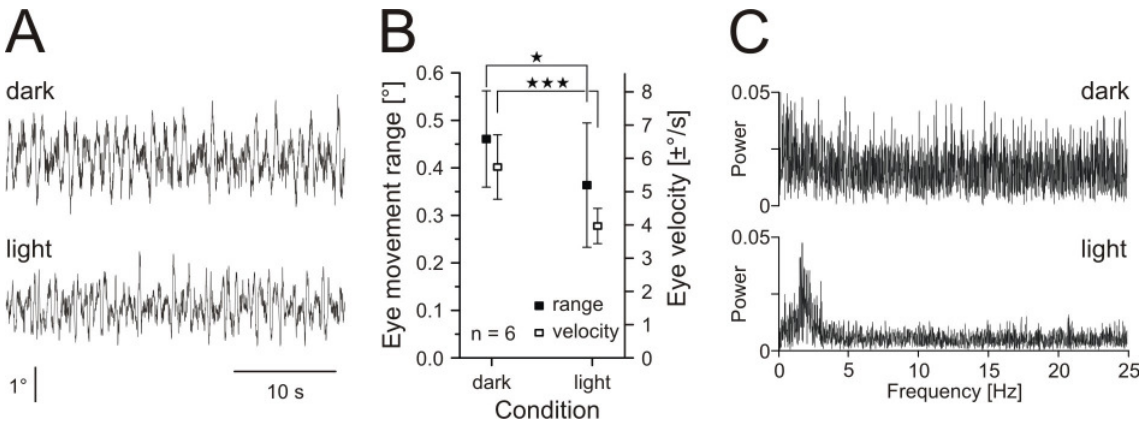

Figure 10: Spontaneous eye movements. (A) Example traces of eye position recordings over 60 seconds during dark and light conditions showed no spontaneous large amplitude eye movements in the horizontal plane (stage 50, right eye). (B) Range (black squares) and velocity (open squares) of spontaneous eye movements were reduced in the presence of a stationary striped pattern. Data indicate mean values ± standard deviations of seven animals. Significance level of $p < 0.05$ (*) and $p < 0.001$ (***). (C) Spectral analysis of the eye position during dark and light conditions (high-pass filtered with 0.1 Hz, n = 6). Frequencies around 2 Hz were represented to a greater extent during the light condition.

3.1.2 Ocular motor range

The ocular motor range was defined as the natural working and operating range of the eye during optokinetically driven slow following movements in the horizontal plane. Calculated as the angular range within which the eyes moved 97 % of the complete experimental measurement time, the ocular motor range had an average value of 21.54 ± 5.58° (n = 9) (Fig. 9A). Referred to the resting position, eye deflection in nasal direction was by trend with 8.37 ± 5.30° smaller than the deflection of 13.17 ± 2.75° in temporal direction (paired t-test, p = 0.053) (Fig. 9B).

3.1.3 Conjugation of left and right eye movements

Movements of the left and right eye were highly conjugated. Horizontal optokinetic stimulation in one direction resulted in following movements of both eyes in the same direction. Linear regression analysis of right versus left eye positions (n = 9) revealed an average slope of 0.97 ± 0.16 with a mean offset of 1.39 ± 6.81° during constant velocity stimulation with ±10 °/s (Fig. 11A). For sinusoidal stimulation of 0.125 Hz with ±10 °/s peak velocity, the slope was 1.08 ± 0.23 with a 4.12 ± 7.06° offset (Fig. 11B). The offset was neglected as it was likely due to mismatches in the horizontal alignment of the animal in the recorded images and had therefore no systematic significance. Plotting eye positions of both eyes, a flattening of the scatter was observed towards the eccentric eye positions, reflecting the asymmetry in the deflection range towards the nasal and temporal borders of the ocular motor range (see 3.1.2).

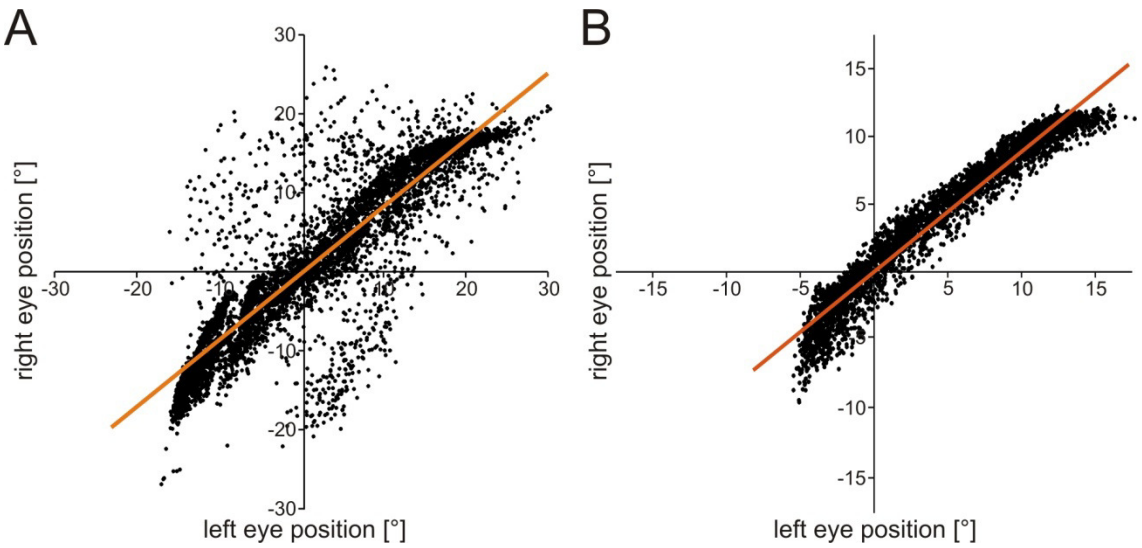

Figure 11: Conjugated eye movements. Relation of the right and left eye positions for (A) constant velocity stimulation with ±10 °/s and (B) sinusoidal stimulation with 0.125 Hz and a peak velocity of ±10 °/s (stage 50, both graphs were corrected for the offset).

The strong conjugation of the left and right eyes over a large portion of the ocular motor range formed the basis of the experiments on the symmetry of the optokinetic system (see 3.1.6) and allowed comparison of the optokinetic

response behavior of one eye to the neuronal signal of the respective extraocular motor nerves of the contralateral eye (see 3.4).

3.1.4 The horizontal optokinetic reflex

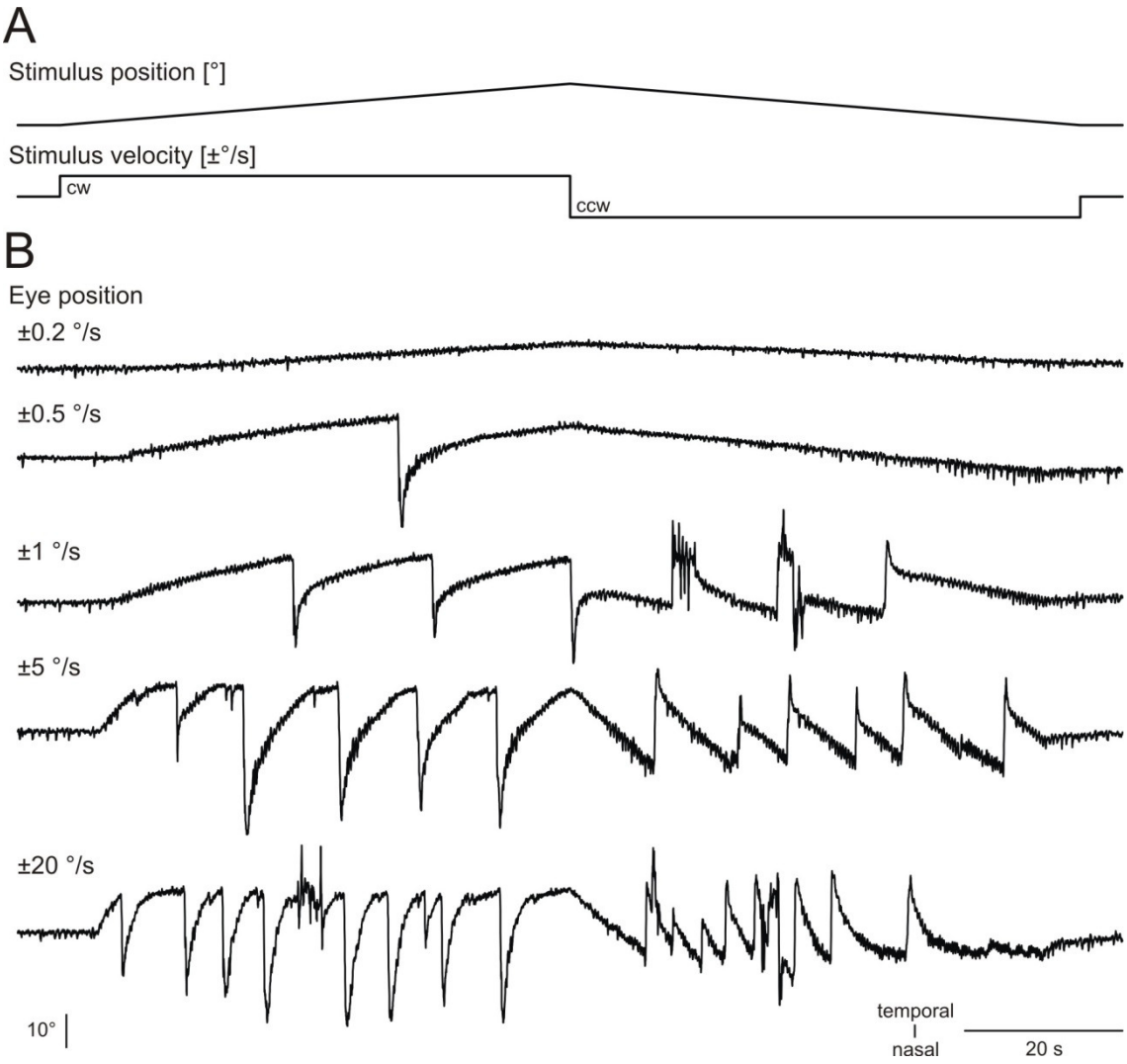

Figure 12: Typical example of the horizontal optokinetic reflex. (A) Constant velocity visual stimulation in clockwise (cw, first half of stimulus) and counterclockwise (ccw, second half of stimulus) direction elicited an optokinetic reflex behavior. (B) Right eye position traces for different stimulus velocities of a representative individual (stage 50). During constant velocity stimulation in clockwise direction the right eye slowly followed the stimulus in temporal direction. Stimulation in counterclockwise direction provoked slow following movements in nasal direction with oppositely directed fast phases.

Out of eleven *in vitro Xenopus* preparations of stages between 50 and 55, nine individuals showed a clearly distinguishable horizontal optokinetic reflex (hOKR). Constant velocity stimulation with a striped drum resulted in a typical reflex behavior (see Fig. 6D): a slow following movement (slow phase, SP) in stimulus direction which was interrupted by a rapid eye movement (fast phase, FP), resetting the eye in the orbit to the opposite direction by overshooting the ocular motor range (further described below in 3.1.4.2.4). The velocity of eye following movements and the number of resetting fast phases (Fig. 12B) were highly dependent on the velocity of the stimulus pattern (Fig. 12A). In the two remaining preparations, visual motion stimulation induced slow phase eye movements, but no resetting fast phases were elicited and the eyes remained at their most eccentric deflection angles until the stimulus changed direction. However, variability in eye movement performance was also detected between the tested OKR-performing individuals.

3.1.4.1 Slow phases

3.1.4.1.1 Slow phase performance

To measure the quality of the eye movements which reduce the image slip on the retina, the gain was calculated as the ratio between eye following movement and stimulus movement (n = 9). At low stimulus velocities the gain was high with a maximum at a stimulus velocity of ±0.4 °/s (0.69 ± 0.18 (N-T)/ 0.64 ± 0.15 (T-N)). A strong decrease of gains was measured with increasing stimulus velocities (0.21 ± 0.11 (N-T)/ 0.18 ± 0.09 (T-N) at ±20 °/s) (Fig. 13).

The direction of stimulation had a minor influence on eye movement gain with slightly lower values in T-N compared to N-T direction. The dependency on the stimulus velocity follows a parallel course for both T-N and N-T directions. Thus, the optokinetic system of *Xenopus* tadpoles is more effective in coping with slow visual displacements than with high velocity changes of the visual surround (Fig. 13).

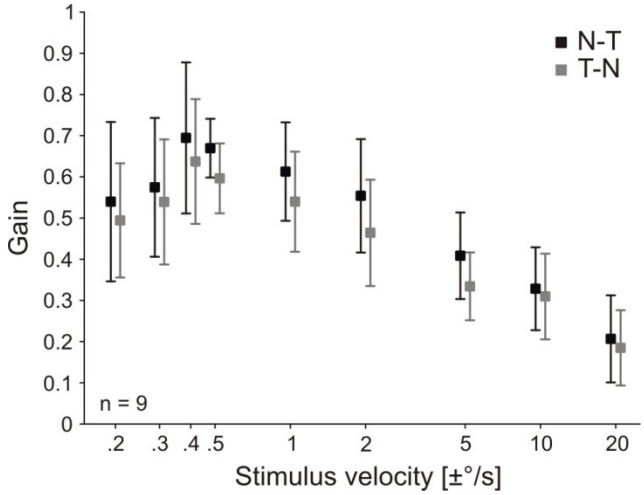

Figure 13: Slow phase gain. Parallel course of stimulus velocity dependence for both eye movement directions, i.e. temporo-nasally (T-N, gray squares) and naso-temporally (N-T, black squares) directed movements. Decline of slow phase performance with increasing stimulus velocities. Values are means ± standard deviations of 9 animals.

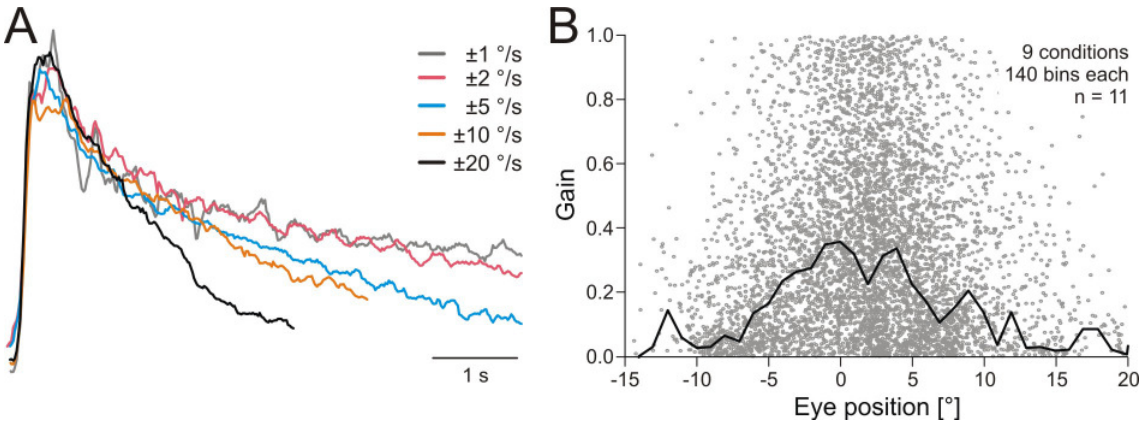

Figure 14: Slow phase shape and gain distribution. (A) Average slow phases of larval *Xenopus* evoked by different stimulus velocities (stage 50, right eye position, normalized to the preceding fast phase amplitudes). (B) Interrelation between gains and eye positions. Data points represent gains of position traces sectioned in 1 s bins (140 bins for 9 constant stimulus velocities, respectively; n = 11). An eye position of zero equals the eye resting position; minimal and maximal position values describe extreme deflections of the eye in counterclockwise (negative) and clockwise (positive) directions. The median of the gain (black line) was calculated for each full degree of eye position. Note the in average higher gains for eye movements around resting position and the lowering of gains with increasing eccentricity of the eyes.

3.1.4.1.2 Slow phase shape

The time course of the slow phase was non-linear. At the beginning of the slow phase, i.e. after a fast resetting phase, the eye was quickly pulled towards its resting position resulting in a rapid change of eye position. With increasing eccentricity of the eye in the stimulus direction, eye velocity decreased and consequently the slope of the eye position trace. The eye movement almost stagnated (i.e. eye velocities = 0) before the next fast phase was triggered (Fig. 14A).

To quantify the influence of eye position on optokinetic performance, the gain was analyzed during slow phases in 1 s time bins within 11 experiments. Gain values reflected the shape of the slow phases described above. When eyes passed resting position, gains were high. With increasing eccentricity of the eye the velocity values and gains decreased again (Fig. 14B).

3.1.4.2 Fast phases

3.1.4.2.1 Fast phase characteristics

Horizontal fast phases in naso-temporal direction (N-T) turned the eye on average by 22.24 ± 3.43° in opposite direction to the stimulus direction within 0.35 ± 0.05 s (n = 8). Temporo-nasal (T-N) directed FPs had a mean amplitude of 25.67 ± 3.42° and a duration of 0.38 ± 0.06 s (Fig. 15A), and were thus larger and longer than fast phases in N-T direction (paired t-test, p = 0.004 (amplitude)/ p = 0.012 (duration)) (Fig. 15C). However, eyes reached comparable peak velocities of 201.26 ± 35.64 °/s in N-T and 210.26 ± 33.67 °/s in T-N direction during resetting phases (paired t-test, p = 0.296) (Fig. 15B).

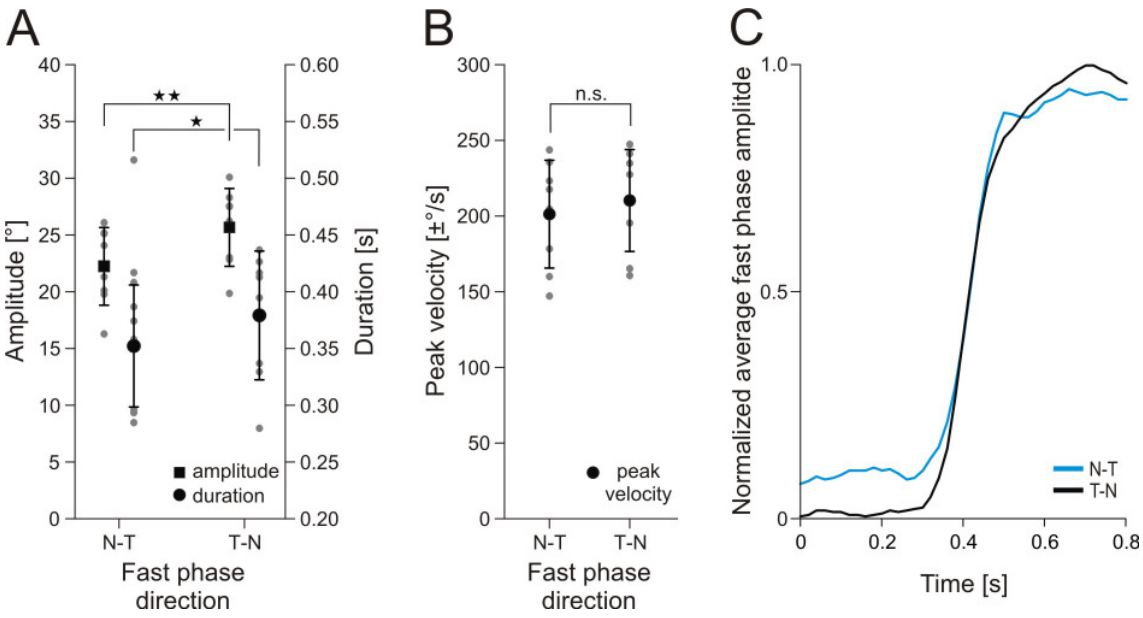

Figure 15: Fast phase appearance and shape. (A) Amplitude (black squares) and duration (black dots) were smaller for FPs in naso-temporal (N-T) direction. Significance level of $p < 0.05$ (*) and $p < 0.01$ (**). (B) Similar peak velocities of N-T and temporo-nasally (T-N) directed FPs, non-significant (n.s.). Black symbols and whiskers for means ± standard deviations, gray dots are individual data (n = 8). (C) Right eye position showing the average fast phases in N-T (blue) and T-N (black) directions calculated from all FPs during constant velocity stimulation of one experiment. The average fast phase amplitude in T-N direction is normalized to 1. The N-T directed FP is proportionally represented.

3.1.4.2.2 Fast phase occurrence

Fast phase occurrence was tightly coupled in the left and right eye as shown in Fig. 16A. The fast phases (FPs) of the right eye of eight animals were pooled for each stimulus condition (120 s stimulation per trial) in order to evaluate stimulus velocity dependency. Stimulus velocity had a strong influence on fast phase occurrence (One-way ANOVA, $F(8, 63) = 18.32$, $p < 0.001$). The number of FPs within the 120 s stimulus sequences increased monotonously for stimulus conditions with higher stimulus velocities (Kendall rank correlation, $\tau = 0.94$, $p < 0.001$). At a low stimulus velocity of ±0.2 °/s only 5 FPs were elicited, whereas the number of FPs at ±2 °/s increased to 65 FPs and reached the maximum of 91 FPs at ±10 and ±20 °/s respectively (Fig. 16D).

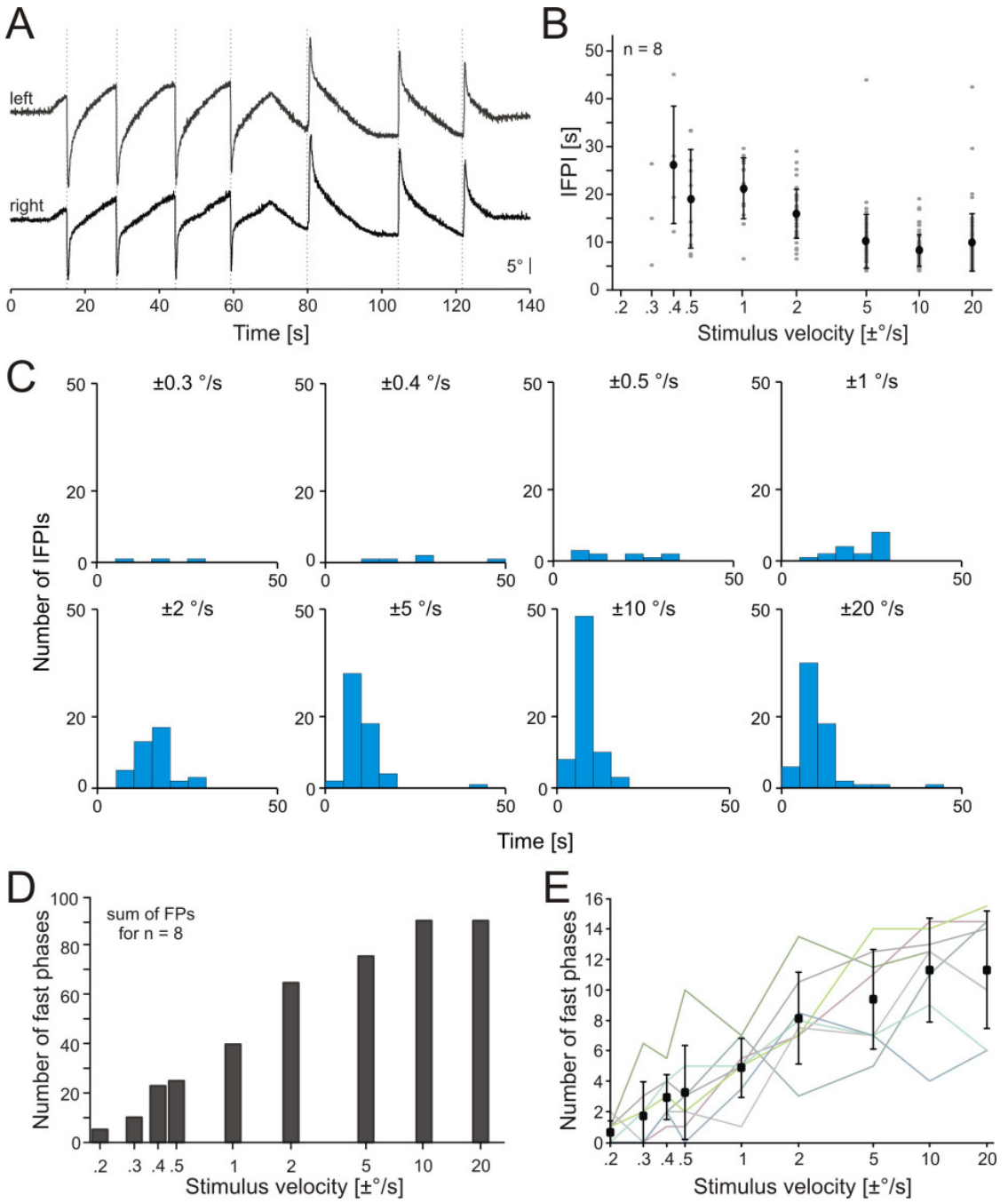

Figure 16: Fast phase occurrence and distribution. (A) Example for synchronous fast phases of the left and right eye at constant velocity stimulation of ±2 °/s (stage 52). (B) The length of the inter-fast-phase-intervals (IFPIs) shortened with higher stimulus velocities. No reliable IFPI lengths for stimulus velocities of ±0.2 and ±0.3 °/s due to no or little FPs at these stimulus velocities. Data indicate mean values ± standard deviations, gray dots represent single IFPIs. (C) At higher stimulus velocities fast phases became more regularly distributed as the number of fast phases increased with increasing stimulus velocities, shown in D and E. (D) Sum of FPs per stimulus for 8 animals. (E) Mean FP number per stimuli ± standard deviations. Colored lines are data of individuals. All data for B-E for n = 8.

Animals exhibited on average 0.63 ± 0.74 FPs at ±0.2 °/s, 8.13 ± 3.02 FPs at ±2 °/s and 11.31 ± 3.87 FPs at ±20 °/s for a sequence of 120 s of constant velocity stimulation (Fig. 16E).

As a consequence, the inter-fast-phase-intervals (IFPIs) shortened with higher stimulus velocities. No reliable length of IFPIs could be calculated for stimulus velocities below ±0.4 °/s, due to no or little FP occurrence at these velocities. Up to a stimulus velocity of ±1 °/s IFPIs were large with a high variability (Fig. 16B). At ±1 °/s stimulus velocity IFPIs averaged out at 21.19 ± 6.40 s. With higher stimulus velocities, the distribution of fast phases became more regular and inter-fast-phase-intervals shortened (Fig. 16C). At ±20 °/s stimulus velocity IFPIs were in average 9.90 ± 6.01 s long (Fig. 16B).

3.1.4.2.3 Fast phases – triggered by eye position?

In general, fast phases in N-T direction were elicited at eye positions beyond resting position in nasal direction (Fig. 17, blue bars), fast phases in T-N direction at eye positions beyond resting position in temporal direction (Fig. 17, red bars). The eyes were reset from varying deflection angles and fast phases were not triggered at distinct eye positions. However, the range of eye positions where fast phases start gets narrower with higher stimulus velocities at constant stimulation (Fig. 17). At a stimulus velocity of ±2 °/s starting positions for FPs were broadly distributed. For stimulus velocities of ±5 °/s and higher, starting positions around 8° for N-T directed and around 10° for T-N directed fast phases were represented to a greater extent.

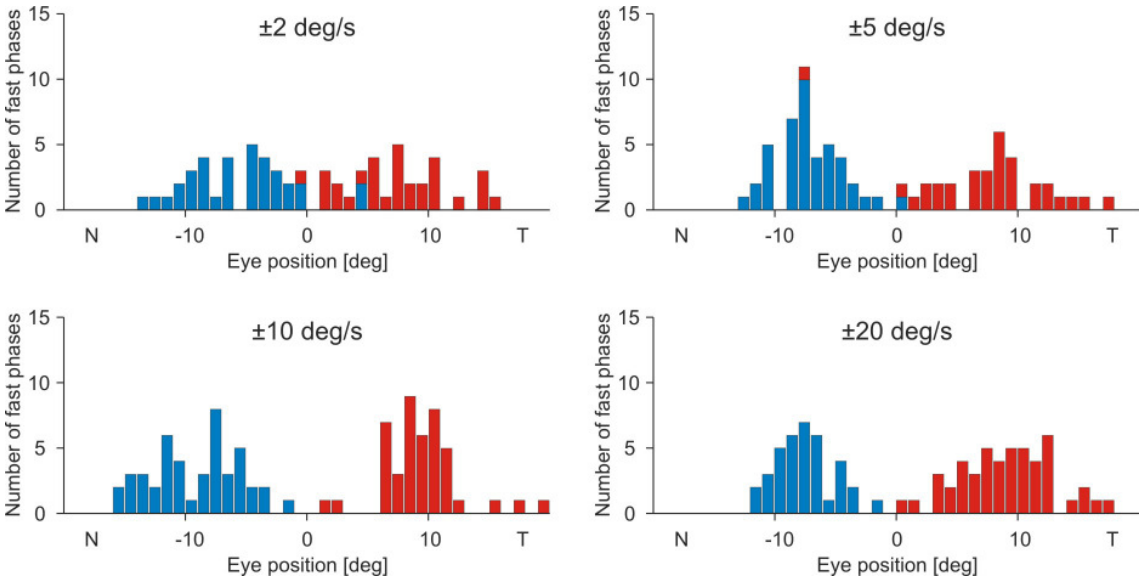

Figure 17: Eye positions at the beginning of fast phases. Starting positions of the right eye of nine animals for all fast phases in naso-temporal (blue bars) and temporo-nasal (red bars) directions. Fast phases were not triggered by concrete eye positions, but showed a higher probability of resetting movements at deflections of the eye from resting position (i.e. zero degree) towards 8° in nasal (N) or 10° in temporal (T) directions.

3.1.4.2.4 Exceeding the ocular motor range during fast phases

During fast phases the eyes regularly overshot the ocular motor range (for definition see methods section 2.4.2), i.e. the eyes were shifted to extreme positions, to which they were not able to be moved by visually elicited slow following movements (Fig. 18, red arrows). The mean magnitude of the overshoots varied between animals (n = 9) and surpassed on average the ocular motor range by 11.98 ± 3.11° in temporal direction and by 15.45 ± 3.43° in nasal direction.

To counteract the exceeding of the ocular motor range, eyes were pulled back into their operating range instantaneously after the fast phases (Fig. 18, blue arrows). These rapid horizontal movements were superimposed on the slow phases and were involved in the non-linear appearance of the SP (see Fig. 14A). The pull-back movements apparently corrected for the FP overshoots. The underlying mechanism might be – unlike visually induced slow following movements – a consequence of the extraocular muscles'

characteristics such as elastomechanical time constants. Nonetheless, no consistent pattern of the pull-back time in relation to the overshoot amplitude could be found.

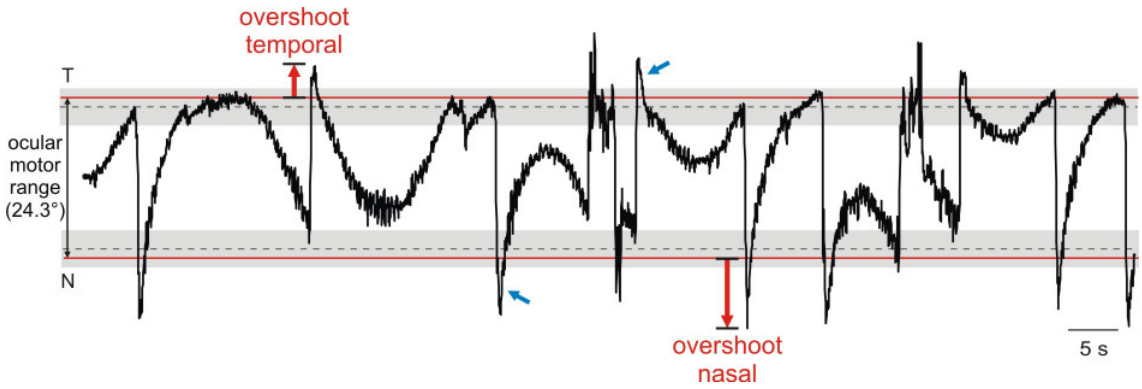

Figure 18: Fast phase overshoot. Right eye position during sinusoidal large amplitude stimulation (0.032 Hz with ±10 °/s, stage 50). Red lines mark the ocular motor range, calculated as the range within which the eye was moving during 97 % of the stimulus time (in this example: 24.3°). During FPs the eye exceeded the ocular motor range resulting in an overshoot in temporal (T) and nasal (N) directions (red arrows). Blue arrows mark pull-back movements which followed the fast phases and moved the eye back into the ocular motor range. Area between the dashed lines indicates the mean ocular motor range with standard deviation (gray areas) of 9 animals.

3.1.5 Optokinetic working range

To determine the working range of the optokinetic system of larval *Xenopus*, sinusoidal stimulation at different frequencies and peak velocities was applied. Eyes followed the stimulus pattern in a sinusoidal manner generally without exhibiting fast phases (Fig. 19). The sole exception existed for stimuli at 0.032 and 0.065 Hz at ±10 °/s: because of the large stimulus amplitude during these stimuli eyes reached the most eccentric positions of the ocular motor range, leading in nine out of the eleven tested preparations to fast resetting phases as described for the optokinetic reflex pattern during constant velocity stimulation (see 3.1.4).

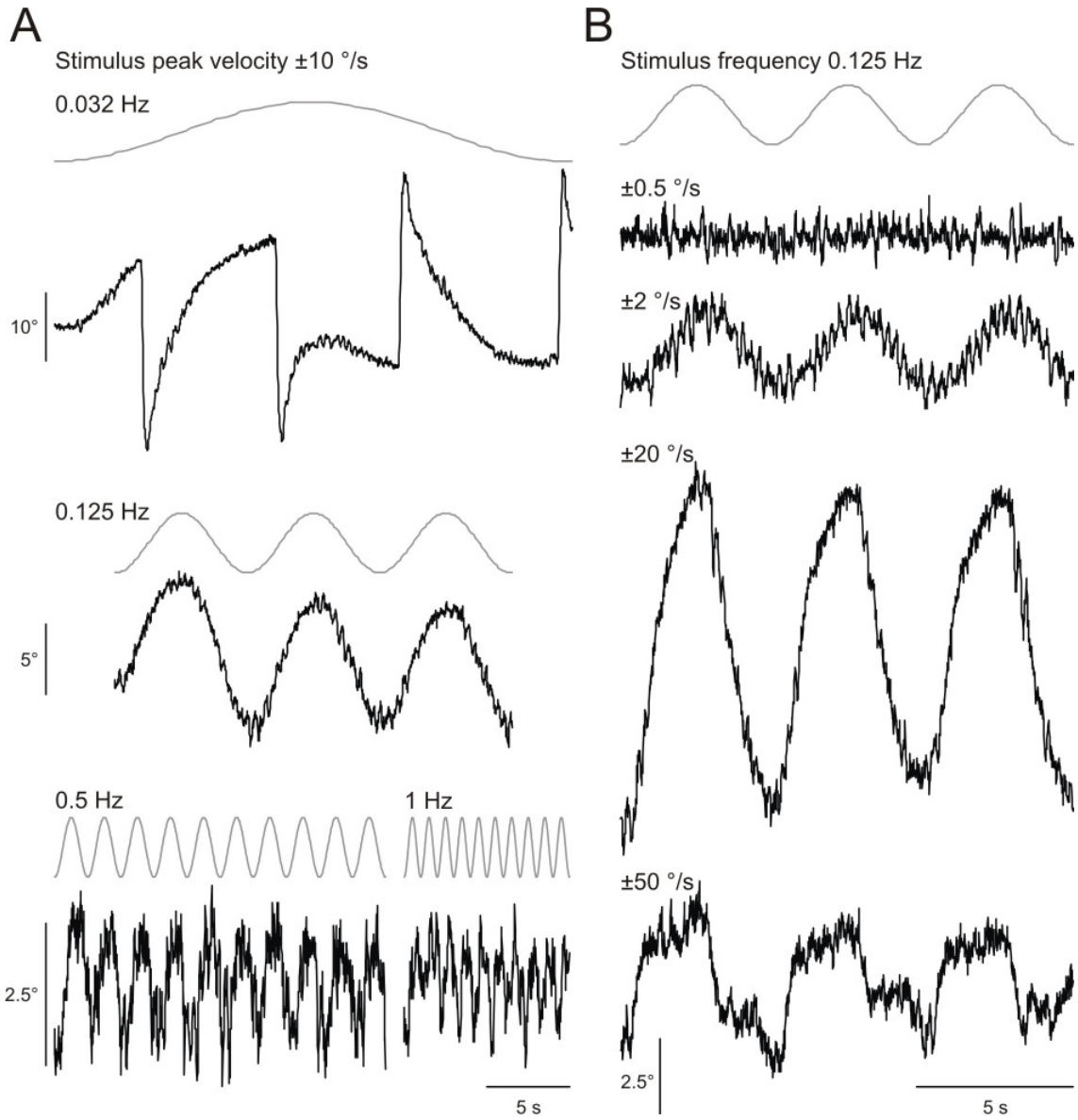

Figure 19: Typical optokinetic response to sinusoidal stimulation. (A) Exemplary position traces for different stimulus frequencies with a peak velocity of ±10 °/s (stage 50, right eye, note the different calibration bars). Eyes followed the stimulus in a sinusoidal manner for the tested frequency range of 0.032 to 1 Hz (gray curves). At 0.032 Hz, the large stimulus amplitude elicited fast phases. (B) Position traces for different stimulus peak velocities at a sinusoidal frequency of 0.125 Hz. Eye movement performance decreased at high stimulus velocities.

3.1.5.1 Frequency dependence

Frequency response analysis of eye movements during sinusoidal stimulation (peak velocity: ±10 °/s) was performed over a frequency range between 0.032 and 1 Hz. Maximal performance of the optokinetic system was

observed at a sinusoidal stimulus frequency of 0.125 Hz with a gain of 0.32 ± 0.12 and a small phase lag of -2.79 ± 7.92°. A frequency-dependent drop of performance, manifested as a gain decrease and the existence of a phase lead or a larger phase lag, occurred below and above this optimal stimulus frequency (One-way ANOVA, $F(5, 47) = 3.71$, $p = 0.007$/ $F(5, 47) = 56.17$, $p < 0.001$). At a frequency of 0.032 Hz gain was low (0.13 ± 0.05), increased up to a frequency of 0.125 Hz and remained slightly below this value for higher frequencies (Fig. 20A). The elevated average gain of 0.37 with an enormous phase lag of -100.80 ± 42.22° was found at a stimulus frequency of 1 Hz. However, the gain's high standard deviation of ±0.18 (Fig. 20A, 1 Hz) led to the assumption that the high gain values were due to noise within the recordings as the 1 Hz stimulus was of little amplitude. Over all stimulus frequencies a change of phase shift was observed. A phase lead of 54.21 ± 15.00° at 0.032 Hz decreased to a phase lag of -100.80 ± 42.22° at 1 Hz, with the response being almost in phase with the stimulus at 0.125 Hz (Fig. 20B).

3.1.5.2 Velocity dependence

By varying the stimulus peak velocities (±0.5 to ±50 °/s) and keeping the stimulus frequency constant during sinusoidal stimulation, the capacity of the ocular motor system to respond to stimuli of increasing amplitudes was tested. As frequency analysis showed optokinetic performance to be most robust at 0.125 Hz, this frequency was used for stimulation. A low gain with a high variability between animals (0.25 ± 0.25) was measured for a peak velocity of ±0.5 °/s. With increasing stimulus peak velocities, a maximal average gain of 0.42 ± 0.11 was detected at a peak velocity of ±2 °/s. Further increase of stimulus peak velocity lead to a non-linear decrease of gain with 0.19 ± 0.08 at ±20 °/s and a gain close to zero (0.02 ± 0.01) at ±50 °/s (Fig. 20C).

The phase shift increased from a phase lag of -60.23 ± 32.05° at the low peak velocity of ±0.5 °/s to a phase lead at high stimulus peak velocities of 31.17 ± 11.82° at ±50 °/s. The response being almost in phase with the stimulus

was found at ±10 °/s stimulus peak velocity (-1.48 ± 7.94°) as also seen in the frequency analysis (Fig. 20D).

In summary, the gains for stimulus peak velocities below and above ±2 °/s showed a non-linear velocity-dependent attenuation (One-way ANOVA, $F(8, 27) = 16.06$, $p < 0.001$). The phase of the optokinetic response shifted from a lag to a lead with increasing stimulus peak velocities and matched the phase of the stimulus best at ±10 °/s (One-way ANOVA, $F(8, 27) = 28.47$, $p < 0.001$).

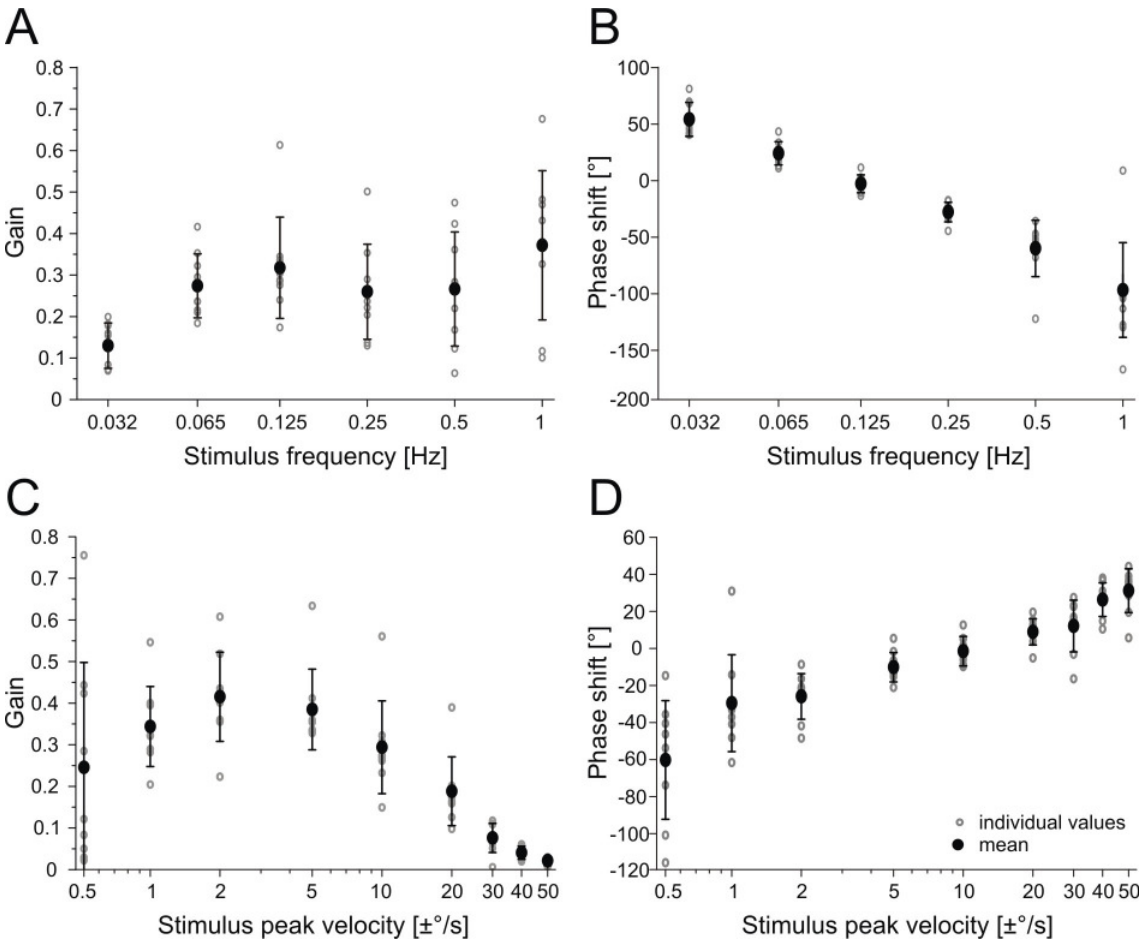

Figure 20: Gain and phase shift during sinusoidal stimulation. (A) Bode gain plot and (B) corresponding phase shift for sinusoidal stimulation with a constant peak velocity of ±10 °/s. Best performance at a stimulus frequency of 0.125 Hz – maximal gain and in phase with the stimulus. (C) Gain and (D) phase shift for different stimulus peak velocities at a stimulus frequency of 0.125 Hz. Black dots are mean values ± standard deviations (n = 9), gray dots show data of individuals. Phase lag < 0, phase lead > 0.

3.1.6 The optokinetic system – symmetric?

Movements of the left and right eyes were strongly conjugated during binocular optokinetic stimulation in *Xenopus* tadpoles (see 3.1.3). Many other afoveate, lateral-eyed animals with coupled eye movements were reported to exhibit an optokinetic asymmetry with a reduced or abolished response to naso-temporally directed stimuli, hypothesizing the prevention of optokinetic stimulation by translational movements during forward locomotion (Fritsches and Marshall, 2002). Thus, the possible asymmetry of the optokinetic system and the level of linkage between the two eyes of *Xenopus* tadpoles were investigated using monocular visual stimulation under two different conditions: first, stimulation was restricted to the right eye by covering the left half of the drum by a stationary white background which prevented stimulation of the left eye with the moving striped pattern, and second, by cutting the left optic nerve which prohibited the information transfer from the left eye to central areas and thus the interaction with information from the intact right eye (n = 6) (see 2.3.3). Optokinetic responses during binocular visual stimulation served as natural control condition. Sinusoidal stimulation was used to compare the optokinetic performance of the intact eye and the non-stimulated or disconnected eye. Constant velocity stimulation provided the basic functional characteristics on the symmetry of the optokinetic system.

3.1.6.1 Differences in optokinetic performance of right and left eye

Gain during binocular sinusoidal stimulation with 0.125 Hz and a peak velocity of ±10 °/s was 0.26 ± 0.10 and 0.23 ± 0.08 for the right and the left eye, respectively. Under both monocular conditions a decrease of the gain was observed for both eyes (Fig. 21A). Monocular sinusoidal stimulation where a white background covered the left half of the drum produced gains of 0.17 ± 0.07 and 0.07 ± 0.03 for the right and left eye, respectively – a drastic drop of eye movement performance in both eyes (paired t-test, right: $p = 0.003$; left: $p < 0.001$) when compared to the gains during binocular stimulation. Also

for the condition with a severed left optic nerve, the gain was decreased for the right eye (0.19 ± 0.08) and significantly reduced for the left eye (0.08 ± 0.03) compared to the gains during binocular stimulation (paired t-test, right: p = 0.144, left: p = 0.0012). Hence, under both monocular conditions sinusoidal stimulation of the right eye provoked eye movements of the – not visually stimulated or disconnected – left eye, although with a considerably reduced gain performance.

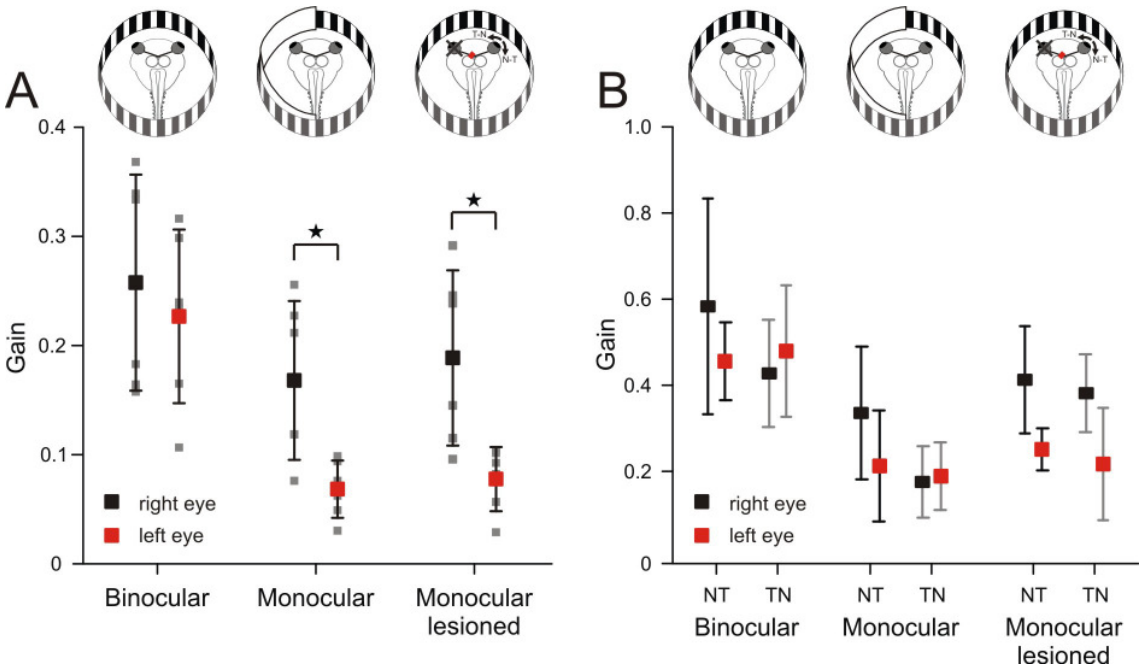

Figure 21: Monocular performance. (A) Decline of the optokinetic response of both eyes for monocular conditions during sinusoidal stimulation, with a stronger abatement of gains for the left eye. Note that albeit the missing visual stimulation of the left eye during monocular conditions, eye movements of the left eye were present. (B) No response asymmetry of the right or the left eye in naso-temporal (N-T) versus temporo-nasal (T-N) direction for all three conditions (constant velocity stimulation with ±1 °/s, n = 6). Data are mean values ± standard deviations.

3.1.6.2 Direction asymmetry of the optokinetic system

For investigation of a possible directional asymmetry of the optokinetic system of tadpoles, i.e. a stronger optokinetic response to one of the stimulus directions, eye movement responses of the intact right eye and the 'blind' left eye were examined. For each eye, respectively, optokinetic response in

naso-temporal (N-T) versus temporo-nasal (T-N) direction was compared at constant velocity stimulation with ±1 °/s (n = 6). Slightly different gains in T-N and N-T direction were observed during binocular stimulation (Fig. 21B), but differences for the two directions were nonsignificant (paired t-test, right: p = 0.113, left: p = 0.708). As in the case of sinusoidal stimulation, gains were drastically reduced for monocular optokinetic stimulation of the right eye (right: 0.34 ± 0.15 (N-T)/ 0.19 ± 0.08 (T-N), left: 0.22 ± 0.13 (N-T)/ 0.20 ± 0.08 (T-N)) compared to gains provoked by the binocular stimulus condition. By lesion of the left optic nerve the performance increased compared to the monocular condition with the white background, but only for the right eye (right: 0.47 ± 0.17 (N-T), 0.42 ± 0.12 (T-N), left: 0.26 ± 0.05 (N-T)/ 0.23 ± 0.13 (T-N)) and not to the initial values elicited by binocular stimulation. For both monocular conditions no significant difference between gains for the two stimulus directions was detected (paired t-test, right: p = 0.155 and p = 0.370, left: p = 0.754 and p = 0.464) (Fig. 21B).

Stimulation was also done for higher stimulus velocities of ±10 and ±20 °/s. The mean number of fast phases within the two trials was high for binocular stimulation (right: 5.58 ± 3.28 FPs (mean over sum of FPs for ±10 and ±20 °/s for n = 6)). Fast phases were still elicited in both directions and the ratio between FPs in T-N direction and FPs in N-T direction was unchanged under the two monocular conditions, although total numbers were smaller compared to binocular optokinetic stimulation. Average FP number under the monocular condition with an intact left optic nerve was with 2.83 ± 2.07 FPs comparable to the fast phase occurrence under the monocular condition with a severed optic nerve (right: 2.33 ± 2.73 FPs).

Thus, with the missing cumulative excitatory input of the left eye a reduction of gain and fast phase numbers was detected for both monocular conditions compared to binocular stimulation. The fact, that the non-stimulated left eye still moved during monocular stimulation of the right eye, supports the existence of a central neural integrator as shown in goldfish (Pastor et al., 1994) and a

shared signal encoding. Nonetheless, no asymmetry in optokinetic responses in temporo-nasal and naso-temporal stimulus directions was observable during both monocular stimulus conditions, leading to the conclusion that each eye is also partially self-controlled, i.e. monocularly driven (Debowy and Baker, 2011).

3.2 ONTOGENY OF HORIZONTAL EYE MOVEMENT BEHAVIOR

During development, eye movements and the horizontal optokinetic reflex (hOKR) in *Xenopus laevis* change drastically. Based on behavioral optokinetic characteristics, animals were divided into different ontogenetic age groups. Larvae of stages 45 and 46 already showed visually-elicited eye movements, but overall optokinetic performance was low and no conventional optokinetic reflex with slow following and regular fast resetting phases was detectable. Beginning at stages 47 to 49, larvae exhibited large eye movements and an optokinetic reflex, yet still slightly irregular and uncoordinated. As described in the first result section, larvae between stages 50 and 55 possessed a regular hOKR with relatively high gains (see 3.1.4). With increasing age, eye movement performance decreased. A reduced gain and a lack of fast phases characterized the pre-metamorphic larvae between stages 57 to 59. A further drop in ocular motor response was detected in larvae at metamorphic climax (stages 60 to 62) and after metamorphosis in froglets, what became noticeable by a considerably reduced ocular motor range and gains close to zero. In the following paragraph, these age-dependent changes are described in detail, comparing eye resting positions, ocular motor ranges and optokinetic response characteristics.

3.2.1 Eye resting position during ontogeny

During rest, eyes were oriented laterally in the head in the younger stages. The mean angle between the eye and the rostrocaudal midline of the animal was 88.9 ± 4.4° for stages between 45 and 49 (n = 13) and 87.5 ± 4.9° for stages between 50 and 55 (n = 15). During metamorphosis, a more nasal orientation of the eyes was detected. The angle of eye resting position changed from 80.0 ± 4.8° in stages 57-59 (n = 8), to 74.2 ± 2.5° in stages 60-62 (n = 15) and 55.6 ± 3.3° in froglets (n = 9) (Fig. 22A). In addition, the change of eye position in the horizontal plane was accompanied by a translocation of the eyes

to a more dorsal position in young adults compared to the laterally directed position in larvae.

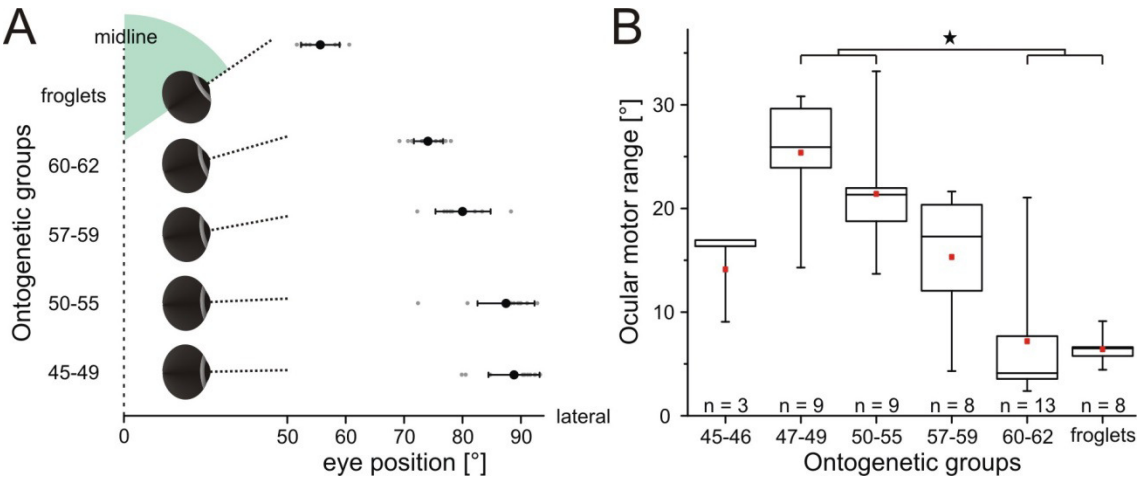

Figure 22: Change of eye resting position and ocular motor range during ontogeny. (A) Eye position in head changed from completely lateral in young larvae to a more frontally directed position in young adults. The angle between eye and the rostrocaudal midline of the animal in the horizontal plane (green area) decreased during metamorphosis. Data indicate means ± standard deviations, gray dots are individual values. (B) Reduction of the ocular motor range during metamorphosis. Box plot with median, 25 and 75 % quartiles and whiskers for an area of 5 to 95 %, red squares are mean values. Significance level of $p < 0.05$ (*).

3.2.2 Alteration of the ocular motor range during ontogeny

The ocular motor range was defined as the natural working range in the horizontal plane, within which the eyes moved during visually elicited following movements. An ocular motor range of 14.21 ± 5.46° in the youngest animals was measured (stages 45-46). The largest average range of 25.54 ± 5.46° was present in stages 47-49. With ongoing ontogeny eye movement angles decreased drastically. A range of 21.54 ± 5.58° for larvae between stages 50-55 declined to 15.41 ± 6.08° in pre-metamorphic stages 57-59. A further reduction during metamorphosis restricted eye movements to a range of 7.23 ± 6.70° in stages 60-62 and to 6.46 ± 1.53° in froglets (Fig. 22B). The small ocular motor range in *Xenopus laevis* froglets is thus consistent with earlier reported findings in adult *Rana temporaria* (amplitude of eye movements: ±3-6°) (Dieringer and Precht, 1982).

3.2.3 Correlation of left and right eye movements during ontogeny

Linear correlation analysis of left versus right eye position was done for all stimulus conditions and within all ontogenetic groups. Coherence in younger animals (stages 45-46) was lower than in stages 47-49 and 50-55, for which correlation was highest. While stages 57-59 showed only slightly less conjugated eye movements, the level of correlation decreased drastically during metamorphosis. The generally decreased conjugation of left and right eye movements for animals from stage 60 onwards was likely also due to the overall decreased optokinetic performance in these animals. The low signal-to-noise ratio of the position traces for these stages impaired noticeably the synchrony of eye movements.

During constant velocity stimulation the coordinated movements of both eyes were not influenced by the stimulus velocities (Fig. 23A) and the degree of correlation remained constant for the whole range of stimulus velocities (±0.5 to ±20 °/s). At a constant stimulus velocity of ±10 °/s, the correlation coefficient rho was with 0.95 highest for stages 47-49 and decreased with development to values of 0.12 and below at stages older than stage 59 (Fig. 23D).

During sinusoidal stimulation the developmental pattern was similar to that for constant velocity stimulation with eye movements less correlated in young larvae (stages 45-46) and animals of stage 57 and above (Fig. 23B, C). At a stimulus frequency of 0.125 Hz and a stimulus velocity of ±10 °/s, the correlation coefficient rho peaked with 0.95 and 0.94 at stages 47-49 and stages 50-55, respectively. Rho decreased with metamorphosis to values below 0.04 and below for ontogenetic stage 60 and older (Fig. 23D). The conjugation of eye movements was further influenced by the stimulus frequencies and velocities.

For sinusoidal stimulation with a frequency of 0.125 Hz and different peak velocities between ±0.2 and ±50 °/s, correlation was low for low stimulus velocities and increased with increasing stimulus velocities reaching a maximal

correlation for stimulus velocities of ±10 and ±20 °/s. For higher velocities the coherence of left and right eye motion dropped slightly (Fig. 23B).

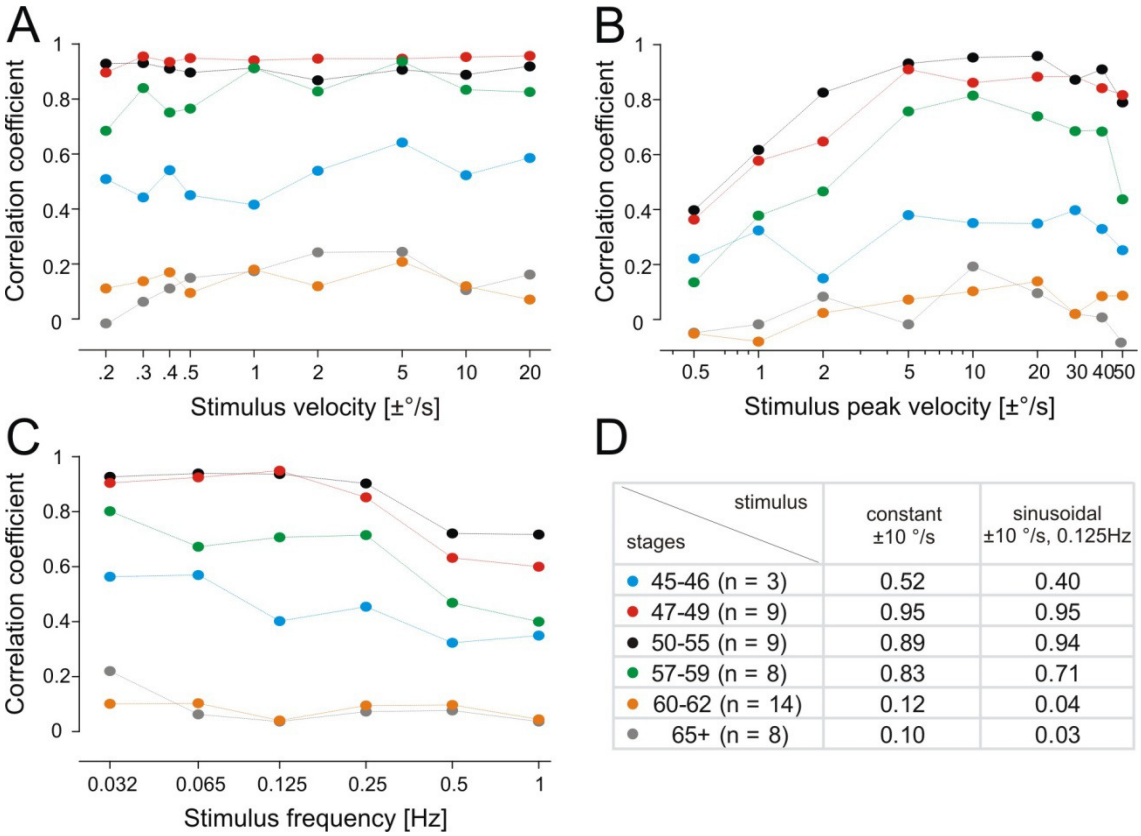

stages \ stimulus	constant ±10 °/s	sinusoidal ±10 °/s, 0.125Hz
45-46 (n = 3)	0.52	0.40
47-49 (n = 9)	0.95	0.95
50-55 (n = 9)	0.89	0.94
57-59 (n = 8)	0.83	0.71
60-62 (n = 14)	0.12	0.04
65+ (n = 8)	0.10	0.03

Figure 23: Correlation of left and right eye movements during ontogeny. Correlation coefficient rho obtained by the correlation of left and right eye positions during (A) stimulation with different constant velocities, (B) sinusoidal stimulation at 0.125 Hz and varying peak velocities and (C) sinusoidal stimulation with a peak velocity of ±10 °/s at varying stimulus frequencies. Ontogenetic age groups are color coded. Data indicate the mean values of rho over all animals within each group. (D) Mean of the correlation coefficient rho for the different developmental groups for constant velocity stimulation with ±10 °/s and sinusoidal stimulation at 0.125 Hz with a peak velocity of ±10 °/s. An extreme decrease of correlation with development was distinctive.

For sinusoidal stimulation at a stimulus peak velocity of ±10 °/s and varying stimulus frequencies between 0.032 and 1 Hz, the conjugation of right and left eye movements remained largely constant up to about 0.25 Hz and then dropped with increasing stimulus frequencies for stages 47 throughout 55 (Fig. 23C). Younger and older stages (45-46 and 57-59) showed a decreasing

coherence of eye movements or remained roughly constant at low levels (stages 60 and older).

3.2.4 Ontogeny of the horizontal optokinetic reflex

No robust and reliable horizontal optokinetic reflex was observed in *Xenopus laevis* tadpoles below stage 47: although visual stimulation provoked eye following movements of low performance, fast resetting phases appeared not at all in some animals or very sporadically in others. Stages 47 to 55 showed a horizontal optokinetic reflex with slow following and fast resetting movements. In stages 47-49 fast phase regularity and slow phase gain increased. Since stages 50-55 exhibited an optokinetic response with a stable slow and fast phase performance, those stages were often used as a reference group for ontogenetic comparisons of optokinetic performance in this study. With the change of body morphology during proceeding metamorphosis a decline in slow phase performance as well as a lack of resetting fast phases was observed from stage 57 onwards.

3.2.4.1 Onset of the horizontal optokinetic reflex

Even though tadpoles of stages 45 and 46 showed visually elicited eye movements, no typical optokinetic reflex in the horizontal plane was observed. Fast resetting phases appeared only in one out of four larvae of stage 45/46. At this stage, fast phases were elicited on a random basis (see below in chapter 3.2.4.3) and could not be referred to as typical fast phases as described in chapter 3.1.4.2. In addition, twitches of the eyes in stimulus directions were recorded (Fig. 25, Animal 4). In another preparation the eyes followed the stimulus, but lacked fast phases and stayed at the most eccentric positions until the stimulus changed direction or stopped (Fig. 25, Animal 3). In the remaining two preparations, slow phases were of small amplitudes and often stopped by retraction of the eye bulb into the head (Fig. 25, Animal 1 and 2). The gain of the slow following movements was generally low during constant velocity

stimulation and reached a maximal average value of 0.34 ± 0.10 at a stimulus velocity of ±0.2 °/s (Fig. 26A).

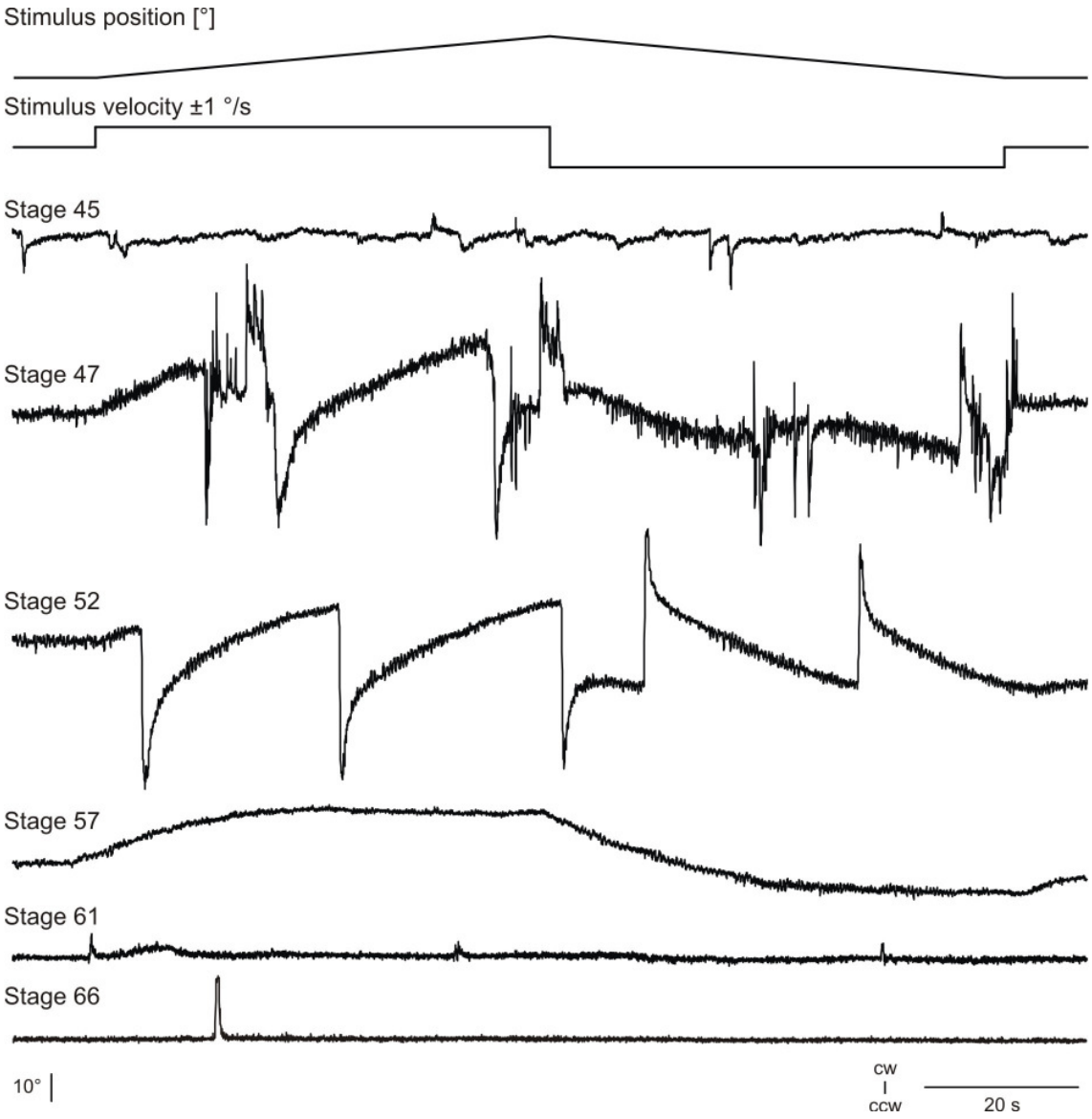

Figure 24: Ontogeny of the horizontal optokinetic reflex. Characteristic right eye position traces for the different developmental groups showing no OKR at stage 45, the onset of the OKR (stage 47), a regular hOKR (stage 52), the loss of fast phases at stage 57 and a drastic reduction of the optokinetic performance for older stages 61 and 66. The first two traces visualize the stimulus (±1 °/s constant velocity). Ccw, counterclockwise; cw, clockwise.

A typical hOKR with clearly observable slow following phases (SPs) interrupted by fast resetting phases (FPs) in opposite direction was detected starting at the transition to stage 47 (Fig. 24). For stages 47-49 (n = 9) slow

phase performance increased to a maximum average gain of 0.61 ± 0.09 at a constant stimulus velocity of ±0.5 °/s (Fig. 26A). Eight out of nine preparations showed fast resetting phases – more fast phases were elicited, but the regularity was still erratic. However, an increase of regularity in fast phase emergence with proceeding ontogeny within the group was evident, leading to a clear and largely periodic SP-FP pattern in animals of stages 50-55 (Fig. 24) (also see Chapter 3.1.4).

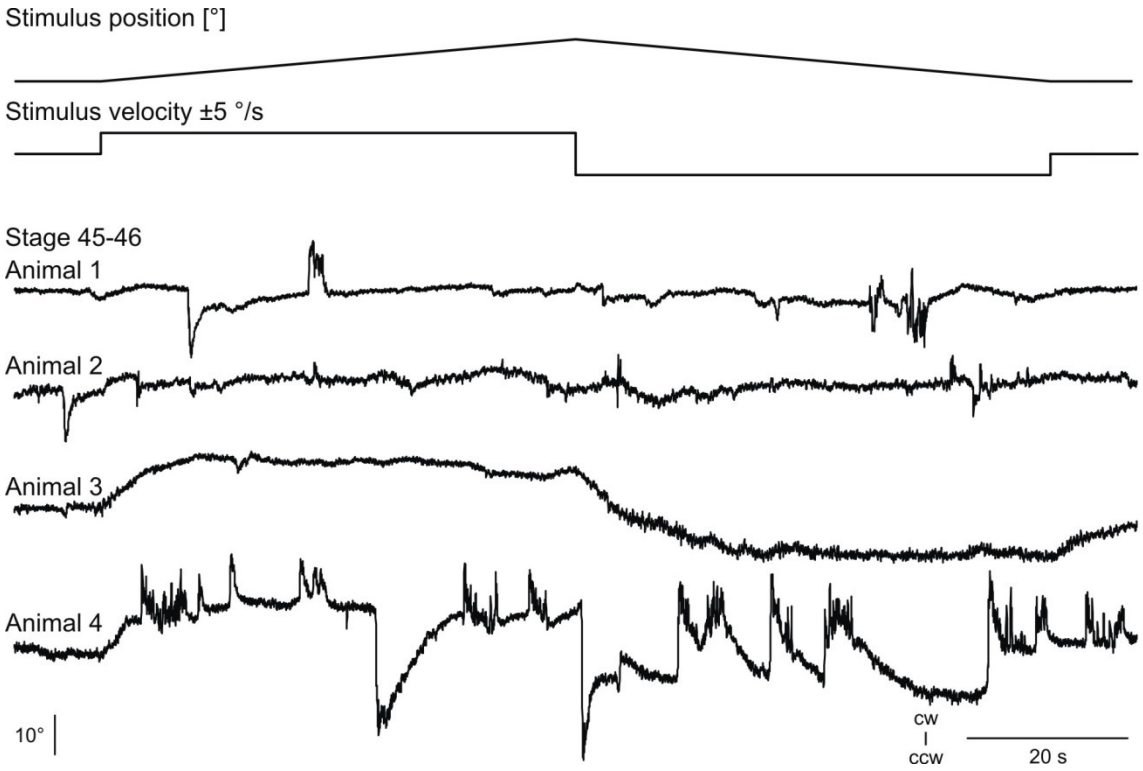

Figure 25: Four examples of the optokinetic performance in stages 45 and 46. Optokinetic stimulation with a constant velocity of ±5 °/s (two upper traces). Note the variability of eye movement responses between the animals. Ccw, counterclockwise; cw, clockwise.

3.2.4.2 Horizontal optokinetic reflex during metamorphosis

A considerable loss of the optokinetic reflex during metamorphosis was detected. The clear and regular hOKR pattern performed by animals between stages 50-55 was absent later in development.

From stage 57 onwards, slow phase gain decreased and resetting fast phases disappeared (Fig. 24). In stages 57-59, only two out of eight larvae

showed a regular optokinetic reflex behavior, while the eyes of the other six animals followed the stimulus pattern and remained at the most eccentric position until stimulation stopped or changed direction (Fig. 24). The slow phase gain decreased to an average gain of 0.44 ± 0.21 at ±0.2 °/s constant velocity stimulation (Fig. 26B).

In stages 60-62, the optokinetic performance was further reduced. In five out of 14 larvae eye movement patterns were similar to the slow phase responses observed in stages 57-59 (Fig. 24), but the slow following movements were of small amplitudes and low gains. In only one preparation fast phases were observed. In the other eight larvae eye movements were almost absent. Thus, the average gains in stages 60-62 diminished to mean values below 0.1 for all tested constant stimulus velocities (Fig. 26B).

Also in froglets (65 and older) fast phases were absent and only little following movements were detected. Mean gains over all animals (n = 9) were below 0.1 for all stimulus velocities, which was comparable to the gains in stages 60-62 (Fig. 26B).

3.2.4.3 Stimulus velocity-dependent changes of slow phase performance and fast phase quantity during ontogeny

The different slow phase response gains of the developmental groups gave an indication about the quality of optokinetic performance during *Xenopus* ontogeny. In young larvae of stages 45-46 a maximal gain of 0.34 ± 0.10 was reached at a stimulus velocity of ±0.2 °/s (Fig. 26A, blue circles). With hOKR onset, gains increased for stages 47-49 to 0.61 ± 0.09 at ±0.5 °/s (Fig. 26A, red circles) and were comparably high as the gain values observed for stages 50-55 (0.63 ± 0.11 at ±0.5 °/s) (Fig. 26A, black circles). Furthermore, optokinetic performance was with a maximal gain of 0.44 ± 0.21 at ±0.2 °/s limited in stages 57-59 (Fig. 26B, green circles). A drastic decline of the overall optokinetic performance was observed in developmental stages 60-62 (Fig. 26B, orange

circles) and in juvenile froglets (Fig. 26B, gray circles). Gains remained below 0.1 for all stimulus velocities.

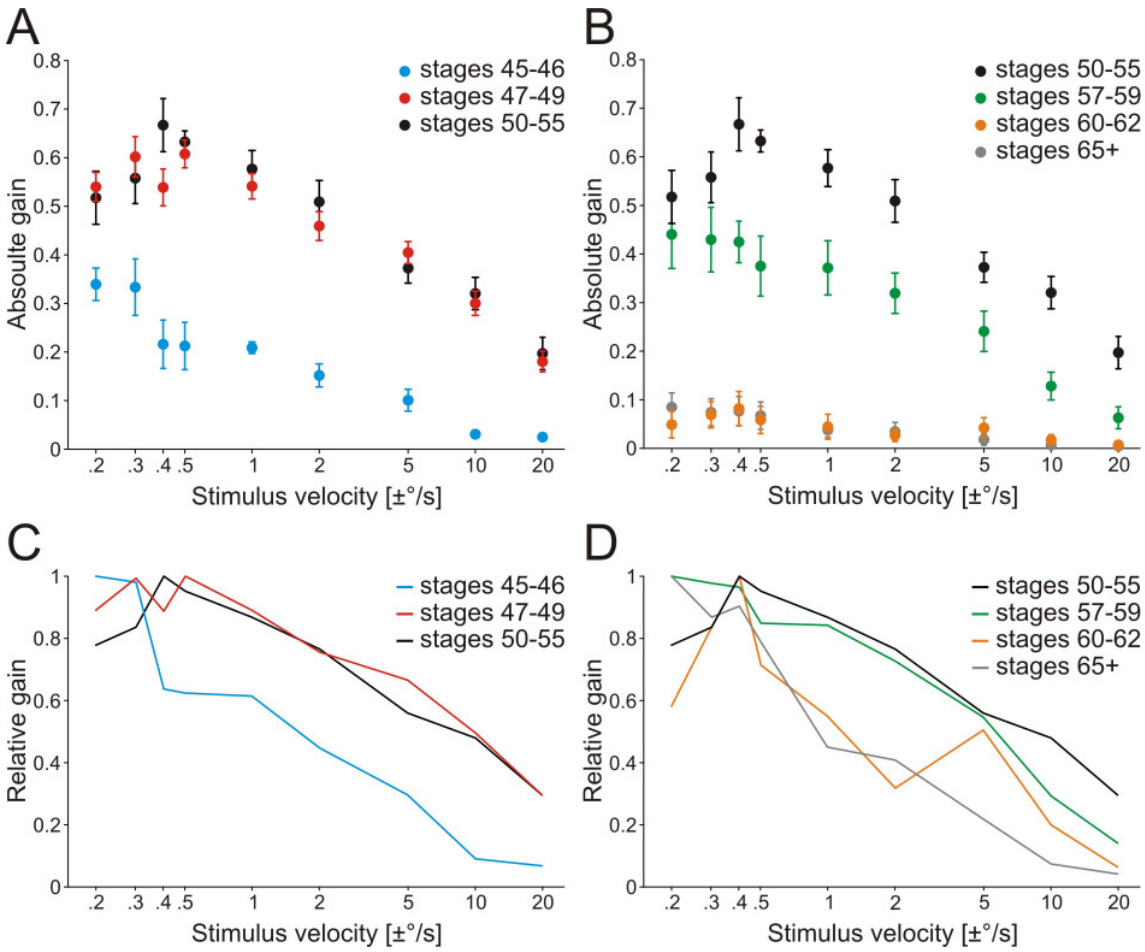

Figure 26: Slow phase gain during ontogeny. (A, B) Absolute gains for constant velocity stimulation with different velocities for the six developmental groups. Values are mean gains averaged over both stimulus directions (naso-temporal and temporo-nasal) and over all animals of each group with the standard error of the mean indicated. (C, D) Relative gains calculated from A and B by normalizing the gain values for each stimulus velocity to the maximum gain within each ontogenetic age group. Developmental groups are color coded (stages 45-46: n = 4; 47-49: n = 9; 50-55: n = 9; 57-59: n = 8; 60-62: n = 14; 65+: n = 9).

The stimulus velocity-dependent change of response performances followed the same pattern in all ontogentic age groups: The highest average gains were measured for low constant stimulus velocities between ±0.2 and ±0.5 °/s. Above ±0.5 °/s, gains decreased with increasing stimulus velocity. However, the stimulus velocity-dependent decrease of the gain was more pronounced in stages 45-46 (Fig. 26C, blue line) and stages 60 and older (Fig. 26D, orange

and gray lines) compared to stages between 47 and 59 (Fig. 26C, red and black lines; Fig. 26D, black and green lines). These observations suggested a tuning of response behavior towards low stimulus velocities in stages 45-46 and animals older than stages 59.

Because no or very few fast phases were generally detected before stage 47 (Fig. 27A, blue), this was defined as the OKR onset (see 3.2.4.1). Starting at stage 47, larvae performed fast phases until ontogenetic stage 55. While animals of stages 47 to 49 (n = 9) exhibited 7.22 ± 5.14 FPs within 120 s step stimulation at a constant velocity of ±20 °/s, larvae of stages 50-55 (n = 8) exhibited in average 11.31 ± 3.87 FPs for the same stimulus. Thus, the variability of fast phase appearance in animals of stages 47 to 49 was larger and the number of fast phases was less compared to stages 50 to 55 (Fig. 27A).

Regarding how the occurrence of fast phases depends on stimulus velocity, the number of fast phases for the different stimulus velocities in both groups followed the same pattern and there was no ontogenetic difference within the two groups. For stages 47-49 as well as for 50-55 more fast phases were elicited the higher the stimulus velocity was, reaching the maximal number of fast phases at a stimulus velocity of ±20 °/s (Kendall rank correlation, stages 47-49: $\tau = 0.89$, $p < 0.001$; stages 50-55: $\tau = 0.94$, $p < 0.001$) (Fig. 27A, red and black).

During further ontogeny, fast phase occurrence changed drastically (Fig. 27B), resulting in a decline or a complete loss of fast phase generation from stage 57 onwards. Out of 8 animals only 2 larvae between stages 57 and 59 exhibited fast phases during constant velocity stimulation. The other 6 preparations only showed slow following movements as already described above (Fig. 24). The maximum average fast phase number of 1.06 ± 2.08 at a constant stimulus velocity of ±2 °/s and a stimulus duration of 120 s clearly demonstrated the reduced fast phase generation (Fig. 27B, green) in comparison to the preceding ontogenetic stages.

In 13 out of 14 animals of stages 60-62 and eight out of nine animals of stages 65 and older no fast phases were elicited at all (Fig. 27B, orange and gray). Only one preparation in each group showed resetting fast phases, respectively. Resetting fast phases in the animal of stage 61 reached high peak velocities (177.31 ± 57.32 °/s) only slightly below those measured in the younger stages 50-55. In the single juvenile frog resetting movements were limited in amplitude (6.49 ± 1.55°) and peak velocity (16.38 ± 4.49 °/s) and thus were not taken into account as fast phases due to the definition of the later (see 2.4.2.1). Excluding these two exceptions, the absence of fast phases in stages 60-62 (n = 13) and older (n = 8) suggested a functional change in the fast phase signal-generating structures during metamorphosis.

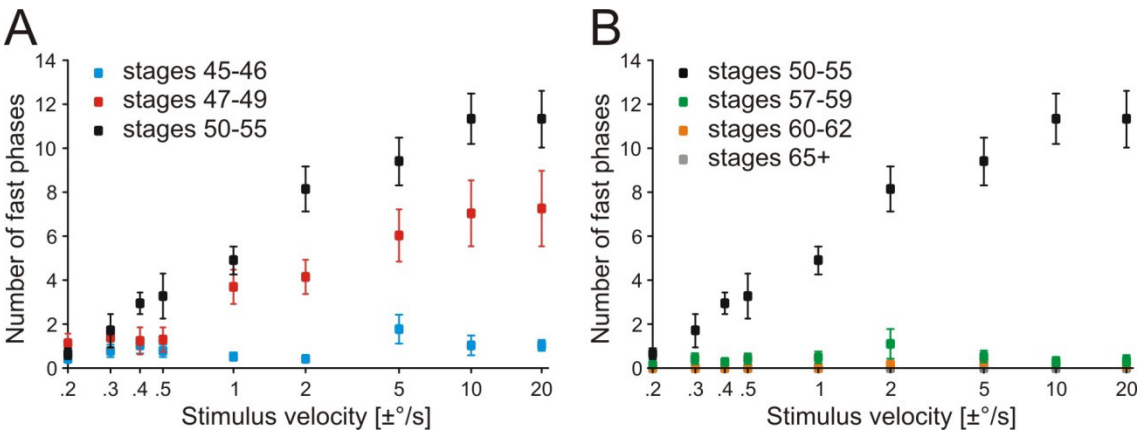

Figure 27: Number of fast phases during ontogeny. Number of fast phases during optokinetic stimulation with different constant stimulus velocities for the six ontogenetic age groups. Values are mean numbers of fast phases across animals with the error bars indicating the standard error of the mean. Developmental groups are color coded (stages 45-46: n = 4; 47-49: n = 9; 50-55: n = 8; 57-59: n = 8; 60-62: n = 14; 65+: n = 9).

3.2.5 Optokinetic working range during ontogeny

For assessing developmental changes in frequency and velocity response profiles, sinusoidal stimulation with different frequencies and peak velocities was presented to the classified ontogenetic groups. As eye movement responses for stages 60-62 and 65+ did not differ to a greater extent, data for sinusoidal stimulation for those animals were pooled for analysis (Fig. 28).

3.2.5.1 Change in frequency responses

Frequency response analysis for a sinusoidal frequency range between 0.032 and 1 Hz with a peak velocity of ±10 °/s allowed comparison of the gain and phase among the five developmental groups (Fig. 28A).

The highest gain values were reached of stages 47 to 55. With a gain of 0.32 ± 0.12, eye movements were almost in phase (-2.79 ± 7.92°) at a stimulus frequency of 0.125 Hz in stage 50-55 (Fig. 28A_3) (also see 3.1.5.1). Comparable response properties were observed for stages 47-49 (gain: 0.33 ± 0.10, phase lead: 8.26 ± 12.21°) (Fig. 28A_2), while optokinetic performance decreased in stages 57-59 to a mean gain of 0.16 ± 0.10 and a phase lead of 9.89 ± 16.49° at 0.125 Hz stimulus frequency (Fig. 28A_4). Although relatively constant gains were detected for stimuli between 0.125 and 1 Hz in these three groups, phase values changed considerably. Eye movements increasingly lagged the stimulus for a stimulus frequency of 0.25 Hz and higher. At lower stimulus frequencies (0.032 and 0.065 Hz) gains were smaller and eye movements exhibited a phase lead compared to the stimulus (Fig. 28A_2-A_4, open circles).

In larvae younger than stage 47 (stages 45-46) (Fig. 28A_1) or in older animals (stages 60-62 and 65+) (Fig. 28A_5) the optokinetic performance was low. Average gains remained below 0.12 for the young animals (stages 45-46) and below 0.06 for the older animals (stages 60-62 and 65+) at all stimulus frequencies. A frequency-dependent change of the phase shift, as reported for stages 47-57, was visible in younger animals (Fig. 28A_1, open circles), while no trend concerning the phase values was detectable above stage 59 (Fig. 28A_5, open circles).

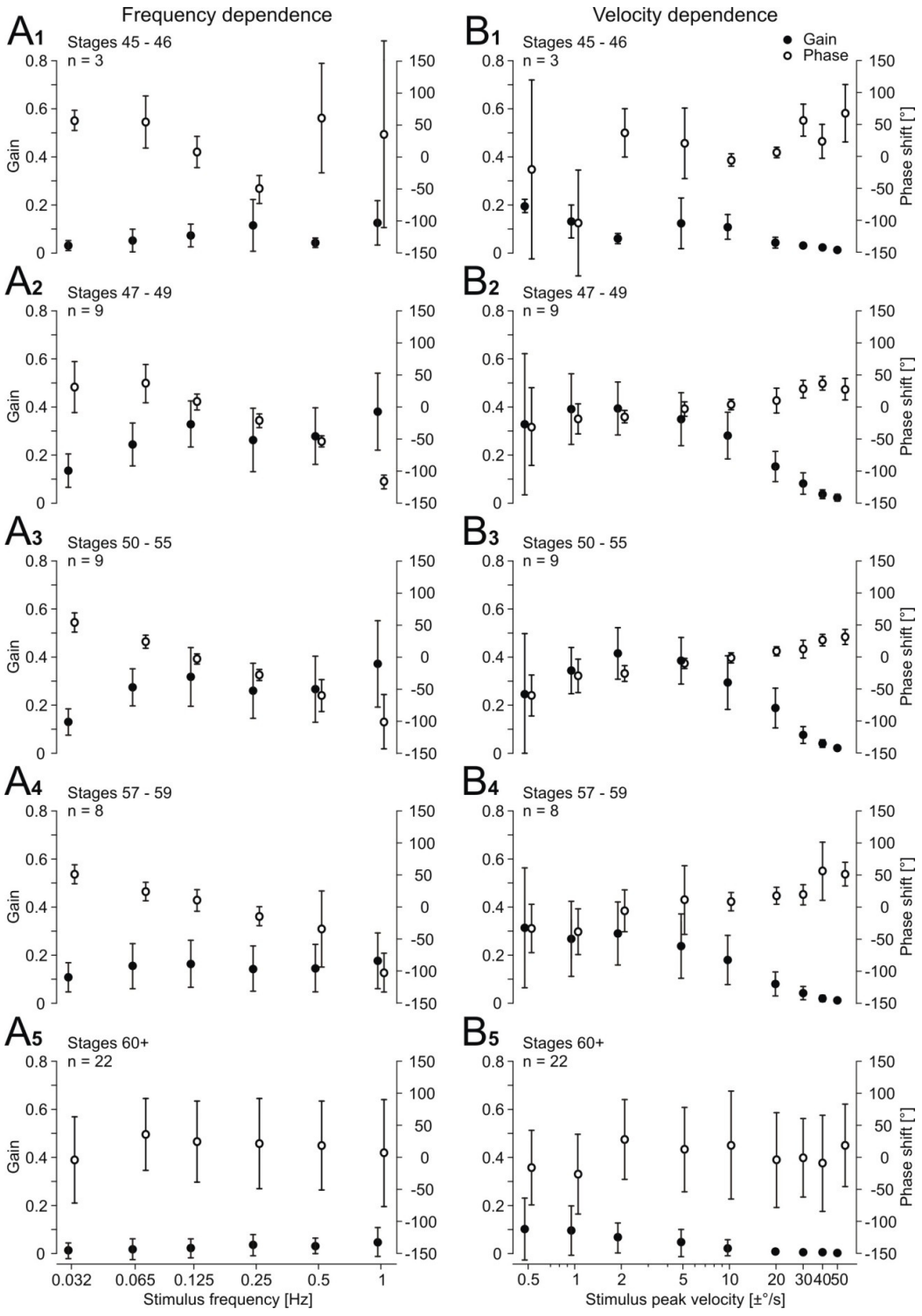

Figure 28: Frequency- and velocity-dependent optokinetic response during ontogeny. Gains and phase shifts for the different ontogenetic groups at ($A_{1\text{-}5}$) sinusoidal stimulation at varying stimulus frequencies with a peak velocity of ±10 °/s and ($B_{1\text{-}5}$) sinusoidal stimulation with varying peak velocities at a stimulus frequency of 0.125 Hz. Data are mean values ± standard deviations.

3.2.5.2 Change in velocity responses

Different sinusoidal stimuli with a peak velocity over a range of ±0.5 to ±50 °/s were used to test possible changes of velocity-dependent eye movement responses among the different ontogenetic groups (Fig. 28B). Stimulus frequency was kept constant at 0.125 Hz as eye movements were most robust for this frequency during frequency analysis.

Maximal average gain values were reached of stages 47 to 55 as already reported above (see 3.2.5.1). Response performance was highest at a stimulus peak velocity of ±2 °/s with gains of 0.42 ± 0.11 for stages 50-55 (Fig. 28B_3) and 0.39 ± 0.11 for stages 47-49 (Fig. 28B_2). For the lower stimulus velocities of ±0.5 and ±1 °/s, gains were slightly lower. With increasing stimulus peak velocities (±5 to ±50 °/s) gains decreased non-linearly to values below 0.1. A comparable velocity-dependent response profile, but with overall lower gains (0.29 ± 0.13 at ±2 °/s) was present in stage 57-59 animals (Fig. 28B_4). Also phase relations behaved similarly in the three developmental groups (Fig. 28B_2-B_4, open circles). Eye movements lagged the stimulus for low peak velocities (stages 50-55: -60.23 ± 32.05° at ±0.5 °/s), were almost in phase at a peak velocity of ±10 °/s and started to lead the stimulus for higher stimulus velocities (stages 50-55: 31.17 ± 11.82° at ±50 °/s).

The optokinetic response was reduced in ontogenetic groups of stages 45-46 (Fig. 28B_1) and stage 60 and older (Fig. 28B_5). Gains for all stimulus velocities were consistently below 0.2 (stages 45-46) and 0.1 (stages 60 and older). While a less distinct trend of phase shifts as reported for stages 47-59 was observed prior to stage 47, no velocity-dependent phase shift was distinguishable for animals at metamorphic climax (stages 60-62) and in froglets (Fig. 28B_1 and B_5, open circles).

3.3 CENTRAL CIRCUITS FOR THE HORIZONTAL OPTOKINETIC REFLEX

To elicit eye movements as a response to large-field visual motion stimulation, the sensory signals are transformed into motor commands. The photoreceptors with their interconnections on a retinal level function as sensors, the extraocular muscles as motor effectors. The intermediate connectivity of the neuroanatomical substrates involved in horizontal eye movement generation was visualized by tracing experiments.

In order to trace the optic tract, Alexa dextran was applied into the eye ball of isolated preparations of *Xenopus laevis* tadpoles (n = 11), where it was taken up by retinal ganglion cells. All anterogradely labeled fibers crossed the midline via the optic chiasm (Fig. 29A). Apart from projections to the nucleus of the basal optic roots in the accessory optic system (Fig. 29B_2, to nBOR) and massive projections to the optic tectum (Fig. 29B_2, OT), fibers projected to the dorsal pretectal area, i.e. the nucleus lentiformis mesencephali in *Xenopus* (Fig. 29B_1, to nLM), which is the first relay station of the horizontal optokinetic reflex (hOKR) circuitry.

By combined tracing of the optic tract and hindbrain structures at the level of the nucleus abducens (n = 4), projection neurons connecting the pretectum and the extraocular motor nucleus were identified. The cell bodies of these neurons were located close to the pretectal termination area of the retinal ganglion cell fibers of the contralateral eye (Fig. 29C). Their axons projected to the ipsilateral nucleus abducens, the final relay station of the hOKR.

The abducens motoneurons located in the fifth rhombomere (Straka et al., 1998) innervate the ipsilateral lateral rectus muscle and thereby form the final element of the horizontal optokinetic three-neuronal reflex circuit. The interconnection of the abducens nucleus to the contralateral oculomotor nucleus via abducens interneurons contributes to the synergistic concurrence of the left and right eyes. Both motor nerves, i.e. ipsilateral abducens and contralateral oculomotor nerves, relay the motor command to the extraocular muscles

resulting in a movement of both eyes in the same direction. The firing patterns, recruitment thresholds and task-specific response dynamics of the different subsets of extraocular motoneurons affect the precision and range of the various dynamic components of the visually-elicited horizontal eye movements.

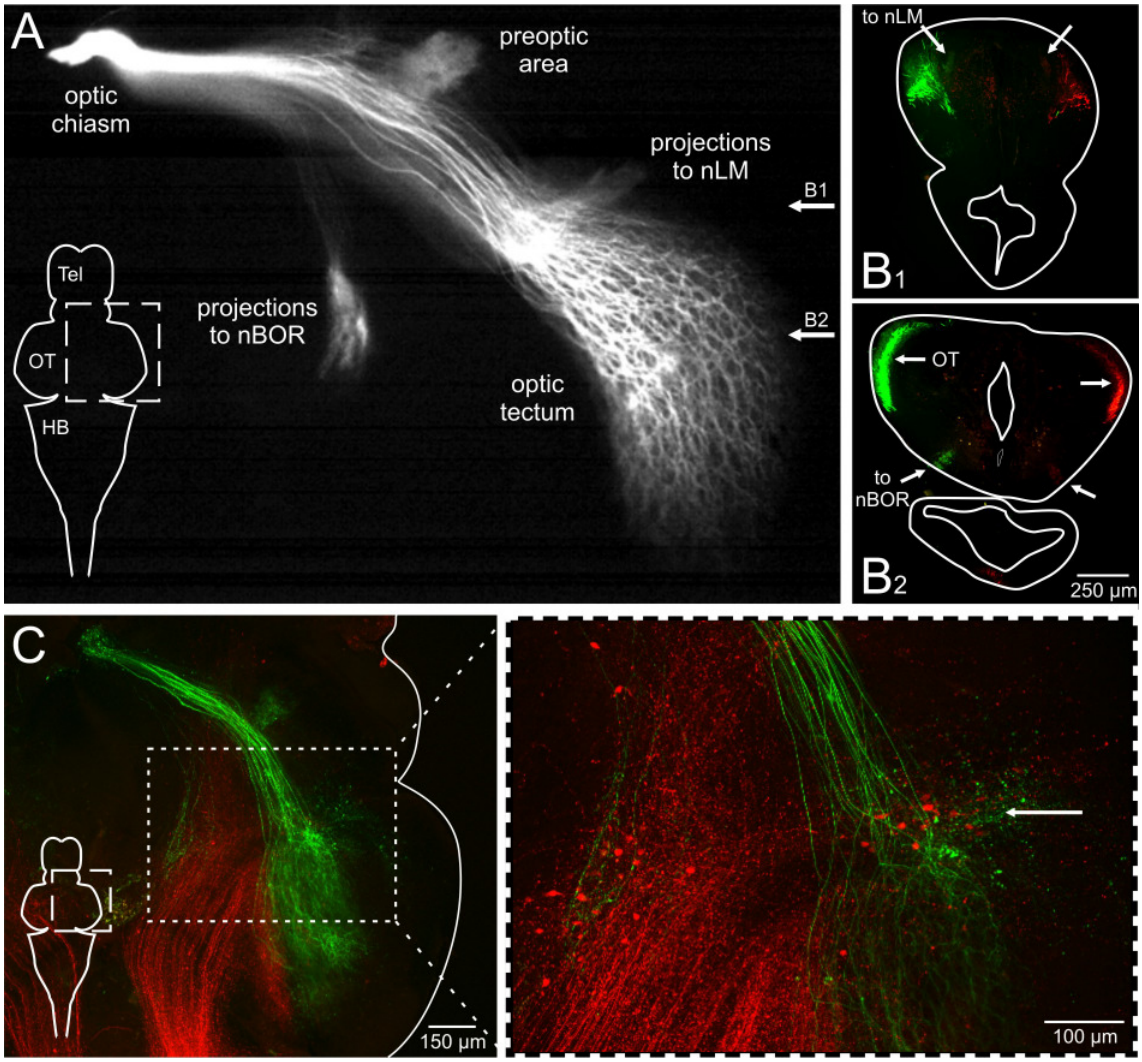

Figure 29: Optokinetic relay stations. (A) Visualization of the optic tract in a whole mount brain preparation of *Xenopus laevis* (stage 50) after anterograde staining with Alexa dextran of the left eye's retina. Note that all retinal ganglion cell fibers crossed the midline. Arrows indicate the locations of the transverse sections. Retinal projections to the pretectal area (B_1 – nLM) and the accessory optic system (B_2 – nBOR) in transverse brain sections (30 µm) after anterograde staining with Alexa dextran of left (green) and right (red) retina. (C) Whole mount preparation with anterograde staining of the left retina (green) and retrograde staining of the right nucleus abducens (red). Inset: Neurons (arrow, red) projecting to the abducens nucleus were located in the pretectal termination area of the retinal ganglion cells. HB, hindbrain; nBOR, nucleus of the basal optic roots; nLM, nucleus lentiformis mesencephali; OT, optic tectum; Tel, telencephalon.

3.4 EXTRAOCULAR NERVE ACTIVITY AND MOTOR OUTPUT

The horizontal optokinetic performance in the tadpole is controlled by the spike discharges of the abducens and oculomotor nerve branches which innervate the lateral and medial rectus muscles, respectively. Non-invasive video recordings of the right eye's movements were combined with simultaneous electrophysiological recordings of the motor nerves innervating the left, i.e. the contralateral eye's extraocular muscles (Fig. 30A) in order to directly compare the motoneuronal signals with the effective behavioral output. Multi- and single-unit discharges were recorded during constant velocity and sinusoidal stimulation in 17 preparations and gave insight into the firing and coding characteristics of the extraocular nerves. For the sake of convenience and relevance for the study of the horizontal optokinetic reflex, the terms *abducens nerve* and *oculomotor nerve* will only refer to the extraocular motor *nerve branches* of the abducens and oculomotor nerves which innervate the lateral and medial rectus muscles, respectively.

3.4.1 Multi-unit discharge during optokinetic stimulation

Based on the findings that *Xenopus* tadpoles exhibit highly conjugated eye movements (see 3.1.3), the spike discharges of the nerves of one eye could be directly compared to the actual eye movements of the contralateral eye. Recordings of the extraocular nerve fibers of the left side mirrored the right eye's effective motor output on a neuronal basis. Multi-unit discharge of the left oculomotor nerve increased during stimulation in clockwise direction – the ensuing contraction of the medial rectus muscle would have induced a temporo-nasally directed movement of the left eye in an intact organism. Conversely, the abducens nerve spike discharge rose during stimulation in counterclockwise direction, provoking a fictive contraction of the lateral rectus muscle and a movement of the associated eye in naso-temporal direction. During stimulation in the opposite direction the firing rates decreased in the respective nerves and the target muscles relaxed (Fig. 30B).

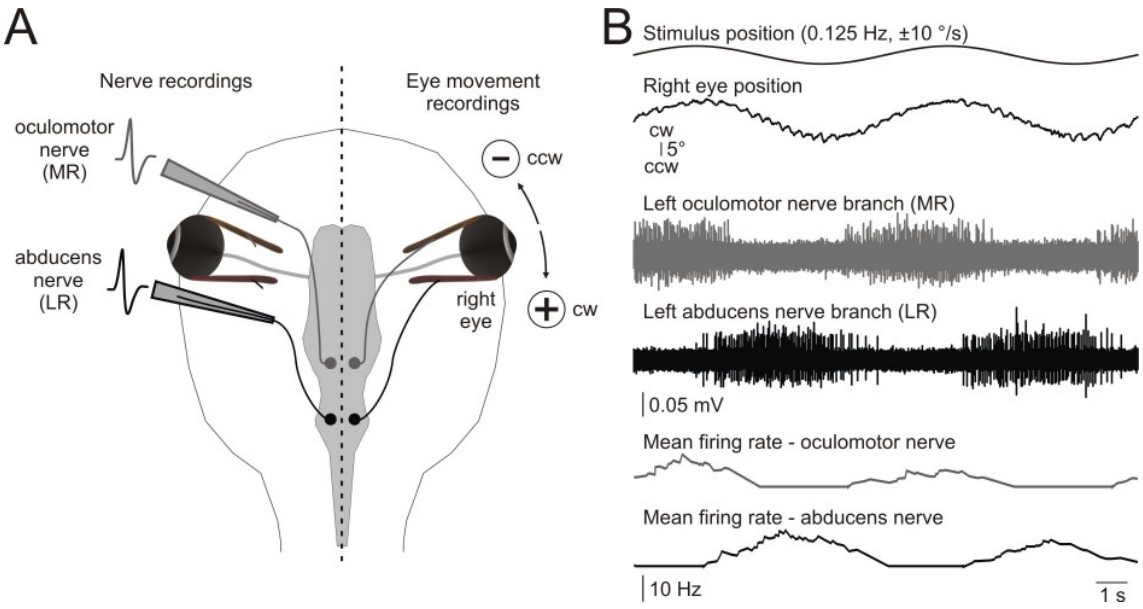

Figure 30: Motoneuronal signals and the motor output during optokinetic stimulation. (A) Experimental setting for simultaneous extraocular nerve recordings on the left side and eye movement recordings of the right eye. Either the oculomotor nerve or the abducens nerve was recorded. Increase of eye position angle for eye movements in clockwise (cw) direction, decrease for eye movements in counterclockwise (ccw) direction. (B) Alternating firing activity and mean firing rate of the oculomotor and abducens nerves during sinusoidal optokinetic stimulation (0.125 Hz, ±10 °/s). LR, lateral rectus muscle; MR, medial rectus muscle.

Optokinetic stimulation with constant stimulus velocities elicited an optokinetic reflex of the intact right eye. Slow following phases in stimulus direction were interrupted by fast resetting phases in opposite direction. For constant velocity stimulation in clockwise direction, the firing rate of the left abducens nerve decreased to zero during slow following movements (Fig. 31A, first half of the stimulus). To reset the eye in counterclockwise direction, the nerve fired in a burst-like manner, causing a rapid contraction of the eye muscle and thereby the fast phase (Fig. 31A, left inset). During stimulation in counterclockwise direction the abducens nerve activity increased during slow following movements (Fig. 31A, second half of the stimulus). For fast phases in clockwise direction sudden drops of the firing rate to zero interrupted the slow phases leading to relaxation of the lateral rectus muscle (Fig. 31A, right inset).

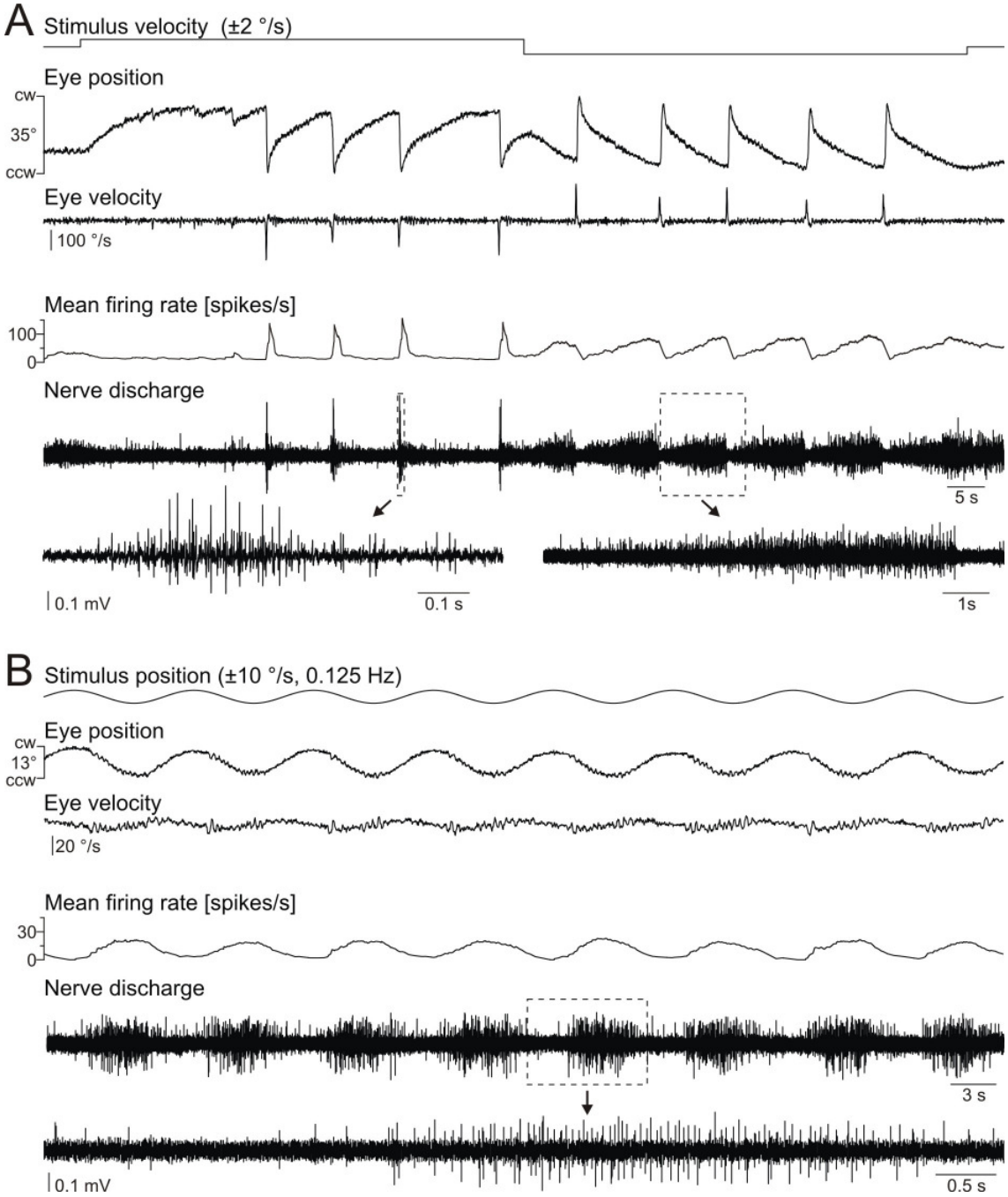

Figure 31: Extraocular nerve activity during optokinetic stimulation. Simultaneous motion recordings of the right eye and extracellular multi-unit recordings of the abducens nerve innervating the lateral rectus muscle of the left eye during optokinetic stimulation. (A) Constant velocity stimulation with ±2 °/s. Left inset: Nerve activity during counterclockwise directed fast phases. Right inset: Nerve discharge during slow phases in counterclockwise direction. (B) Sinusoidal stimulation at 0.125 Hz and with a peak velocity of ±10 °/s. Inset: Firing activity during a single stimulus cycle. Ccw, counterclockwise; cw, clockwise.

For sinusoidal stimulation, the same general pattern appeared. The left abducens nerve was silent during stimulation in clockwise direction and discharge increased with stimulation in counterclockwise (i.e. lateral for the left eye) direction (Fig. 31B). However, abrupt changes of nerve discharge – as seen during fast phase generation – were absent. Instead, a smooth rise and fall of firing rate dependent on stimulus frequency and velocity was prevalent (Fig. 31B, inset).

3.4.2 Extraocular nerve activity – coding of eye position or eye velocity?

Single-unit recordings of 23 units of the left abducens nerve and two units of the left oculomotor nerve provided data to correlate the neuronal discharge of single motoneurons to eye position and eye velocity. The pattern of spike activity of the single units was consistent with the findings for multi-unit recordings described above (see 3.4.1).

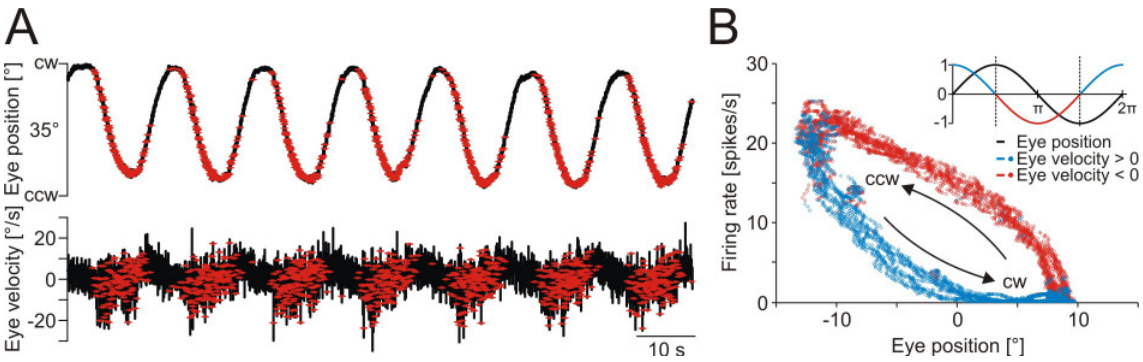

Figure 32: Correlation of extraocular nerve activity and eye movements. (A) Example of the neuronal discharge of a single unit of the left abducens nerve (red asterisks) projected on the simultaneously recorded position and velocity traces of the right eye (black traces) during sinusoidal stimulation at 0.065 Hz with ±10 °/s (stage 54). (B) Firing rate of the single unit versus the right eye position described in A: Constant increase of the spike discharge for eye movements in counterclockwise (ccw) direction (red); rapid decrease to zero for eye movements in clockwise (cw) direction (blue).

During sinusoidal optokinetic stimulation, the firing rate of single abducens units increased for stimuli in counterclockwise direction (Fig. 32A). The eye followed in stimulus direction with the eye movement velocity being negative by definition (Fig. 32B, red symbols). The further the eye was deflected during slow

following movements in counterclockwise direction, the higher was the firing rate. Nerve activity was maximal shortly before the eye was at its most eccentric position where it reversed its moving direction. A quick drop of the firing rate towards zero coincided with the change of eye movement direction, a positive eye movement velocity (Fig. 32B, blue symbols) and an increasing deflection in clockwise direction (Fig. 32A). Thus, the combined activity of all units of the abducens nerve provoked a controlled contraction of the lateral rectus muscle for an eye movement in lateral direction. The close connection of the maximization and minimization of the firing rate of abducens units and the movement of the eye towards the eccentric positions in on- and off-direction suggested a motoneuronal coding of eye position.

To further reveal the position and velocity sensitivity of single motor units, linear regression analysis between the firing rate of a single unit and the corresponding eye position as well as eye velocity was used. A graphical representation of the obtained regression coefficients $ß_{Position}$ and $ß_{Velocity}$ gave insight in the coding specificity of the motoneurons and pictured two coding types (Fig. 33A). Units with $ß_{Position}$-values of zero and $ß_{Velocity}$-values of non-zero would have been pure eye velocity encoders, but none of these units were found in the recordings. Instead, many units with non-zero $ß_{Position}$-values and $ß_{Velocity}$-values of close to zero were present (Fig. 33B). These units primarily encoded eye position (Fig. 33A, unit 1). All other units besides the strongly eye position-encoding units encompassed both eye position and eye velocity control (Fig. 33A, unit 2). For these units both regression coefficients were non-zero (Fig. 33B) and the ratio between the two coefficients characterized the relative weight of coding for position and velocity in abducens (Fig. 33C) and oculomotor units (Fig. 33D).

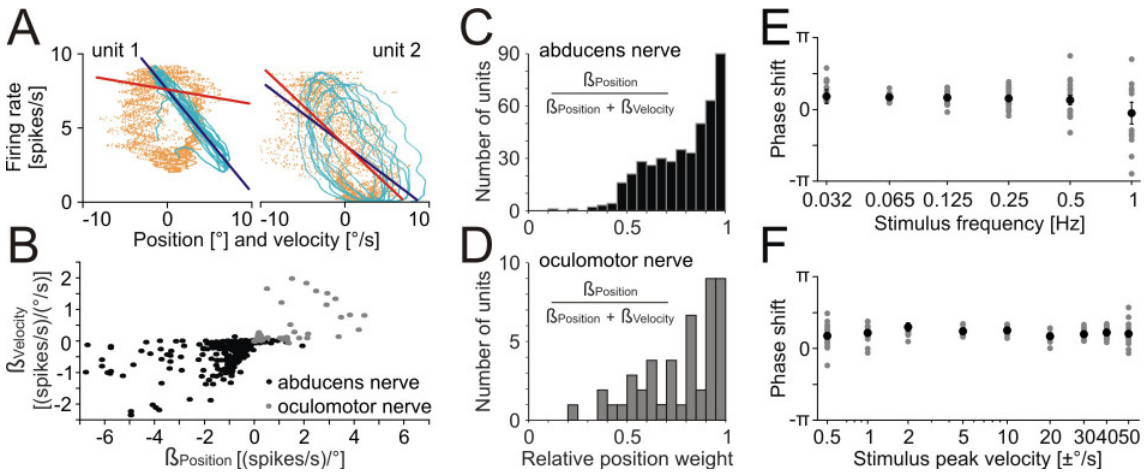

Figure 33: Neuronal coding of eye position and eye velocity. (A) Position (blue circles) and velocity (orange circles) coding profiles of two abducens units during sinusoidal stimulation (0.25 Hz, ±10 °/s) with the linear regression lines indicated (blue – eye position to firing rate; orange – eye velocity to firing rate). Unit 1 coded mainly for eye position, unit 2 for eye position and eye velocity. (B) Linear regression coefficient $ß_{Position}$ versus $ß_{Velocity}$ of 23 abducens (black circles) and two oculomotor units (gray circles) for several sinusoidal (0.032-1 Hz, ±0.5-±50 °/s) and constant velocity (±0.2-±20 °/s) stimuli. Each data point represents one stimulus condition for each single unit. (C) Histogram of the eye position and eye velocity coding of abducens neurons and (D) of oculomotor units. Relative position weight: 0 = eye velocity coding, 1 = eye position coding. (E) Constant phase lead of the maximum abducens discharge compared to the maximum eye deflection in counterclockwise direction for sinusoidal stimulation with ±10 °/s at different stimulus frequencies and (F) with different peak velocities at 0.125 Hz. Data show the mean phase shifts (black dots) with the standard deviations of 18 single units. Gray dots represent single values.

Also the phase relation between the ocular motor nerve discharge and the eye position underlined the strong but not absolute position tuning of the motor units. If the units had been complete position encoders, no phase shift would have been detected. Rather, during sinusoidal stimulation with different stimulus frequencies (Fig. 33E) and peak velocities (Fig. 33F), the maximal firing rate of the abducens nerve always led the maximal deflection of the eye in the corresponding, i.e. counterclockwise direction. A similar phase shift was detected for all stimulus conditions, allowing the conclusion of a strong coupling of the motor units and effector organs for signal transmission.

3.4.3 Modulation of abducens nerve discharge

To classify potential subunits with different recruitment thresholds and tuning properties within the abducens nerve, average eye positions and average spike discharge were compared in the form of peri-stimulus time histograms. Data were taken from 18 single units responding to sinusoidal stimulation at different frequencies (Fig. 34A) and peak velocities (Fig. 34B). Modulation depth was defined as the difference between maximal and minimal activity in the circular normal distribution fit curves on the peri-stimulus time histograms. A broadening or narrowing of the firing pattern was expressed as a change in the half width of modulation depth and revealed the units' recruitment threshold and sensitivity for different stimulus velocities and frequencies.

During sinusoidal stimulation with a peak velocity of ±10 °/s, modulation depth was high for frequencies between 0.032 and 0.125 Hz. Frequencies of 0.25 Hz and higher led to a drop of the mean firing rates. While the absolute change of modulation depth with increasing stimulus frequencies varied between units (Fig. 34C_1), the relative change of modulation depth decreased equally with increasing stimulus frequency for all units (Fig. 34C_2). The half width of modulation depth was invariant up to a stimulus frequency of 0.25 Hz (Fig. 34C_3). For higher stimulus frequencies, firing patterns became more irregular (Fig. 34A) and the half width decreased for most units (Fig. 34C_3).

For sinusoidal stimulation with a stimulus frequency of 0.125 Hz, the modulation depth rose with increasing stimulus velocities up to a maximum at ±10 °/s (Fig. 34B). For higher velocities of ±20 to ±50 °/s mean firing rates declined. Again, the absolute magnitudes of modulation depth varied between units (Fig. 34D_1), but the relative change of modulation depth was similar for all units (Fig. 34D_2). The half width of modulation depth remained invariant between ±2 and ±30 °/s, but fluctuated between units for lower and higher stimulus velocities (Fig. 34D_3).

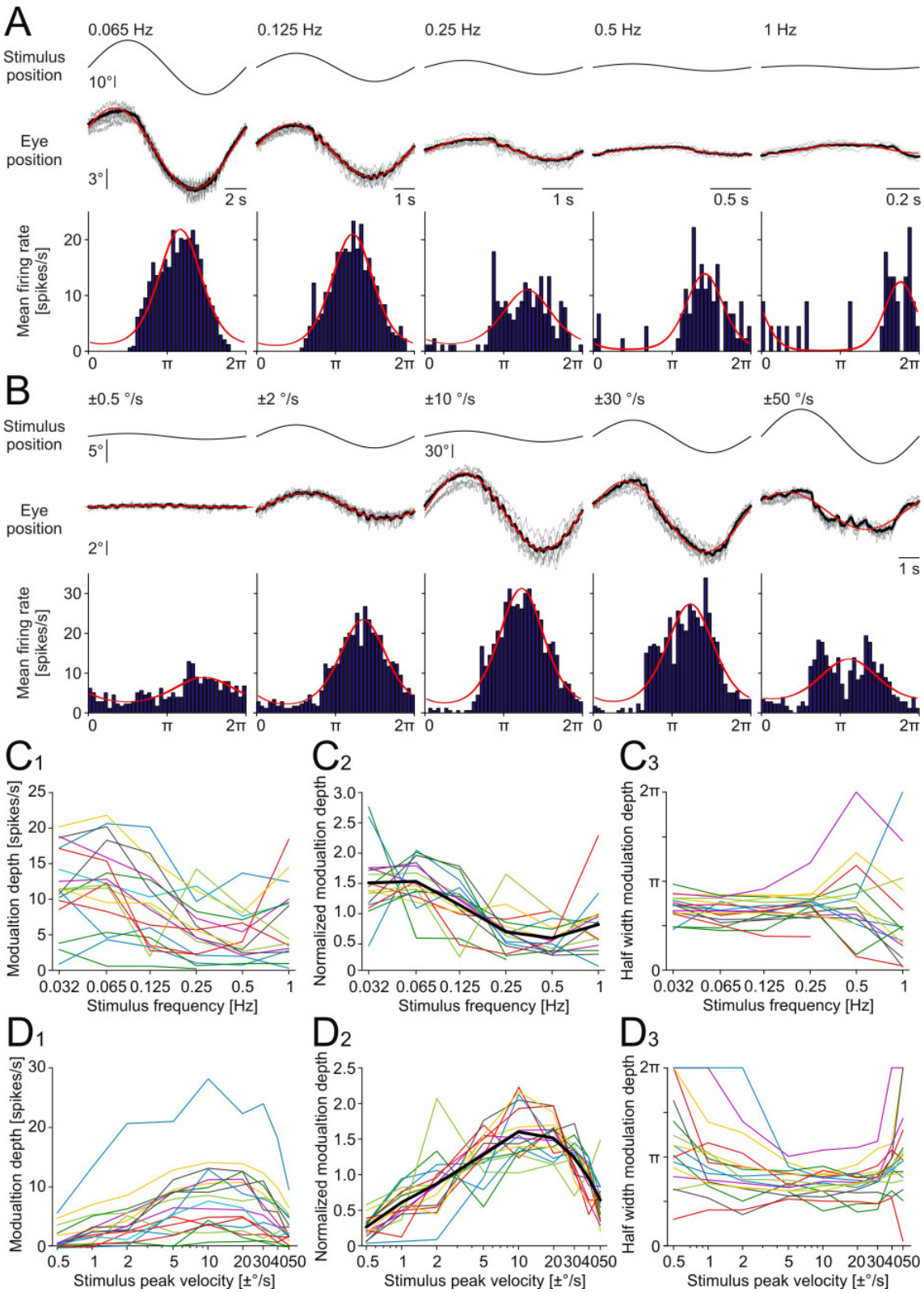
A
0.065 Hz
0.125 Hz
0.25 Hz
0.5 Hz
1 Hz
Stimulus position
10°
Eye position
3°
2 s
1 s
1 s
0.5 s
0.2 s
Mean firing rate [spikes/s]
B
±0.5 °/s
±2 °/s
±10 °/s
±30 °/s
±50 °/s
5°
30°
2°
1 s
C1
C2
C3
Modulation depth [spikes/s]
Normalized modulation depth
Half width modulation depth
Stimulus frequency [Hz]
D1
D2
D3
Stimulus peak velocity [±°/s]

Figure 34: Modulation of abducens nerve discharge. Simultaneously recorded right eye position and single unit discharge of the left abducens nerve during sinusoidal stimulation at (A) different stimulus frequencies with a peak velocity of ±10 °/s and (B) at 0.125 Hz with different peak velocities (stage 53). Eye position traces: sinusoidal fit (red curves) to the average eye position (black traces) calculated from 9 eye position cycles (gray traces). Spike firing rate: peri-stimulus time histograms (PSTHs) with circular normal distribution fits (red curves). (C, D) Firing activity of 18 abducens single units (colored lines) during sinusoidal stimulation at (C_{1-3}) different frequencies with a peak velocity of ±10 °/s and (D_{1-3}) at 0.125 Hz with different peak velocities. (C_1, D_1) Modulation depth (difference between maximal and minimal discharge rates in the circular normal distribution fit) (C_2, D_2) Modulation depth of the same units normalized to the mean modulation depth of each single unit, respectively. Black lines indicate the mean of the normalized values. (C_3, D_3) Tuning width of the single units delineated as half width of modulation depth calculated from the circular normal distribution fits of the PSTHs.

Thus, for a stimulus range of peak velocities between ±2 and ±30 °/s and frequencies up to 0.25 Hz an increase in modulation depth was accompanied by a broadening of the firing pattern and a decrease of modulation depth by a narrowing of firing pattern for all units. For lower and higher stimulus velocities, some units did not respond at all and the firing rate modulated only little or not at all during the whole stimulus cycle, while other units were more sensitive and strongly modulated as seen for the intermediate velocities and lower frequencies. Overall, the frequency- and velocity-dependent modulation of the neuronal discharge of the abducens units corroborated the findings for the frequency and velocity dependence of eye movement gains as described in 3.1.5.

3.4.4 Task-specific motor units

All single units described so far responded to optokinetic stimulation. The sensitivity to different stimulus frequencies and velocities, a progressive increase of firing rates during abducting slow phases as well as the activation during fast phases in this direction characterized these units (Type I) (see 3.4.3).

A second type (Type II) of abducens motor units did not participate in the generation of slow eye movements during optokinetic stimulation. The

immediate detection of the latter during recordings was impeded by the missing resting discharge of the units and their inactivity during visually induced following movements of the eye. Thus, a minority of only four type II units was recorded. The units fired exclusively during resetting fast phases (Fig. 35A). Additionally, a rhythmical activation of type II units during spinal efference copy-driven eye movements became apparent in two preparations (Fig. 35B). Compared to type I units, the spikes of type II units were of particularly large amplitudes and appeared in a burst-like manner. In general, type II units resemble in their firing activity the silent but in motion sensitive abducens motor units, which were found in studies on the vestibular system in *Xenopus* tadpoles (Dietrich et al., 2017).

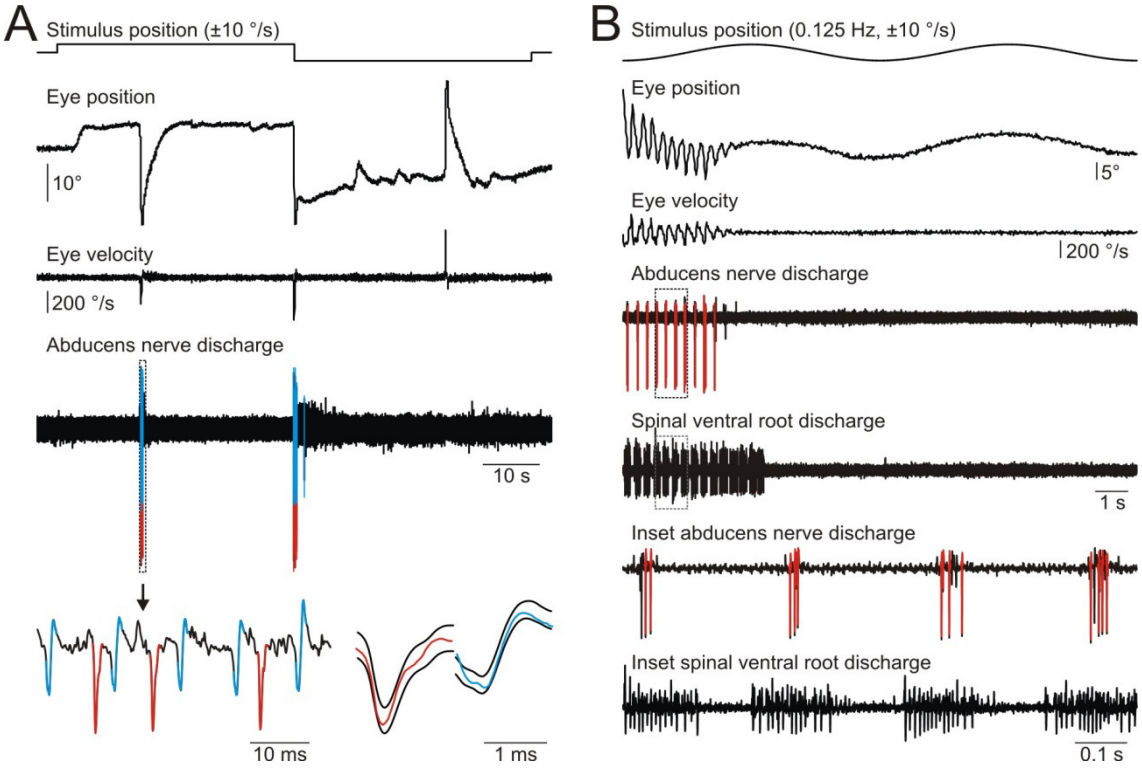

Figure 35: Task-specific motoneurons. (A) Type II abducens motor units (2 units, red and blue, stage 56) showed no spike discharges at rest and fired only during fast resetting phases in counterclockwise direction during constant velocity stimulation (±10 °/s). (B) The same unit (red) rhythmically modulated during fictive swimming (contralateral spinal ventral root discharge), but was not involved in the generation of eye following movements during sinusoidal stimulation (0.125 Hz, ±10 °/s).

4 DISCUSSION

The optokinetic system works hand in hand with the vestibular and proprioceptive systems to guarantee visual acuity. By detection of remaining retinal slip, the system elicits an adequate motor output to optimize gaze stabilization. So far, the optokinetic system is well explored in adult frogs (Cochran et al., 1984; Dieringer, 1987; Dieringer et al., 1982; Grüsser and Grüsser-Cornehls, 1976), but not in tadpoles. In this study, visually induced eye movement responses and the optokinetic reflex of tadpoles of the African clawed frog *Xenopus laevis* are described. An optokinetic performance of tadpoles is observed at stage 45 concurrent with swimming onset (Currie et al., 2016; Nieuwkoop and Faber, 1994) and matures progressively up to morphological stages 50-55. At full manifestation, horizontal visual motion stimulation evokes eye following movements in a range larger than 20°. Constant velocity stimulation provokes a robust optokinetic reflex with slow following and fast resetting phases. Electrophysiological activities of the extraocular motor nerves go along with the behavioral pattern and two subtypes of abducens motoneurons were identified. Type I motoneurons are active during slow following movements of different frequencies and velocities as well as during fast phases; motoneurons of type II fire during fast phases only. The optokinetic reflex starts to weaken around stage 57 and eye movement performance declines drastically. With metamorphosis the optokinetic reflex is largely lost and the remaining limited eye movement amplitudes are comparable to those reported in former studies in adult *Rana* (Dieringer and Precht, 1982).

4.1 ANATOMICAL CONNECTIONS – HOMOLOGY OF PATHWAYS IN VERTEBRATES

The neuronal structures underlying the optokinetic system are well preserved among vertebrate species (Fite, 1985; Masseck and Hoffmann, 2009). Although additional ocular motor features such as smooth pursuit have

developed, homologous structures in the pretectum, mesencephalon and hindbrain form a consistent neuronal substrate of the reflex circuitry in all vertebrates (Huang and Neuhauss, 2008). Earlier lesioning studies in frog revealed the two retinal projection sites relevant for the optokinetic reflex circuitry – the nucleus of the basal optic roots (nBOR) as part of the accessory optic system and the pretectal nucleus lentiformis mesencephali (nLM) (Lazar, 1989; Lazar et al., 1983). Besides strong projections to the optic tectum (Fig. 29A), retinal ganglion cell projections to these relay stations could also be identified in *Xenopus* tadpoles (Fig. 29B_1 and B_2). The direct projection via interconnecting neurons from the nLM to the ipsilateral abducens nucleus in tadpoles (Fig. 29C) is consistent with the findings of Cochran et al. (1984) and Montgomery et al. (1981). These authors reported projections from the retinal termination site in the pretectum to the abducens nucleus and of the direct vicinity of the nBOR to the oculomotor and trochlear nucleus. Some controversy exists on how the optokinetic response to the direction of visual stimulation is implemented by different target areas of retinal ganglion cells. Some studies claim that temporo-nasal stimulation is operated via nLM (Katte and Hoffmann, 1980) and naso-temporal stimulation via nBOR (Cochran et al., 1984), while others found no direction selectivity in pretectal neurons (Fite et al., 1989). Nonetheless, the direct connections of these structures to oculomotor and abducens neurons which innervate the medial and lateral rectus muscles is a sign of their involvement in horizontal eye movement control. Indeed, as suggested by Cochran et al. (1984), such a three-neuronal retino-pretectal reflex arc might predominantly enact the initiation of ocular movements and accelerate the eye. Since the direct input, i.e. the retinal slip signal, is diminished as soon as the eye is in motion, the task to hold the eye in the proper position and to achieve velocity-to-position integration involves more indirect connections in the control network (Dieringer and Precht, 1986). Such neural mechanisms reside in distinct hindbrain nuclei as for example area I and area II in goldfish (Pastor et al., 1994) and the prepositus hypoglossi and medial vestibular nuclei in mammals (Cannon and Robinson, 1987).

4.2 VISUAL PERFORMANCE

4.2.1 The optokinetic system – a low-pass filter

The optokinetic system in *Xenopus* tadpoles showed its best frequency performance in terms of maximal gain and minimal phase shift at 0.125 Hz with a peak velocity of ±10 °/s. At higher stimulus frequencies (0.25-1 Hz), only slightly lower gains (Fig. 20A) but increasing phase lags (Fig. 20B) were detected. Frequencies above 1 Hz could not be tested due to the small stimulus amplitudes at the used peak velocity of ±10 °/s and the poor signal-to-noise ratio of the eye movement response which were already apparent in the eye movement recordings at 0.5 and 1 Hz (Fig. 19A). However, the increasing inability of the eyes to follow the stimulus in phase at higher stimulus frequencies identifies the optokinetic system of tadpoles as a low-pass filter. Strongly affected by the long latency of visual processing in the vertebrate retina (Berry et al., 1999), similar low-pass filtering characteristics have been found for the optokinetic system in a wide range of vertebrates – for example in pigeon (Gioanni, 1988), rat (Hess et al., 1985), cat (Maioli and Precht, 1984) and monkey (Cohen et al., 1977). Although the optokinetic frequency bandwidth in tadpoles matches the one of zebrafish, medaka and goldfish (Beck et al., 2004b), the maximal gain in the frog larvae (0.32 at 0.125 Hz) remains clearly below the gain values found in these three fish species (> 0.8). As the optokinetic response gain also depends on stimulus parameters such as contrast (Gravot et al., 2017) and spatial frequency (Borst and Egelhaaf, 1989), the difference could be due to the different experimental setups used in the studies and should not be over-interpreted. In any case, the low response performance might indicate a lesser role of the optokinetic system for gaze stabilization in *Xenopus* than in other species like e.g. goldfish (Keng and Anastasio, 1997) or zebrafish which rely on vision for prey capture (Gahtan et al., 2005).

4.2.2 Phase lead of the eyes at low stimulus frequencies

At stimulus frequencies below 0.125 Hz, an effective phase lead of the eye was observed (Fig. 20B). The effect seems to be a product of the quick saturation of the eye plant by the large stimulus amplitude of the low frequency stimuli and the decreasing stimulus velocity approaching the turning point. The eyes follow the stimulus to the maximal deflection, i.e. the extremes of the ocular motor range in the respective direction, and remain at this eccentric position, while the stimulus continues to move. The low velocity of the stimulus approaching the turning point is insufficient to sustain the prevailing firing rate of all units to hold the eye at the eccentric position. With the decline in recruitment of motoneurons, the tension of the extraocular muscle decreases. This – in conjunction with an increase of the firing rate of the antagonistic extraocular motor nerve – causes a movement towards resting position before the stimulus inverses. A phase lead is the consequence.

The frequency-independent phase relation of the maximal firing rate of abducens motoneurons and the maximal deflection of the eye in the on-direction (Fig. 33E) excludes a passive pull-back movement due to mechanical properties of the eye plant as an origin of the phase lead. A learning process as a reason is also unlikely. The cerebellum which is – together with the vestibular nucleus – the critical site for motor learning and adaptation (Dietrich and Straka, 2016), is only anatomical mature starting at stage 52-53 (C.M. Gravot, personal communication, 2016), but the phase lead was already detected at stages before the functional onset of the cerebellum (Fig. 28A_1 and A_2). Moreover, the applied stimulus consisted of only 10 sine waves. In former studies a one hour sustained horizontal sinusoidal oscillation was used to induce an adaptation of the horizontal optokinetic response in form of an increased gain (Nagao, 1988 (rabbit); Shutoh et al., 2006 (mouse)) and a decrease of the eye movement velocity up to two seconds before the change in direction of stimulus velocity (Marsh and Baker, 1997 (goldfish)). Also in the vestibulo-ocular reflex circuitry of *Xenopus laevis* tadpoles,

cerebellum-dependent homeostatic plasticity was found to enable the system to adapt and optimize the encoding of motion signals to maintain an optimal working range for sensory-motor transformations (Dietrich and Straka, 2016). Thus, whether and in which form an adaptation of the optokinetic response is also present in *Xenopus*, remains to be answered.

4.2.3 Linearity of optokinetic response behavior

By increasing the stimulus velocities, the capacity of the optokinetic system to respond to large amplitude stimuli and the velocity profile of the system was tested. For sinusoidal stimulation at 0.125 Hz the gain was maximal at a stimulus peak velocity of ±2 °/s (Fig. 20C). Gains declined in a non-linear manner with higher velocities and larger stimulus amplitudes. The same effect was visible for the eye movement amplitudes, which decreased drastically for stimulus velocities above ±20 °/s (Fig. 19B). The limitations of the system to respond to high stimulus velocities and large amplitudes could either be caused by the sensory or the motor branch of the optokinetic circuitry. A restriction of signal processing on the level of the neuro-muscular connection can be excluded as the phase relation between the motoneuronal peak discharge and the equivalent maximal eye deflection remained constant throughout the relevant velocity and amplitude range (Fig. 33F). The limitations rather arise already at a retinal level. A higher stimulus velocity means an increased spatial displacement of the stimulus pattern over time and a change in the time course of activation of adjacent photoreceptors (Borst and Euler, 2011). This implies a modification of the dynamic interplay of excitatory and inhibitory influences in the lateral interacting retinal elements. The specific spatiotemporal integration properties of the convergent and divergent pathways of the retina (Adelson and Bergen, 1985) finally determine the response features of the optokinetic control circuit (Hartline, 1969). Therefore, the deterioration of the optokinetic response at higher stimulus velocities is likely due to signal processing at the retinal level, rather than restricted by central neuronal properties.

This non-linearity of the optokinetic system in the tadpole also applies to constant velocity stimulation. The maximal gain was observed at ±0.4 °/s and the response performance declined with increasing stimulus velocities. A considerable non-linear reduction of gains started at a stimulus velocity of ±0.5 °/s (Fig. 13) and coincided with the appearance of fast resetting phases (Fig. 12). Thus, the optokinetic system of *Xenopus* tadpoles is designed to compensate slow visual stimuli of moderate amplitudes. At large amplitude stimuli fast resetting phases are elicited to maintain the eyes in the working range.

4.3 TASK SPECIFICITY – NEURONS

A high diversity of eye movement patterns was elicited by optokinetic stimulation. Eye movements span the whole range from slow continuous to fast twitch-like eye movements. The system performs following movements of different frequencies and velocities at sinusoidal stimulation and an optokinetic reflex with slow following and fast resetting phases is the response to constant velocity stimulation. To understand how closely these movement patterns are a direct consequence of the discharge patterns of the controlling motoneurons was the major objective of the neuronal recordings conducted in this study. On the basis of the discharge patterns, abducens motoneurons could be subdivided into two major classes which may contribute to the different features of eye movement patterns in specific ways.

The units of the first type were active during both the slow following and the fast resetting phases of the optokinetic nystagmus (Fig. 31A, insets: small and medium units) as well as during following movements elicited by sinusoidal optokinetic stimulation. All these neurons exhibited a resting discharge and were characterized by an increase of the firing rate in on-direction and a decrease of the firing rate in off-direction (Fig. 32) comparable to the discharge properties of abducens axons with small spike amplitudes in *Rana temporaria* (Dieringer and Precht, 1986). Within this class of motoneurons (Type I), some

units encoded eye position only, while others controlled eye position and velocity (Fig. 33A, B and C). Besides these two subpopulations, a third population of abducens neurons which mediates signals related to retinal image slip velocity was found in frog (Dieringer and Precht, 1986), but could not be identified in *Xenopus* tadpoles. Also in cat, similar discharge classifications were found in abducens neurons and distinguished as phasic, tonic and intermediate (Davis-López de Carrizosa et al., 2011). The tonic neurons with a low recruitment threshold and no interdependence to eye velocity resemble the eye position coding units in *Xenopus* larvae. The intermediate, i.e. tonic-phasic neurons in cats with a high discharge correlation to eye position and eye velocity have similar properties as the second group of type I neurons in the tadpole.

Furthermore, Davis-López de Carrizosa and colleagues (2011) correlated lateral rectus muscle tension to motoneuronal discharges. They demonstrated that muscle tension which increases with increasing eccentric position of the eye is determined by the ensemble innervation and activation of motoneurons. Their findings suggest that similar mechanisms may exist in the tadpole, in that large response amplitudes of the eyes result from high activation dynamics of the motoneurons (Fig. 34A and B, compare eye position and mean firing rate) and that increasing numbers of active units are involved during large amplitude eye movements (Fig. 34C_1 – low frequencies, D_1 – ±10 °/s). This recruitment of motor units for a larger eccentricity of the eye was also observed in multi-unit recordings in the tadpole (Fig. 31). Although the comparison should take into account the difference in species and the correlation of motoneuronal discharges in one case to the tension of the eye muscle (cat) and in the other case to the behavioral response in the form of eye deflection (tadpole), it reveals interesting basic organizational principles of ocular motor control.

The stimulus condition which elicited maximal eye movement performances did not coincide with the stimulus condition which evoked maximal modulation depths of abducens units. Contrary to the actual behavioral response to

optokinetic stimulation (Fig. 20A/C), the dynamic range of the motoneurons was shifted to a lower stimulus frequency and a higher stimulus velocity range (Fig. 34C_2/D_2), provided that the recorded units constitute a representing sample of abducens motoneurons. Consequently, several mechanisms may be responsible for the decline of the optokinetic response of *Xenopus* larvae at low and high stimulus velocities. On the one hand, the low-pass filtering characteristics of the visual system and its sensory processing lead to the reduced performance at higher stimulus velocities (see 4.2.3). On the other hand, the reduced recruitment of motoneurons at low stimulus velocities (Fig. 34D_1) restricts the optokinetic response at these velocities and together with the limitations of the eye plant for large amplitude eye movements sets boundaries to the motor performance of the optokinetic system at large amplitude stimulus conditions.

The second class of units, type II units, fired only during high velocity eye movements such as the fast resetting phases of the optokinetic nystagmus (Fig. 35A). Remarkably, this motoneuron type is also involved in the generation of oscillatory horizontal eye movements during tadpole undulatory swimming. Locomotor efference copies are known to directly recruit extraocular motoneurons during locomotion (Lambert et al., 2012) and hence spike discharge of type II abducens motoneurons is synchronized to the contralateral spinal root discharges during episodes of fictive swimming (Fig. 35B). In contrast to type I motoneurons, type II units were silent at rest and exhibited a burst-like firing pattern instead of gradual changes in discharge rates. Also the amplitude of spikes differed considerably between type I and type II units, with much larger amplitudes found in type II units (Fig. 31A, left inset: large units).

Similar subtypes of response patterns in ocular motoneurons innervating the lateral rectus muscle have been distinguished in *Xenopus* larvae if eye movements were elicited by vestibular instead of visual stimulation (Dietrich et al., 2017). One subgroup coded for head frequency and velocity, the other encoded angular head velocity only. Additionally, they reported a minority of

motoneurons which were insensitive to vestibular stimulation and proposed that these might be the neurons responsible for fast resetting phases of the optokinetic reflex as published in abstract form (Schuller et al., 2014). The amplitude of these units was comparable to the spike amplitude of type II units measured in this study. However, the vestibular study was performed in the absence of visual input and lacks evidence to actual eye movement performance. This issue could be clarified by an experimental design which enables both vestibular and optokinetic stimulation, together with extraocular motor nerve recordings and concurrent imaging of the eye movements. Such an experimental approach should show whether type II units, which are active during fast phases, are also active during vestibular elicited eye movements or silent which would prove the previous prediction that they are motion insensitive.

4.4 SLOW AND FAST COMPONENTS OF THE OPTOKINETIC REFLEX

4.4.1 Slow phase shape

The shape of the slow phase in *Xenopus* tadpoles follows a non-linear time course. After a resetting fast phase a quick pull back movement drives the eye towards its resting position. The eye position around resting position changes linearly (Fig. 12), and the gain is generally high when the eye passes through the resting position (Fig. 14B). With increasing eccentricity in stimulus direction, the velocity of the eye decreases and finally the movement stagnates (Fig. 14A). This non-linear shape of the slow phase can be interpreted as a result of the successive recruitment of extraocular motoneurons and specific characteristics of the eye plant. During nasally directed fast phases, motoneurons in the abducens nerve are silent and the lateral rectus muscle is passively elongated by the sudden contraction of the medial rectus muscle. With relaxation of the latter, i.e. directly after the fast phase and with ongoing visual stimulation in naso-temporal direction, the activity of the type I abducens units increases. A nearly linear increase of firing rate of the single units

(Fig. 32B – red asterisks) as well as a position- and velocity-dependent gradual recruitment of further motoneurons (Fig. 31A, right inset) lead to the controlled contraction of the abducens muscle during the slow phase. When eyes move linearly to more eccentric positions the required muscle force increases exponentially (Davis-López de Carrizosa et al., 2011). Recruitment of motoneurons and their discharge activity, however, do not grow exponentially, but rather reach their maximum and a state of saturation at eccentric eye positions which results in the decrease of eye velocity towards maximal deflection.

These smooth eye movements as observed during slow following movements suggest a type of innervation that allows for a gradual contraction of the eye muscles. Type I units targeting multiply innervated muscle fibers (MIFs) lend themselves to a well-controlled activation of these fibers. The distribution of motor endplates all along these fibers facilitate a progressive contraction of the non-twitch fatigue resistant fibers (Horn and Leigh, 2011). A completely different mechanism governs the singly innervated muscle fibers (SIFs), also called twitch fibers, which respond with an all-or-nothing response to activation of the input motoneurons (Büttner-Ennever et al., 2001). Heterogeneity of twitch and non-twitch muscle fibers was shown in the extraocular muscles of frogs and toads (Nowogrodzka-Zagórska, 1974). As optokinetic behavior of tadpoles mainly comprises slower movements, albeit interrupted by fast resetting movements, the constitution of the lateral and medial rectus muscles in *Xenopus* larvae with a higher number of multiply innervated fibers than singly innervated fibers (M. Faust, personal communication, 2016) is not surprising, although a ratio of slow-tonic to twitch fibers of about 1:1 for the lateral rectus muscle of frogs was reported earlier (Dieringer and Rowlerson, 1984; cited by Straka and Dieringer, 2004).

4.4.2 Overshoot during fast resetting phases

In tadpoles of stages 50-55, eye following movements spanned a maximal ocular motor range of 21.5° (Fig. 9A). The additional activation of type II motor units leads to a rapid acceleration of the eye to a speed of around ±200 °/s (Fig. 15B) during fast phases (FPs). It is assumed that singly innervated muscle fibers of the respective extraocular muscle are maximally contracted by type II unit activity. The burst-like discharge of these units combined with the innervation pattern provokes a rapid contraction of the singly innervated muscle fibers (Spencer and Porter, 2006). The parallel activation of type I units and thus contraction of multiply innervated fibers supports the resetting movement. The eye moves to the maximal mechanical position by overshooting the ocular motor range (Fig. 18). The discharge of type II units comprises only several spikes to kick on the resetting movement and with an activation period of about 0.3 s lasts in most cases shorter than the complete fast phase (duration approx. 0.4 s). Consequently, it is unlikely that the overshoot is directly caused by activity of type II motoneurons. Rather the shape of the fast phase with the quick slow-down of eye velocity towards the reversal point of the eye (Fig. 15C) suggests that the overshoot is caused by the inertia of the eye. Additionally, the discharge of type I units lasts slightly longer than type II unit activity, but decreases quickly at the end of the fast phase. Thus, it seems that type I units influence and stabilize the eye position towards the end of the fast phase and during the overshoot. The antagonistic nerves, which are supposed to activate the respective muscles to shift the eye back into the ocular motor range, are completely silent directly after the fast phase (Fig. 31A, right inset). Hence, the subsequent quick pull-back movement of the eye at the end of the fast phase can also be attributed to the mechanical characteristics of the eye plant. A mismatch between the tensions produced by twitch and non-twitch muscle fibers can provoke such a quick movement even without corresponding motor signals (Dieringer and Precht, 1986). The elastomechanical pulling force of the extraocular muscles (here lateral rectus muscle) has a time constant of about

330 ms in tadpoles (stage 55) (Schuller et al., unpublished data) and is only counteracted by the contraction of the antagonistic muscle pulling the eye against stimulus direction due to the residual activity of type I units at the end of the fast phase.

4.4.3 Fast phase generation

In *Xenopus* tadpoles, the amplitude and duration of fast phases in temporo-nasal (T-N) direction were slightly larger (~3.5°) and longer (~0.03 s) than in naso-temporal (N-T) direction (Fig. 15A). No difference was observed in maximal peak velocities for the two directions (Fig. 15B). The differences in fast phase amplitude in T-N and N-T direction could result from different properties of the medial and lateral rectus muscles. The fact that the lateral rectus muscle has a larger diameter and consists of more fibers than the medial rectus muscle, otherwise having the same ratio of thick and thin fibers (M. Faust, personal communication, 2016), would rather argue for the direction imbalance of the fast phases being the other way around. The differences in muscle properties could, however, be compensated and reversed by an according disparity in innervation and activation strength.

Fast phases are supposed to reset the eye in the orbit to enable a continuous reduction of retinal image slip without driving the eye into a position of maximal deflection. Higher constant stimulus velocities and amplitudes evoked an increase of fast phase quantity (Fig. 16C, D and E) and a decrease of the length of inter-fast-phase-intervals (Fig. 16B). This relation between fast phase quantity and stimulus velocities was also reported in e.g. goldfish (Anastasio, 1996) and turtle (Balaban and Ariel, 1992) and can be attributed to the increase of retinal slip at higher stimulus velocities. One explanatory mechanism was suggested by Anastasio (1996): the visual system provides a noisy velocity signal, which is integrated to provide eye position commands for the slow phase and passed on to the fast phase generator. Thus, the signal is composed of an integrated constant, i.e. the internal velocity signals,

superimposed with a random walk, i.e. the integrated noise. Whenever this signal surpasses the threshold for triggering a fast phase, the burst neurons of the fast phase generator discharge (Anastasio, 1996). Thus, with a higher retinal slip signal the fast phase generator is charged quicker and reaches the activation threshold in a shorter time. The random walk process would also explain the broad range of deflection angles of which fast phases are triggered (Fig. 17).

Schoonheim and colleagues (2010) discovered a small area in the hindbrain of zebrafish which is responsible for the generation of fast phases and proposed that it is homologous or at least functionally equivalent to the burst generator in mammals which drives horizontal saccadic eye movements. Excitatory burst neurons are supposed to directly activate abducens neurons on the ipsilateral side, while inhibitory burst neurons project to the contralateral abducens nucleus, resulting in conjugate fast phases to the ipsilateral side (Schoonheim et al., 2010). The tight coupling of left and right eye during fast resetting phases in tadpoles (Fig. 16A) argues for the presence of such a central neuronal circuit with comparable connectivity in *Xenopus*.

4.5 DIRECTIONAL SYMMETRY OF THE OPTOKINETIC SYSTEM

The optokinetic responses of the eyes in naso-temporal (N-T) and temporo-nasal (T-N) direction during binocular stimulation were largely balanced in *Xenopus* tadpoles, with a minor trend to smaller gain values in T-N direction than in N-T direction (Fig. 13). Though, studies on binocularly tested optokinetic direction asymmetry are rare (Easter, 1972 (goldfish); Gioanni, 1988 (pigeon)), a variety of studies on the optokinetic response to monocular stimulation exist. The majority of afoveate, lateral-eyed animals with conjugated eye movements possess an optokinetic preference for T-N stimulation and show a reduced response to movements from front to back (Fritsches and Marshall, 2002 (butterflyfish); Wallman and Velez, 1985 (chicken); Grüsser-Cornehls and Böhm, 1988 (mouse)). Within the order anura, frog species *Rana*

esculenta (Jardon and Bonaventure, 1992; Yücel et al., 1990) and *Rana temporaria* (Dieringer and Precht, 1982) were reported to exhibit this asymmetry, whereas no data on directionality are available for the clawed frog *Xenopus*. However, tadpoles of *Xenopus laevis* do not show such an asymmetrical directionality of horizontal eye movements which may infer that optokinetic response directionality in the clawed frog differs from that in other anurans. When binocular input to the system was prevented either by a monocular stimulus condition or by severing one optic nerve, the gain of both eyes decreased distinctly (Fig. 21A), but no significant asymmetry in the optokinetic response for one of both stimulus directions was observed in the intact eye (Fig. 21B).

Several criteria were discussed to explain the occurrence of an asymmetric horizontal optokinetic behavior – a missing fovea (Tauber and Atkin, 1968) in combination with a lateral position of the eyes and a small or nonexistent binocular visual field (Gioanni et al., 1981), a high degree of crossing retinofugal fibers in the optic chiasm (Fukuda and Tokita, 1957) and a conjugated movement of the left and right eye (Masseck and Hoffmann, 2009). These criteria also apply to *Xenopus* tadpoles. Indeed, frogs are afoveates (Walls, 1942). The ganglion cell axons of *Xenopus* decussate completely in the optic chiasm (Fig. 29A) and both eyes move highly conjugated in the horizontal plane (Fig. 11; Fig. 16A) due to the presence of abducens interneurons (Straka and Dieringer, 1991, 1993). The eyes in the larvae are positioned laterally (Fig. 9A) and essentially no binocular overlap of the visual fields exists before metamorphic climax beginning at stage 60 (Beazley et al., 1972; Grant and Keating, 1986). Thus, why is the optokinetic response in *Xenopus* tadpoles symmetric? The dramatic change of eye position throughout the ontogenetic development of *Xenopus* might be a key feature for the symmetry of the optokinetic response. With the gradual change in body plan, the lateral facing eyes in the tadpole migrate to a fronto-dorsal position in the adult with an interocular angle in the horizontal meridian of around 110° (Fig. 22A) and a dorsal inclination of 50° (Grant and Keating, 1986). Hence, the binocular visual

field increases from around 30° in developmental stage 60, to 100° in stage 66, and up to 160° in the adult (Udin and Grant, 1999). Although the nasal position of the eyes in the horizontal plane of the adult *Xenopus* is comparable to *Rana*, the eyes are located more dorsally (dorsal inclination *Rana*: 15°) and the binocular field is considerably larger (*Rana*: 100°) (Gaze and Jacobson, 1962). If eye position and size of the binocular field play a crucial role in the symmetry of the optokinetic response, the different response patterns of the frog species might be owed to the different morphology of the adult animals. Whether the symmetry of the optokinetic system in *Xenopus* larvae is sustained over metamorphosis and whether it is a functional aspect important for the lifestyle of the adult animals, needs to be scrutinized in further experiments on the directionality of the horizontal optokinetic response in mature *Xenopus*.

4.6 ONTOGENY OF THE OPTOKINETIC RESPONSE – FROM TADPOLE TO FROG

During ontogeny, the body plan of *Xenopus* is completely remodeled. Reorganization of almost every structure transforms the swimming larva to a tetrapod (Nieuwkoop and Faber, 1994; Sillar et al., 2008). These changes have a fundamental impact on the functionality and interactions of the animals within their environment. Tadpoles are herbivorous feeders living aquatically, and undergoing metamorphosis, develop into sit-and-wait predators with a carnivorous lifestyle. Accordingly, the changes affecting the ocular motor control system during metamorphosis can be seen in mutual adaptation of optokinetic performance and requirements for visual orientation of the animals in their different environments and different behavioral situations.

As gross anatomical change, the location of the eyes transforms from a lateral position with a monocular field of view in the tadpole to a fronto-dorsal orientation of the eye axes providing a binocular overlap of vision in the frog. The visual neuronal network undergoes a corresponding rewiring which involves the development of new ipsilateral retino-thalamic projections to

guarantee binocular processing (Beazley et al., 1972; Gaze and Jacobson, 1962).

Eye movements show also distinct performance differences in parallel to the anatomical changes. Eye movements in *Xenopus* tadpoles cover a range up to 25° in stages 47-55. The ocular motility declines around stage 57 and the ocular motor range is further drastically reduced in stages 60 and older (Fig. 22A) spanning no more than around 8°. This small eye movement amplitude in froglets of *Xenopus* is consistent with previous findings of up to 12° in adult *Rana temporaria* (Dieringer and Precht, 1982). The concurrent ossification of the orbit and the strengthening of the connective tissue and skin during development might reduce the motility of the eyes, but is rather a consequence and not the reason for it. The narrowing of the ocular motor range during development has to be seen in connection with other changes in the body plan. The body plan of the tadpole is adapted to undulatory swimming (Combes et al., 2004) and the head is conform with the body, so that moving the eyes in the head is the only possibility to stabilize gaze during locomotion. For this purpose eye movements need to cover an ocular motor range that is large enough to compensate for the body undulations while swimming. The differentiation of a head and a neck during metamorphosis uncouples the head with the eyes from the body. Concurrently, locomotor movements shift to more linear motion. In the case of the mainly propulsive forward locomotion in adult frogs (Rauscent et al., 2006), the necessary ocular motor adjustment to stabilize gaze is small since the head is directed straight forward without horizontal right-left oscillation and thus the eye axes deviate little from the moving direction. In addition, the ability to move the head independently of the body enables adult frogs to use head movements to stabilize gaze. A coadaptation of the two motor systems controlling eye and head movements facilitates the reduction of the visual input signal by slow phase head movements and thereby prevents a saturation of the ocular motor system with its restricted working range, resulting in a relatively large contribution of the head to gaze stabilization in frogs (Dieringer, 1987).

Substantial changes go along with the development of the tadpole during metamorphic climax in the response of the eyes to optokinetic stimulation and the functioning of the optokinetic reflex (OKR). In the youngest stages (45/46) investigated in this study visually induced eye movements occur but performance is inconsistent and of low gain (Fig. 25). An optokinetic reflex with slow following and fast resetting movements was observed starting at stage 47 (Fig. 24) and the quantity of fast phases increased in older stages 50-55 (Fig. 27A). This included a tight correlation of left and right eye concordant movements manifested in a strong linkage of slow and fast phases in both eyes (Fig. 16A). The highest correlation of eye movements was observed in stages 47-49 and only slightly declined in stage 50-55 (Fig. 23). With ongoing development and starting at metamorphic climax a complete loss of correlation of both eyes was observed. The gradual increase of eye movement performance, the vanishing of the optokinetic reflex, especially the fast phases, and the loss of the left to right eye correlation coincide with the transformation from the “immobile” embryo over the undulatory swimming tadpole to the mainly linearly forward moving frog.

Self-motion increases the need for gaze stabilization. Developmental stage 45 was the youngest stage investigated in this study. It would not be surprising if visually elicited eye movements occur already at younger stages than 45, as *Xenopus* larvae start swimming at stage 42 (Nieuwkoop and Faber, 1994). The onset of active feeding at stage 45 (Nieuwkoop and Faber, 1994) and thus the requirement of more sustained episodes of locomotor activity, might trigger the appearance of eye following responses. The onset of the horizontal optokinetic reflex at stage 47 coincides with the full maturation of swimming activity (Currie et al., 2016). This concurrence of developmental events hints to a functional link of swimming behavior to the development of optokinetic performance. Further, a massive restructuring of the spinal networks during metamorphosis, affects locomotor as well as ocular motor circuitries throughout. A complete remodeling of central pattern generation in the spinal cord underlies the change of locomotor pattern (Beyeler et al., 2008; Combes et

al., 2004). For young frogs there is no behavioral advantage of concordantly coupled eye movements, whereas a convergence enables them to stabilize a visual target also during linear propulsion (von Uckermann et al., 2013). As there is no more need to compensate for horizontal swimming movements and as angular deviations remain relatively small, slow eye movements and head movements are sufficient for image stabilization. Fast phases are evidently not further needed, which concurs with a complete absence of the latter (Fig. 27B). If fast contractions of the recti muscles in adults are induced, the retractor bulbi muscles are co-activated, resulting in a quick retraction of the eye into the orbit (Dieringer et al., 1982), but not in a fast resetting phase. The loss of fast phases appears with the beginning of the critical intermediate metamorphic period (stages 58-63) when limbs and tail coexist and participate in locomotion (Combes et al., 2004). The question whether the fast phase generating circuit is omitted completely or rewired for other control tasks needs to be investigated in further experiments.

4.7 BIOLOGICAL IMPLICATIONS

The OKR in the tadpole and its nearly absence in the frog can be clearly understood as adaptations to the specific forms of locomotion, feeding and prey catching behavior of the animals. Also in its details like the response dynamics of the optokinetic system in tadpoles, the close adaptation to the specific needs can be recognized.

The visually controlled eye movements must be considered in the context of the concurrently active vestibulo-ocular reflex (VOR) as both systems act together on the common final output, on the extraocular muscles (Robinson, 1981). The optokinetic circuitry forms a closed-loop system. It provides online feedback about the retinal slip and by elicitation of accordant eye movements optimizes the compensation provoked by the fast-acting VOR. Also the working ranges of the two systems complement each other. The semicircular canals of the vestibular system sense angular head acceleration in an intermediate to

high frequency range (Straka and Simmers, 2011). The optokinetic system as a low-pass filter is consequently ideally suited to respond to visual motion at low frequencies and to act in situations where angular acceleration is insufficient to properly elicit reflexive eye movements by the semicircular canals.

This cooperation of the two systems may explain why in experiments on the optokinetic system in head fixed tadpoles the gain generally never reached a higher value than 0.7 at constant velocity stimulation (Fig. 13) and 0.4 at sinusoidal stimulation (Fig. 20A and C). In a freely moving animal the VOR and OKR would have cooperated and the VOR would have contributed the missing drive to the eye movements to stabilize the visual environment. A gain value of one would be necessary to catch up and entirely compensate the retinal slip, which is not to be expected in afoveate *Xenopus*. Without a fovea, a complete compensation does not provide significant additional benefit.

The onset of the angular VOR was determined to be at stage 49 (Lambert et al., 2008). Although the hair cells and the underlying neuronal basis of the vestibulo-ocular system are already operational in younger stages, the small diameters of the semicircular canals restrict detection of head acceleration (Lambert et al., 2008). As visually elicited eye movements were detected at stage 45 and the onset of the optokinetic reflex can be found around stage 47, young tadpoles up to aVOR onset at stage 49 have to rely on the optokinetic system for gaze stabilization. Visually induced eye movements generally decline during metamorphic climax, and the working range of the optokinetic system is shifted towards lower frequencies and velocities (Fig. 28A_4/A_5). The decrease of swimming frequency during larval development diminishes also the dynamic range of angular head motion related vestibular signals (Hänzi and Straka, 2017). Again, the transformation from undulatory swimming tadpole to calmly sitting frog changes the requirements for both systems as larval angular body and head movements are replaced by no or primarily linear forward-directed body movements in the frog.

The functional role of the optokinetic system in *Xenopus* as an afoveate vertebrate is a topic worth to be discussed in the larger context of body movements and visual orientation. More than the optokinetic and the vestibular system, spinal efference copy-derived signals seem to play a major role for gaze stabilization during rhythmic locomotion (Combes et al., 2008; Lambert et al., 2012). Efference copies of the signals driving tail and limb musculature are directly projected from the central pattern generators in the spinal cord onto the extraocular motor nuclei. Contralateral projections in tadpoles provoke synchronous oscillatory eye movements of the left and right eye in the horizontal plane which counteract body movement during right-left undulation of the tail (Combes et al., 2008). Ipsilateral projections in frogs elicit convergent eye movements during linear forward movement by limb kicking (von Uckermann et al., 2013). Vestibular signals were shown to be selectively suppressed during central pattern generator activity during locomotion (Lambert et al., 2012). The question arises in which way optokinetic signals and efference copies interact (Fig. 35B) – do both signals cooperate or do efference copies cancel out the optokinetic signal? Hypothesizing the latter, would imply, that the vestibular and the optokinetic system both are of minor importance for image stabilization during locomotion. The optokinetic system in *Xenopus* would thus rather fulfill the function of detecting passive optic flow as e.g. generated by the water stream around the tadpole or slowly moving prey for the frog.

4.8 CONCLUSION

This study revealed a robust horizontal optokinetic performance in larval *Xenopus laevis*. Eye movements were limited to lower frequencies and velocities due to the long latency of retinal processing, while the response amplitude was restricted by the ocular motor range of up to 20°. Large amplitude stimuli elicited an optokinetic reflex. During slow following and fast resetting phases of the reflex a differential recruitment of two different subtypes of abducens motoneurons became apparent. Type I units coded for eye position

– and some in addition for eye velocity – observable by the successive activation of these units with ongoing deflection of the eye during slow following movements and by a prolonged firing during fast phase overshoot. The burst-like discharge of type II units during fast phases provoked eye velocities of up to 200 °/s. A drastic decline of optokinetic performance during metamorphosis came along with the change of body plan and locomotor pattern from swimming tadpole to limb-kicking frog.

The smooth eye movements evoked by type I units and the fast reset by type II units suggest the activation of different extraocular muscle fibers. Simultaneous recording and labeling of extraocular motoneurons would directly demonstrate a cooperative functionality of the motoneurons and their target muscle fibers. Analysis of the neuro-muscular innervation patterns and fiber structures could further help to categorize and classify type I and II units. Calcium imaging of abducens motoneurons and simultaneous extracellular recordings of the latter could show whether the units are topographically represented in the motor nucleus according to their task-specificity.

New insight into an integration of vestibular and optokinetic commands at the level of the extraocular motor nuclei could emerge from experiments that allow both vestibular and optokinetic stimulation. Analysis of response properties of the same single units during optokinetic stimulation on the one hand and vestibular stimulation on the other hand could identify a potential overlap of the motoneuronal classifications in this study (OKR) and the two recently described motion-sensitive subgroups of abducens neurons (VOR) (Dietrich et al., 2017). Additionally, mismatch experiments, i.e. stimulation of both systems in cooperative or antagonistic directions, could shed light on the adaptability of the working range of the systems.

The reduction of ocular motor range, the decline of optokinetic performance and the almost complete loss of fast phases during metamorphosis coincides with the transformation of body plan and change of locomotor pattern from tail-based undulatory swimming in tadpoles to limb-based linear forward

propulsion in frogs. While the optokinetic response characteristics of tadpoles are similar to that of other lateral-eyed, swimming vertebrates with a comparable lifestyle as e.g. goldfish, the limited optokinetic response behavior in the only sporadically moving frogs resembles that of bottom dwelling fish like toadfish (Dieringer et al., 1992). These findings support the concept that the optokinetic response performance is adapted to the species-specific requirements of the animal. The transformations in the underlying optokinetic circuitry could be tracked by anatomical tracing experiments at different developmental stages. An ontogenetic approach as in zebrafish (Schoonheim et al., 2010) could identify the fast phase generating structures in the hindbrain of *Xenopus* and give an answer to whether the missing fast phases in adult frogs are due to a loss of the neuronal substrate during metamorphosis or to a change in function only.

Semi-intact *in vitro* preparations of *Xenopus laevis* allow various combinations of methods and manipulation of the optokinetic circuitry – e.g. selective lesioning of neural structures, pharmacological manipulation, electrophysiological intra- and extracellular recordings and behavioral studies. The complete transformation of body plan from larval to adult organism makes *Xenopus* a unique animal model for studying the basic control mechanisms of image stabilization during locomotion in vertebrates. The findings in this study of the optokinetic system complement the existing knowledge of the vestibulo-ocular reflex and spinal efference copy signaling in *Xenopus*. Interaction of optokinetic and vestibular systems and their interplay with spinal efference copy signals on the background of two different locomotor strategies can all be investigated in the same species. Therefore, further studies on semi-intact preparations of *Xenopus laevis* open up the possibility for an integrative approach proceeding from investigation of the isolated functions to the analysis of the integrated functionality of systems.

BIBLIOGRAPHY

Adelson, E.H., Bergen, J.R., 1985. Spatiotemporal energy models for the perception of motion. J Opt Soc Am A 2, 284-299.

Allum, J.H., Graf, W., Dichgans, J., Schmidt, C.L., 1976. Visual-vestibular interactions in the vestibular nuclei of the goldfish. Exp Brain Res 26, 463-485.

Anastasio, T.J., 1996. A random walk model of fast-phase timing during optokinetic nystagmus. Biol Cybern 75, 1-9.

Arendt, D., Hausen, H., Purschke, G., 2009. The 'division of labour' model of eye evolution. Philos Trans R Soc Lond B Biol Sci 364, 2809-2817.

Ashley-Ross, M.A., Hsieh, S.T., Gibb, A.C., Blob, R.W., 2013. Vertebrate land invasions - past, present, and future: an introduction to the symposium. Integr Comp Biol 53, 192-196.

Baker, R., Evinger, C., McCrea, R.A., 1981. Some thoughts about the three neurons in the vestibulo-ocular reflex. Ann NY Acad Sci 374, 171-188.

Baker, R., Highstein, S.M., 1975. Physiological identification of interneurons and motoneurons in the abducens nucleus. Brain Res 91, 292-298.

Balaban, C.D., Ariel, M., 1992. A "beat-to-beat" interval generator for optokinetic nystagmus. Biol Cybern 66, 203-216.

Barlow, H.B., Hill, R.M., 1963. Selective sensitivity to direction of movement in ganglion cells of the rabbit retina. Science 139, 412-414.

Beazley, L., Keating, M.J., Gaze, R.M., 1972. The appearance, during development, of responses in the optic tectum following visual stimulation of the ipsilateral eye in *Xenopus laevis*. Vision Res 12, 407-410.

Beck, J.C., Gilland, E., Baker, R., Tank, D.W., 2004a. Instrumentation for measuring oculomotor performance and plasticity in larval organisms. Methods Cell Biol 76, 385-413.

Beck, J.C., Gilland, E., Tank, D.W., Baker, R., 2004b. Quantifying the ontogeny of optokinetic and vestibuloocular behaviors in zebrafish, medaka, and goldfish. J Neurophysiol 92, 3546-3561.

Beraneck, M., Cullen, K.E., 2007. Activity of vestibular nuclei neurons during vestibular and optokinetic stimulation in the alert mouse. J Neurophysiol 98, 1549-1565.

Berry, M.J., Brivanlou, I.H., Jordan, T.A., Meister, M., 1999. Anticipation of moving stimuli by the retina. Nature 398, 334-338.

Beyeler, A., Metais, C., Combes, D., Simmers, J., Le Ray, D., 2008. Metamorphosis-induced changes in the coupling of spinal thoraco-lumbar motor outputs during swimming in *Xenopus laevis*. J Neurophysiol 100, 1372-1383.

Biewener, A.A., 2003. Animal locomotion. OUP, Oxford, NY.

Birukow, G., 1937. Untersuchungen über den optischen Drehnystagmus und über die Sehschärfe des Grasfrosches (*Rana temporaria*). Z Vgl Physiol 25, 92-142.

Birukow, G., 1952. Studien über statisch-optisch ausgelöste Kompensationsbewegungen und Körperhaltung bei Amphibien. Z Vgl Physiol 34, 448-472.

Blanks, R.H., Curthoys, I.S., Markham, C.H., 1975. Planar relationships of the semicircular canals in man. Acta Otolaryngol 80, 185-196.

Blanks, R.H.I., Precht, W., 1976. Functional characterization of primary vestibular afferents in the frog. Exp Brain Res 25, 369-390.

Bonaventure, N., Wioland, N., Jardon, B., 1985. On GABAergic mechanisms in the optokinetic nystagmus of the frog: Effects of bicuculline, allyglycine and SR 95103, a new GABA antagonist. Eur J Pharmacol 118, 61-68.

Borst, A., Egelhaaf, M., 1989. Principles of visual motion detection. Trends Neurosci 12, 297-306.

Borst, A., Euler, T., 2011. Seeing things in motion: models, circuits, and mechanisms. Neuron 71, 974-994.

Brändli, A.W., 2004. Prospects for the *Xenopus* embryo model in therapeutics technologies. Chimia 58, 694-702.

Brecha, N., Karten, H.J., 1979. Accessory optic projections upon oculomotor nuclei and vestibulocerebellum. Science 203, 913-916.

Briggman, K.L., Helmstaedter, M., Denk, W., 2011. Wiring specificity in the direction-selectivity circuit of the retina. Nature 471, 183-188.

Büttner-Ennever, J.A., Horn, A.K., Scherberger, H., D'Ascanio, P., 2001. Motoneurons of twitch and nontwitch extraocular muscle fibers in the abducens, trochlear, and oculomotor nuclei of monkeys. J Comp Neurol 438, 318-335.

Büttner, U., Büttner-Ennever, J.A., 2006. Present concepts of oculomotor organization. Prog Brain Res 151, 1-42.

Butz-Kuenzer, E., 1957. Optische und labyrinthäre Auslösung der Lagereaktionen bei Amphibien. Z Tierpsychol 14, 429-447.

Cannon, S.C., Robinson, D.A., 1987. Loss of the neural integrator of the oculomotor system from brain stem lesions in monkey. J Neurophysiol 57, 1383-1409.

Clifford, C.W., Ibbotson, M.R., 2002. Fundamental mechanisms of visual motion detection: models, cells and functions. Prog Neurobiol 68, 409-437.

Cochran, S.L., Dieringer, N., Precht, W., 1984. Basic optokinetic-ocular reflex pathways in the frog. J Neurosci 4, 43-57.

Cohen, B., Matsuo, V., Raphan, T., 1977. Quantitative analysis of the velocity characteristics of optokinetic nystagmus and optokinetic after-nystagmus. J Physiol 270, 321-344.

Collewijn, H., 1969. Optokinetic eye movements in the rabbit: Input-output relations. Vision Res 9, 117-132.

Collewijn, H., 1975. Oculomotor areas in the rabbits midbrain and pretectum. J Neurobiol 6, 3-22.

Collewijn, H., 1980. Sensory control of optokinetic nystagmus in the rabbit. Trends Neurosci 3, 277-280.

Combes, D., Le Ray, D., Lambert, F.M., Simmers, J., Straka, H., 2008. An intrinsic feed-forward mechanism for vertebrate gaze stabilization. Curr Biol 18, 241-243.

Combes, D., Merrywest, S.D., Simmers, J., Sillar, K.T., 2004. Developmental segregation of spinal networks driving axial- and hindlimb-based locomotion in metamorphosing *Xenopus laevis*. J Physiol 559, 17-24.

Currie, S.P., Combes, D., Scott, N.W., Simmers, J., Sillar, K.T., 2016. A behaviorally related developmental switch in nitrergic modulation of locomotor rhythmogenesis in larval *Xenopus* tadpoles. J Neurophysiol 115, 1446-1457.

Davis-López de Carrizosa, M.A., Morado-Diaz, C.J., Miller, J.M., de la Cruz, R.R., Pastor, A.M., 2011. Dual encoding of muscle tension and eye position by abducens motoneurons. J Neurosci 31, 2271-2279.

Debowy, O., Baker, R., 2011. Encoding of eye position in the goldfish horizontal oculomotor neural integrator. J Neurophysiol 105, 896-909.

Delgado-Garcia, J.M., Del Pozo, F., Baker, R., 1986a. Behavior of neurons in the abducens nucleus of the alert cat--I. Motoneurons. Neuroscience 17, 929-952.

Delgado-Garcia, J.M., Del Pozo, F., Baker, R., 1986b. Behavior of neurons in the abducens nucleus of the alert cat--II. Internuclear neurons. Neuroscience 17, 953-973.

Delgado-Garcia, J.M., Vidal, P.P., Gomez, C., Berthoz, A., 1989. A neurophysiological study of prepositus hypoglossi neurons projecting to oculomotor and preoculomotor nuclei in the alert cat. Neuroscience 29, 291-307.

Dieringer, N., 1987. The role of compensatory eye and head movements for gaze stabilization in the unrestrained frog. Brain Res 404, 33-38.

Dieringer, N., Daunicht, W.J., 1986. Image fading - a problem for frogs? Naturwissenschaften 73, 330-332.

Dieringer, N., Precht, W., 1982. Compensatory head and eye movements in the frog and their contribution to stabilization of gaze. Exp Brain Res 47, 394-406.

Dieringer, N., Precht, W., 1986. Functional organization of eye velocity and eye position signals in abducens motoneurons of the frog. J Comp Physiol A 158, 179-194.

Dieringer, N., Precht, W., Blight, A.R., 1982. Resetting fast phases of head and eye and their linkage in the frog. Exp Brain Res 47, 407-416.

Dieringer, N., Reichenberger, I., Graf, W., 1992. Differences in optokinetic and vestibular ocular reflex performance in teleosts and their relationship to different life styles. Brain Behav Evol 39, 289-304.

Dieringer, N., Rowlerson, A., 1984. Fiber types in the extraocular muscles of the frog. J Physiol 353, 50.

Dietrich, H., Glasauer, S., Straka, H., 2017. Functional organization of vestibulo-ocular responses in abducens motoneurons. J Neurosci 37, 4032-4045.

Dietrich, H., Straka, H., 2016. Prolonged vestibular stimulation induces homeostatic plasticity of the vestibulo-ocular reflex in larval *Xenopus laevis*. Eur J Neurosci 44, 1787-1796.

Distler, C., Hoffmann, K.P., 2003. Development of the optokinetic response in macaques: a comparison with cat and man. Ann NY Acad Sci 1004, 10-18.

Distler, C., Hoffmann, K.P., 2011. The optokinetic reflex. In: Liversedge, S.P., Gilchrist, I., Everling, S. (Eds.), The Oxford handbook of eye movements. OUP, New York, NY, pp. 65-83.

Distler, C., Vital-Durand, F., Korte, R., Korbmacher, H., Hoffmann, K.P., 1999. Development of the optokinetic system in macaque monkeys. Vision Res 39, 3909-3919.

Easter, S.S., Jr., 1972. Pursuit eye movements in goldfish (Carassius auratus). Vision Res 12, 673-688.

Euler, T., Detwiler, P.B., Denk, W., 2002. Directionally selective calcium signals in dendrites of starburst amacrine cells. Nature 418, 845-852.

Evinger, C., 1988. Extraocular motor nuclei: location, morphology and afferents. Rev Oculomot Res 2, 81-117.

Ezure, K., Graf, W., 1984. A quantitative analysis of the spatial organization of the vestibulo-ocular reflexes in lateral- and frontal-eyed animals--I. Orientation of semicircular canals and extraocular muscles. Neuroscience 12, 85-93.

Fan, T.X., Weber, A.E., Pickard, G.E., Faber, K.M., Ariel, M., 1995. Visual responses and connectivity in the turtle pretectum. J Neurophysiol 73, 2507-2521.

Fite, K.V., 1985. Pretectal and accessory-optic visual nuclei of fish, amphibia and reptiles: theme and variations. Brain Behav Evol 26, 71-90.

Fite, K.V., Kwei-Levy, C., Bengston, L., 1989. Neurophysiological investigation of the pretectal nucleus lentiformis mesencephali in Rana pipiens. Brain Behav Evol 34, 164-170.

Fritsches, K.A., Marshall, N.J., 2002. Independent and conjugate eye movements during optokinesis in teleost fish. J Exp Biol 205, 1241-1252.

Fritzsch, B., Beisel, K.W., 2003. Molecular conservation and novelties in vertebrate ear development. Curr Top Dev Biol 57, 1-44.

Fukuda, T., Tokita, T., 1957. Relation of the direction of optical stimulation to the type of reflex of the oculomotor muscles. Acta Otolaryngol 48, 415-424.

Gahtan, E., Tanger, P., Baier, H., 2005. Visual prey capture in larval zebrafish is controlled by identified reticulospinal neurons downstream of the tectum. J Neurosci 25, 9294-9303.

Gaze, R.M., Jacobson, M., 1962. The projection of the binocular visual field on the optic tecta of the frog. Exp Physiol 47, 273-280.

Gehring, W.J., 2011. Chance and necessity in eye evolution. Genome Biol Evol 3, 1053-1066.

Gilland, E., Baker, R., 2005. Evolutionary patterns of cranial nerve efferent nuclei in vertebrates. Brain Behav Evol 66, 234-254.

Gioanni, H., 1988. Stabilizing gaze reflexes in the pigeon (*Columba livia*). I. Horizontal and vertical optokinetic eye (OKN) and head (OCR) reflexes. Exp Brain Res 69, 567-582.

Gioanni, H., Rey, J., Villalobos, J., Bouyer, J.J., Gioanni, Y., 1981. Optokinetic nystagmus in the pigeon (Columba livia). I. Study in monocular and binocular vision. Exp Brain Res 44, 362-370.

Giolli, R.A., Blanks, R.H., Lui, F., 2006. The accessory optic system: basic organization with an update on connectivity, neurochemistry, and function. Prog Brain Res 151, 407-440.

Goldberg, J.M., Wilson, V.J., Cullen, K.E., Angelaki, D.E., Broussard, D.M., Büttner-Ennever, J., Fukushima, K., Minor, L.B., 2012. The vestibular system: A sixth sense. OUP, Oxford, NY.

Gordon, J., Hood, D.C., 1976. Anatomy and physiology of the frog retina In: Fite, K.V. (Ed.), The amphibian visual system: A multidisciplinary approach. Academic Press, New York, NY, pp. 29-86.

Graf, W., Gilland, E., McFarlane, M., Knott, L., Baker, R., 2002. Central pathways mediating oculomotor reflexes in an elasmobranch, *Scyliorhinus canicula*. Biol Bull 203, 236-238.

Grant, S., Keating, M.J., 1986. Ocular migration and the metamorphic and postmetamorphic maturation of the retinotectal system in *Xenopus laevis*: an autoradiographic and morphometric study. J Embryol Exp Morphol 92, 43-69.

Gravot, C.M., Knorr, A.G., Glasauer, S., Straka, H., 2017. It's not all black and white: It's not all black and white: visual scene parameters influence optokinetic reflex performance in *Xenopus laevis* tadpoles. J Exp Biol 220, 4213-4224.

Gruberg, E.R., Grasse, K.L., 1984. Basal optic complex in the frog (*Rana pipiens*): a physiological and HRP study. J Neurophysiol 51, 998-1010.

Grüsser-Cornehls, U., Böhm, P., 1988. Horizontal optokinetic ocular nystagmus in wildtype (B6CBA+/+) and weaver mutant mice. Exp Brain Res 72, 29-36.

Grüsser, O.J., Grüsser-Cornehls, U., 1976. Neurophysiology of the anuran visual system. In: Llinas, R., Precht, W. (Eds.), Frog neurobiology: A handbook. Springer Berlin Heidelberg, pp. 297-385.

Hänzi, S., Straka, H., 2017. Developmental changes in head movement kinematics during swimming in *Xenopus laevis* tadpoles. J Exp Biol 220, 227-236.

Hartline, H.K., 1969. Visual receptors and retinal interaction. Science 164, 270-278.

Hess, B.J., Precht, W., Reber, A., Cazin, L., 1985. Horizontal optokinetic ocular nystagmus in the pigmented rat. Neuroscience 15, 97-107.

Hoffmann, K.P., Garipis, N., Distler, C., 2004. Optokinetic deficits in albino ferrets (*Mustela putorius furo*): a behavioral and electrophysiological study. J Neurosci 24, 4061-4069.

Holstege, G., Collewijn, H., 1982. The efferent connections of the nucleus of the optic tract and the superior colliculus in the rabbit. J Comp Neurol 209, 139-175.

Horn, A.K.E., Leigh, R.J., 2011. The anatomy and physiology of the ocular motor system. In: Kennard, C., Leigh, R.J. (Eds.), Neuro-Ophthalmology, 3 ed. Elsevier, pp. 21-69.

Huang, Y.Y., Neuhauss, S.C., 2008. The optokinetic response in zebrafish and its applications. Front Biosci 13, 1899-1916.

Ilg, U.J., 1997. Slow eye movements. Prog Neurobiol 53, 293-329.

Jardon, B., Bonaventure, N., 1992. The pretectal cholinergic system is involved through two opposite ways in frog monocular OKN asymmetry. Exp Brain Res 90, 72-78.

Katte, O., Hoffmann, K.P., 1980. Direction specific neurons in the pretectum of the frog (*Rana esculenta*). J Comp Physiol 140, 53-57.

Keng, M.J., Anastasio, T.J., 1997. The horizontal optokinetic response of the goldfish. Brain Behav Evol 49, 214-229.

Klar, M., Hoffmann, K.P., 2002. Visual direction-selective neurons in the pretectum of the rainbow trout. Brain Res Bull 57, 431-433.

Lamb, T.D., 2013. Evolution of phototransduction, vertebrate photoreceptors and retina. Prog Retin Eye Res 36, 52-119.

Lamb, T.D., Arendt, D., Collin, S.P., 2009. The evolution of phototransduction and eyes. Philos Trans R Soc Lond B Biol Sci 364, 2791-2793.

Lamb, T.D., Collin, S.P., Pugh, E.N., 2007. Evolution of the vertebrate eye: opsins, photoreceptors, retina and eye cup. Nat Rev Neurosci 8, 960-976.

Lambert, F.M., Beck, J.C., Baker, R., Straka, H., 2008. Semicircular canal size determines the developmental onset of angular vestibuloocular reflexes in larval *Xenopus*. J Neurosci 28, 8086-8095.

Lambert, F.M., Combes, D., Simmers, J., Straka, H., 2012. Gaze stabilization by efference copy signaling without sensory feedback during vertebrate locomotion. Curr Biol 22, 1-10.

Land, M.F., 1999. Motion and vision: why animals move their eyes. J Comp Physiol A 185, 341-352.

Land, M.F., 2015. Eye movements of vertebrates and their relation to eye form and function. J Comp Physiol A 201, 195-214.

Lazar, G., 1989. Altering the direction of optokinetic head nystagmus: a lesion study and a hypothetical model. Exp Brain Res 77, 193-200.

Lazar, G., Bennani, S., Toth, P., 1989. Neuronal pathways involved in the optokinetic head nystagmus of the frog. Acta Biol Hung 40, 107-120.

Lazar, G., Toth, P., Csank, G., Kicliter, E., 1983. Morphology and location of tectal projection neurons in frogs: a study with HRP and cobalt-filling. J Comp Neurol 215, 108-120.

Liem, K.F., Bemis, W., Walker, W.F., Grande, L., 2001. Functional anatomy of the vertebrates: An evolutionary perspective, 3 ed. Harcourt College Publishers, Fort Worth, TX.

Lopez-Barneo, J., Darlot, C., Berthoz, A., Baker, R., 1982. Neuronal activity in prepositus nucleus correlated with eye movement in the alert cat. J Neurophysiol 47, 329-352.

Luksch, H., Walkowiak, W., Munoz, A., ten Donkelaar, H.J., 1996. The use of *in vitro* preparations of the isolated amphibian central nervous system in neuroanatomy and electrophysiology. J Neurosci Methods 70, 91-102.

Maioli, C., Precht, W., 1984. The horizontal optokinetic nystagmus in the cat. Exp Brain Res 55, 494-506.

Marsh, E., Baker, R., 1997. Normal and adapted visuooculomotor reflexes in goldfish. J Neurophysiol 77, 1099-1118.

Martinez-Morales, J.R., Wittbrodt, J., 2009. Shaping the vertebrate eye. Curr Opin Genet Dev 19, 511-517.

Masseck, O., Röll, B., Hoffmann, K.P., 2008. The optokinetic reaction in foveate and afoveate geckos. Vision Res 48, 765-772.

Masseck, O.A., Hoffmann, K.-P., 2009. Comparative neurobiology of the optokinetic reflex. Ann NY Acad Sci 1164, 430-439.

Matesz, C., Kulik, A., Bacskai, T., 2002. Ascending and descending projections of the lateral vestibular nucleus in the frog *Rana esculenta*. J Comp Neurol 444, 115-128.

McKenna, O.C., Wallman, J., 1985. Accessory optic system and pretectum of birds: comparisons with those of other vertebrates. Brain Behav Evol 26, 91-116.

Miles, F.A., Lisberger, S.G., 1981. Plasticity in the vestibulo-ocular reflex: a new hypothesis. Annu Rev Neurosci 4, 273-299.

Montgomery, N., Fite, K.V., Bengston, L., 1981. The accessory optic system of *Rana pipiens*: Neuroanatomical connections and intrinsic organization. J Comp Neurol 203, 595-612.

Nagao, S., 1988. Behavior of floccular Purkinje cells correlated with adaptation of horizontal optokinetic eye movement response in pigmented rabbits. Exp Brain Res 73, 489-497.

Nieuwkoop, P.D., Faber, J., 1994. Normal table of *Xenopus laevis* (Daudin): a systematical and chronological survey of the development from the fertilized egg till the end of metamorphosis. Garland Publishing, New York, NY.

Nilsson, D.E., 2013. Eye evolution and its functional basis. Vis Neurosci 30, 5-20.

Northcutt, R.G., Kicliter, E., 1980. Organization of the amphibian telencephalon. In: Ebbesson, S.O.E. (Ed.), Comparative neurology of the telencephalon. Springer US, pp. 203-255.

Nowogrodzka-Zagórska, M., 1974. The organization of extraocular muscles in Anura. Acta Anat (Basel) 87, 22-44.

Pasik, P., Pasik, T., Krieger, H.P., 1959. Effects of cerebral lesions upon optokinetic nystagmus in monkeys. J Neurophysiol 22, 297-304.

Pastor, A.M., De la Cruz, R.R., Baker, R., 1994. Eye position and eye velocity integrators reside in separate brainstem nuclei. Proc Natl Acad Sci USA 91, 807-811.

Prasad, S., Galetta, S.L., 2011. Anatomy and physiology of the afferent visual system. Handb Clin Neurol 102, 3-19.

Precht, W., 1979. Vestibular mechanisms. Annu Rev Neurosci 2, 265-289.

Purves, D., Augustine, G.J., Fitzpatrick, D., Hall, W.C., LaMantia, A.-S., White, L.E., 2012. Neuroscience, 5 ed. Sinauer Associates, Inc, Sunderland, MA.

Rauscent, A., Le Ray, D., Cabirol-Pol, M.J., Sillar, K.T., Simmers, J., Combes, D., 2006. Development and neuromodulation of spinal locomotor networks in the metamorphosing frog. J Physiol Paris 100, 317-327.

Robinson, D.A., 1981. Control of eye movements. In: Brooks, V.B. (Ed.), Comprehensive physiology: The nervous system, motor control (Supplement 2). American Physiological Society, Bethesda, MD, pp. 1275-1320.

Schoonheim, P.J., Arrenberg, A.B., Del Bene, F., Baier, H., 2010. Optogenetic localization and genetic perturbation of saccade-generating neurons in zebrafish. J Neurosci 30, 7111-7120.

Schuller, J.M., Knorr, A.G., Glasauer, S., Straka, H., 2014. Task-specific activation of extraocular motoneurons in *Xenopus laevis*. Program No. 247.06/HH8. 2014 Neuroscience Meeting Planner. Washington, DC: Society for Neuroscience, 2014. Online.

Shutoh, F., Ohki, M., Kitazawa, H., Itohara, S., Nagao, S., 2006. Memory trace of motor learning shifts transsynaptically from cerebellar cortex to nuclei for consolidation. Neuroscience 139, 767-777.

Sillar, K.T., Combes, D., Ramanathan, S., Molinari, M., Simmers, J., 2008. Neuromodulation and developmental plasticity in the locomotor system of anuran amphibians during metamorphosis. Brain Res Rev 57, 94-102.

Simpson, J.I., Graf, W., 1981. Eye-muscle geometry and compensatory eye movements in lateral-eyed and frontal-eyed animals. Ann NY Acad Sci 374, 20-30.

Spencer, R.F., Porter, J.D., 2006. Biological organization of the extraocular muscles. Prog Brain Res 151, 43-80.

Straka, H., Dieringer, N., 1991. Internuclear neurons in the ocular motor system of frogs. J Comp Neurol 312, 537-548.

Straka, H., Dieringer, N., 1993. Electrophysiological and pharmacological characterization of vestibular inputs to identified frog abducens motoneurons and internuclear neurons *in vitro*. Eur J Neurosci 5, 251-260.

Straka, H., Dieringer, N., 2004. Basic organization principles of the VOR: lessons from frogs. Prog Neurobiol 73, 259-309.

Straka, H., Gilland, E., Baker, R., 1998. Rhombomeric organization of brainstem motor neurons in larval frogs. Biol Bull 195, 220-222.

Straka, H., Holler, S., Goto, F., Kolb, F.P., Gilland, E., 2003. Differential spatial organization of otolith signals in frog vestibular nuclei. J Neurophysiol 90, 3501-3512.

Straka, H., Simmers, J., 2011. *Xenopus laevis*: An ideal experimental model for studying the developmental dynamics of neural network assembly and sensory-motor computations. Dev Neurobiol 72, 649-663.

Suzuki, D.G., Murakami, Y., Yamazaki, Y., Wada, H., 2015. Expression patterns of *Eph* genes in the “dual visual development” of the lamprey and their significance in the evolution of vision in vertebrates. Evol Dev 17, 139-147.

Tauber, E.S., Atkin, A., 1968. Optomotor responses to monocular stimulation: Relation to visual system organization. Science 160, 1365-1367.

Udin, S.B., Grant, S., 1999. Plasticity in the tectum of *Xenopus laevis*: binocular maps. Prog Neurobiol 59, 81-106.

Valentine, J.W., Jablonski, D., Erwin, D.H., 1999. Fossils, molecules and embryos: new perspectives on the Cambrian explosion. Development 126, 851-859.

Ventre, J., 1985. Cortical control of oculomotor functions. I. Optokinetic nystagmus. Behav Brain Res 15, 211-226.

von Uckermann, G., Le Ray, D., Combes, D., Straka, H., Simmers, J., 2013. Spinal efference copy signaling and gaze stabilization during locomotion in juvenile *Xenopus* frogs. J Neurosci 33, 4253-4264.

Wade, N.J., 2010. Pioneers of eye movement research. Iperception 1, 33-68.

Wallman, J., McKenna, O.C., Burns, S., Velez, J., Weinstein, B., 1981. Relation of the accessory optic system and pretectum to optokinetic responses in chickens. In: Fuchs, A.F., Becker, W. (Eds.), Progress in Oculomotor Research. Elsevier North Holland, pp. 435–442.

Wallman, J., Velez, J., 1985. Directional asymmetries of optokinetic nystagmus: developmental changes and relation to the accessory optic system and to the vestibular system. J Neurosci 5, 317-329.

Walls, G.L., 1942. The vertebrate eye and its adaptive radiation. Cranbrook Institute of Science, Bloomfield Hills, MI.

Weber, A.E., Martin, J., Ariel, M., 2003. Connectivity of the turtle accessory optic system. Brain Res 989, 76-90.

Wheeler, G.N., Brändli, A.W., 2009. Simple vertebrate models for chemical genetics and drug discovery screens: lessons from zebrafish and *Xenopus*. Dev Dynam 238, 1287-1308.

Winterson, B.J., Brauth, S.E., 1985. Direction-selective single units in the nucleus lentiformis mesencephali of the pigeon (*Columba livia*). Exp Brain Res 60, 215-226.

Wylie, D.R., Linkenhoker, B., Lau, K.L., 1997. Projections of the nucleus of the basal optic root in pigeons (*Columba livia*) revealed with biotinylated dextran amine. J Comp Neurol 384, 517-536.

Yücel, Y.H., Jardon, B., Kim, M.S., Bonaventure, N., 1990. Directional asymmetry of the horizontal monocular head and eye optokinetic nystagmus: effects of picrotoxin. Vision Res 30, 549-555.

LIST OF ABBREVIATIONS

ANOVA	analysis of variance
AOS	accessory optic system
aVOR	angular vestibulo-ocular reflex
$CaCl_2$	calcium chloride
CN	cranial nerve
CN III	oculomotor nerve
CN IV	trochlear nerve
CN VI	abducens nerve
ccw	counterclockwise
cw	clockwise
DC motor	direct current motor
DMSO	dimethyl sulfoxide
DTN	dorsal terminal nucleus
EOM	extraocular muscle
F	F-value of ANOVA
FP	fast phase
HB	hindbrain
HC	horizontal semicircular canal
hOKR	horizontal optokinetic reflex
IFPI	inter-fast-phase-interval
Int	interneurons
IO	inferior oblique muscle
IR	inferior rectus muscle
KCl	potassium chloride
LR	lateral rectus muscle
LTN	lateral terminal nucleus
lVOR	linear vestibulo-ocular reflex
$MgCl_2$	magnesium chloride

MIF	multiply innervated muscle fiber
MR	medial rectus muscle
MS-222	tricaine methanesulfonate
MTN	medial terminal nucleus
n	number of animals
nIII	oculomotor nucleus
nIV	trochlear nucleus
nVI	abducens nucleus
N	nasal
NaCl	sodium chloride
$NaHCO_3$	sodium hydrogen carbonate
nBOR	nucleus of the basal optic roots
nLM	nucleus lentiformis mesencephali
NOT	nucleus of the optic tract
N-T	naso-temporal
OKR	optokinetic reflex
ON	optic nerve
OT	optic tectum
p	critical level of statistical significance
PB	phosphate buffer
PFA	paraformaldehyde
PSTH	peri-stimulus time histogram
r1-8	rhombomeres 1-8
RB	retractor bulbi muscle
RGC	retinal ganglion cell
ROI	region of interest
SD	standard deviations

SEM	standard error of the mean
SIF	singly innervated muscle fiber
SO	superior oblique muscle
SP	slow phase
SR	superior rectus muscle
T	temporal
Tel	telencephalon
T-N	temporo-nasal
tOKR	torsional optokinetic reflex
VN	vestibular nucleus
vOKR	vertical/oblique optokinetic reflex
VOR	vestibulo-ocular reflex
$ß_{Position}$/ $ß_{Velocity}$	regression coefficient of firing rate to eye position/ eye velocity
°	degree of angle
τ	Kendall's tau coefficient

APPENDIX

COPYRIGHTS

FIGURE 4 (Introduction, p. 16):

FIGURE 5B (Materials and methods, p. 20):

CONFERENCE PRESENTATIONS

Schuller J.M., Knorr A.G., Glasauer S., Straka H. (2014) Task-specific activation of extraocular motoneurons in *Xenopus laevis*. Society for Neuroscience Conference, Washington

Schuller J.M., Knorr A.G., Glasauer S., Straka H. (2013) Different extraocular motoneuronal subgroups control fast and slow phase components of the optokinetic reflex in *Xenopus laevis*. Meeting of the German Neuroscience Society, Göttingen

Schuller J.M., Knorr A.G., Glasauer S., Straka H. (2012) Differential organization of extraocular motoneurons for slow and fast phase components of the horizontal optokinetic reflex in *Xenopus laevis*. Forum of the Federation of European Neurosciences Society, Barcelona

Knorr A.G., **Schuller J.M.**, Straka H. and Glasauer S. (2012) A model of the optokinetic reflex system in larval *Xenopus*. Bernstein Conference, Munich

Schuller J.M., Chagnaud B.P., Straka H. (2011) Interaction of visual and spinal central pattern generator-derived signals during locomotor activity in larval *Xenopus*. Society for Neuroscience Conference, Washington

AFFIDAVIT

Hiermit versichere ich an Eides statt, dass ich die vorliegende Dissertation “Functional organization and ontogeny of the optokinetic reflex in *Xenopus laevis*” selbstständig angefertigt habe, mich außer der angegebenen keiner weiteren Hilfsmittel bedient und alle Erkenntnisse, die aus dem Schrifttum ganz oder annähernd übernommen sind, als solche kenntlich gemacht und nach ihrer Herkunft unter Bezeichnung der Fundstelle einzeln nachgewiesen habe.

I hereby confirm that the dissertation “Functional organization and ontogeny of the optokinetic reflex in *Xenopus laevis*” is the result of my own work and that I have only used sources or materials listed and specified in the dissertation.

München, den / Munich, 29.08.2017

Johanna Schuller

DECLARATION OF AUTHOR CONTRIBUTIONS

Contributions of Johanna Schuller

- Planning of all experiments
- Performance of all experiments
- Analysis of all data
- Design and assembly of all figures
- Writing of the manuscript

Munich, 29.08.2017

Johanna Schuller Prof. Hans Straka